LIEGE UNIVERSITY

Second Colloquium on the Hydrodynamics

of the Ocean

Small Scale Processes in the Deep Ocean

March 17-20, 1970

UNIVERSITÉ DE LIÈGE

Cahiers de mécanique mathématique n° 26

LIEGE UNIVERSITY

Second Colloquium on the Hydrodynamics of the Ocean

March 17-20, 1970

Held at the

Institut de Mathématique

Avenue des Tilleuls, 15 - 4000 LIÈGE

Sponsored by the

Centre belge d'Océanographie

and the

Academic Authorities of the University of Liege

Papers edited by

Claude J. FRANKIGNOUL

Colloquium Planning Committee :

Jacques C.J. NIHOUL - Claude J. FRANKIGNOUL

TABLE OF CONTENTS

FOREWORD

In 1969, the University of Liège organized a small invitational symposium on some selected topics in Ocean Hydrodynamics. Several scientists from different countries met at the University of Liège to discuss both theoretical and experimental problems in recent attempts to understand the mechanism of internal waves and turbulent patches in the ocean.

During and following this symposium, feeling developed among participants that it was a valuable type of meeting, that scientific benefit would come from continuation of it. Consequently, a second symposium was held at the Institute of Mathematics of Liège University, in March 17 - 20, 1970, with Dr. Ferris Webster and Mr. J. Gonella as invited lecturers.

This document contains papers by the speakers at this second symposium. Some of the papers were prepared by the authors for the colloquium, some are summarized versions of more extended works (which will also appear, in parts, in current scientific journals). One paper has been established from the recording of the talk by the editorial board with the author's help and another one is reproduced from Nature (whose kind collaboration is acknowledged), following the author's suggestion.

Financial support for the second symposium came from the Centre Belge d'Océanographie and from the University of Liège.

The organizers wish to express their gratitude to Professor M. Dubuisson, Recteur de l'Université de Liège and Président du Centre Belge d'Océanographie and to Professor A. Distèche, Secrétaire du Centre Belge d'Océanographie for their sustained advice, encouragement and support ; to Prof. J. Etienne, Directeur administratif de l'Institut de Mathématique and to Dr. M. Thyssen, conservateur de la bibliothèque, who place the Institute facilities to their disposal.

Madame Gilnay's precious help is greatly acknowledged in the organization of the colloquium. The organizers are endebted to Madame Desaive for her hearty welcome at the Château de Colonster.

COLLOQUIUM PROGRAMME

Tuesday, 17th March.

Small scale erratic motions in the ocean. *By Jacques C.J. Nihoul*

Introduction to the W.H.O.I. moored array experiments ; aims techniques, overall results, future directions. *By Ferris Webster*

La Méditerranée occidentale, modèle réduit d'océan. La Bouée Laboratoire : description ; projection d'un film. *By J. Gonella*

Wednesday, 18th March.

Variability of ocean currents ; low-frequency oscillations, mean currents, representativeness. *By Ferris Webster*

On the fine structure of ocean variables and its correlation with the field of motion. *By G. Siedler*

Small scale processes and antarctic bottom water formation. *By A.E. Gill*

On horizontal coherence and internal wave propagation in the Northern North Sea. *By F. Schott*

Thursday, 19th March.

Inertial oscillations in the deep sea : review of observations, scales of coherence, local vs. global generation. *By Ferris Webster*

Quelques résultats d'observations (vent, courants et température). Synthèse : le modèle d'Ekman en régime impulsionnel. *By J. Gonella*

Wave driven inertial oscillations. *By K. Hasselmann*

The effects of horizontal density gradients on the propagation of inertial-internal waves. *By Christopher N.K. Mooers*

Friday, 20th March.

Internal waves and turbulence : energy relationships, equipartition, vertical profiles, dissipation, anisotropy. *By Ferris Webster*

Generation of transient nearly inertial oscillations by the interaction of internal waves with a shear flow. *By Claude J. Frankignoul*

General discussion.

LIST OF PARTICIPANTS

Prof. K.K. Bajaj, University of Kansas, U.S.A.

Mr. D. Bay, Lc. sc., Université de Liège, Belgium.

Dr. A.G. Cavanié, Centre Océanologique de Bretagne, France.

Dr. J. de Boer, Hydrographic Office, The Hague, Netherlands.

Prof. A.E. Distèche, Université de Liège, Belgium.

Ing. A.E. Eskenazy, Université de Liège, Belgium.

Ing. C.J. Frankignoul, Université de Liège, Belgium.

Prof. J.P. Germain, Laboratoire de Mécanique des Fluides, Grenoble, France.

Dr. A.E. Gill, University of Cambridge, England.

Mr. J. Gonella, anc. él. de l'école polytechnique, Museum d'Histoire Naturelle, Paris 5e, France.

Dr. G. Grancini, Osservatorio Geophisico sperimentale, Trieste, Italy.

Prof. K. Hasselmann, Universität Hamburg, Germany.

Dr. J.L. Hyacinthe, Centre Océanologique de Bretagne, France.

Dr. K.P. Klotermann, Deutsches Hydrographisches Institut, Hamburg, Germany.

Dr. G. Lebon, Université de Liège, Belgium.

Ing. J. Lebrun, Université de Liège, Belgium.

Ing. A. Lejeune, Université de Liège, Belgium.

Ing. H. Libens, Université de Liège, Belgium.

Mr. P. Liden, University of Cambridge, England.

Mr. A. Maftei, Lc. sc. (France), Université de Liège, Belgium.

Dr. C.N.K. Mooers (U.S.A.), University of Liverpool, England.

Ing. N. Mpeye, Université de Liège, Belgium.

Prof. J.C.J. Nihoul, Université de Liège, Belgium.

Mr. A. Pequeux, Lc. sc., Université de Liège, Belgium.

Ing. J.M. Quitin, Université de Liège, Belgium.

Dr. F. Schott, Universität Kiel, Germany.

Prof. G. Siedler, Universität Kiel, Germany.

Prof. R. Spronck, Université de Liège, Belgium.

Dr. J.L. Van Hamme, Institut Royal Météorologique, Belgium.

Dr. F. Webster, Woods Hole Oceanographic Institution, U.S.A.

STUDENTS

MM. A. Bernard
M. Betz
Miss C. Bon
B. Delcourt
R. Henrion
MM. G. Jeuris
F. Ronday
Miss M. Wiser
C. Zeyen
Y. Adam

SMALL-SCALES ERRATIC MOTIONS IN THE DEEP OCEAN

By Jacques C.J. Nihoul
Institut de Mathématique, Université de Liège
4000 Liège

1. INTRODUCTION -

In the ocean, under the surface layer, the flow is quieter and some authors do not hesitate to describe the fluid motion in these regions as a laminar flow displaying occasional disorganized patches answerable to turbulence (Woods, 1969).

In a non-homogeneous medium like the ocean, however, the word "laminar" cannot possibly refer to the sort of peaceful motion one can produce in a pipe or a laboratory channel. Between subsurface layers of varying density, undulating swells, called internal waves, form and multiply by non-linear interactions. These interactions, on the one hand, and the variety of their sources on the other hand, produce an intricated collection of motions of various scales which is best described by a statistical analysis.

The same approach applies then to waves and to turbulence and, indeed, if one defines "turbulence" as a field of chaotic vorticity (Saffman, 1968), the rotational random waves can be incorporated in the definition and the ocean can be regarded as completely turbulent.

The first objective of the study of ocean flow is then the determination of the energy spectrum function which associates to each scale of motion (indicated by its wave number vector $\underline{K}$) a density of energy $F(\underline{K})$ and the definition of transport coefficients describing the average diffusion by erratic stirring and mixing of momentum, heat, salt, radioactivity, pollution etc...

This study has been first approached from two extremes and

methods of linear wave analysis (Fofonoff,1969) have been tried simultaneously with phenomenological descriptions of ordinary homogeneous turbulence.

An artificial distinction has thus been introduced, inducing several authors to consider two quite separate types of motions in the deep ocean and Townsend (1958) writes that, dispite "the gradual transition from one flow to another","the two flows are so distinct that no common description is likely to be valid".

It is difficult to accept this opinion, however, in view of the recent works in the domain which, proceeding from the two extremes, have successfully narrowed the difference and support the idea of a unified description.

Standard perturbation techniques, starting from the linear wave model, allowed Hasselmann (1962,1963,1966,1967,1968) and other authors to develop a "weak interaction" theory of ocean waves, analogous to weak plasma turbulence (Kadomtsev,1965), interacting phonon ensembles (Peierls,1955) and to the recent description of Clear Air turbulence proposed by Bretherton (1969). This theory approaches the controversed but enthralling theory propounded by Kraichnan (1959) for homogeneous turbulence. Examining the problem from the other side, Webster (1969) has shown that, even in a range of wave-numbers where one would expect wave models to be very accurate, experimental data were not in disagreement with the famous Kolmogorov law for strong turbulence.

These results, which contribute to the construction of a unified description, agree well with the actual trend, in the theory of non-homogeneous turbulence, to represent a fully developed turbulent shear flow as a superposition of waves (Landahl, 1967, Reynolds, Nihoul,1969, 1970).

The purpose, here, is to present the philosophy of some important features of the existing models and the elements of a general description, in the simplest context possible.

2. FOURIER ANALYSIS -

Ocean hydrodynamics is currently described by the Boussinesq equations. This is an approximation which consists in assuming that the fluid is incompressible and the density constant but taking into account the density variation in the gravity force by the introduction of a buoyancy force.
Let the Brunt-Väisälä frequency N and the buoyancy velocity V_4 be introduced by

$$(1),(2) \qquad N^2 = -\frac{g}{\rho_o}\frac{d\bar{\rho}}{dX_3} \quad ; \quad V_4 = \frac{-g\rho'}{\rho_o N}$$

where the X_3-axis is vertical upwards, g is the acceleration of gravity, ρ_o the reference constant density, $\bar{\rho}$ the average deviation from ρ_o and ρ' the fluctuation around $\bar{\rho}$.

Neglecting the Coriolis effects and assuming the Brunt-Väisälä frequency constant, for simplicity, the Boussinesq equations may be written :

$$(3) \qquad \nabla \cdot \underline{V} = 0$$

$$(4) \qquad \frac{\partial V_1}{\partial t} + \underline{V} \cdot \nabla V_1 + \frac{\partial q}{\partial X_1} - \nu \nabla^2 V_1 = 0$$

$$(5) \qquad \frac{\partial V_2}{\partial t} + \underline{V} \cdot \nabla V_2 + \frac{\partial q}{\partial X_2} - \nu \nabla^2 V_2 = 0$$

$$(6) \qquad \frac{\partial V_3}{\partial t} + \underline{V} \cdot \nabla V_3 + \frac{\partial q}{\partial X_3} - NV_4 - \nu \nabla^2 V_3 = 0$$

$$(7) \qquad \frac{\partial V_4}{\partial t} + V \cdot \nabla V_4 + NV_3 = 0$$

where q denotes the pressure counted from the reference state and divided by ρ_o; V_1, V_2, V_3 are the components of the velocity vector and ∇ is the vector-operator $\left(\frac{\partial}{\partial X_1}, \frac{\partial}{\partial X_2}, \frac{\partial}{\partial X_3}\right)$. The Coriolis

forces have been neglected to lighten the writing. Since the corresponding terms are linear, there would be no difficulty in incorporating them in the subsequent analysis. The approximation merely excludes the very small frequencies, and disregards eventual complicated interactions between the oscillations considered here and other low frequency mechanisms.

Let

$$(8) \qquad V_1(\underline{X},t) = \int W_1(\underline{K},\omega)\, e^{i(\underline{K}.\underline{X}-\omega t)} d\underline{K}\, d\omega$$

$$(9) \qquad V_2(\underline{X},t) = \int W_2(\underline{K},\omega)\, e^{i(\underline{K}.\underline{X}-\omega t)} d\underline{K}\, d\omega$$

$$(10) \qquad V_3(\underline{X},t) = \int W_3(\underline{K},\omega)\, e^{i(\underline{K}.\underline{X}-\omega t)} d\underline{K}\, d\omega$$

$$(11) \qquad V_4(\underline{X},t) = i\int W_4(\underline{K},\omega)\, e^{i(\underline{K}.\underline{X}-\omega t)} d\underline{K}\, d\omega \ .$$

Four dimensional Fourier transforms of eq(3) to (7) yield, after eliminating the pressure :

$$(12) \qquad A_{\alpha\beta}W_\beta = \int C_{\alpha\beta}K_\gamma W_\beta(\underline{K}-\underline{K}',\omega-\omega')W_\gamma(\underline{K}',\omega')d\underline{K}'\, d\omega'$$

where the greek subscripts can take values from 1 to 4. (Note $K_4=0$) and where a sum is understood whenever a subscript is repeated.

The matrix elements $C_{\alpha\beta}$ and $A_{\alpha\beta}$ are given by

$$(13) \qquad C_{\alpha\beta} = (\delta_{\alpha\beta} - \frac{K_\alpha K_\beta}{K^2})$$

$$(14) \qquad A = \begin{pmatrix} \omega+i\nu K^2 & 0 & 0 & -N\frac{K_1K_3}{K^2} \\ 0 & \omega+i\nu K^2 & 0 & -N\frac{K_2K_3}{K^2} \\ 0 & 0 & \omega+i\nu K^2 & N(1-\frac{K_3^2}{K^2}) \\ 0 & 0 & N & \omega \end{pmatrix}$$

Denoting ensemble averages by angular brackets, the energy spectrum tensor $\underline{\underline{H}}$ is defined by

$$(15) \qquad H_{\alpha\beta}(\underline{K},\omega)\ \delta(\underline{K}-\underline{\mu})\ \delta(\omega-\sigma)=\langle W_\alpha(\underline{K},\omega)W^*_\beta(\underline{\mu},\sigma)\rangle\ .$$

Energy spectrum functions, measuring the energy distribution in wave number space, are then introduced by :

$$(16) \qquad F_h(\underline{K},\omega) = H_{11}+H_{22}$$

$$(17) \qquad F_c(\underline{K},\omega) = H_{11}+H_{22}+H_{33}$$

$$(18) \qquad F_T(\underline{K},\omega) = H_{11}+H_{22}+H_{33}+H_{44}\ .$$

Four-dimensional Fourier transforms are appropriate to describe fluid motions which are homogeneous in space and time.

This cannot be the case here. On the one hand, no attention has been paid to possible sources of energy (they would appear in the right hand side of eq (4) to (7)) and the dynamics of the random field in consideration may only result in a general decay. On the other hand, the assumption of space homogeneity obviously disregards boundary effects at the surface or the bottom of the ocean and is related to the hypothesis of constant Brunt-Väisälä

forces have been neglected to lighten the writing. Since the corresponding terms are linear, there would be no difficulty in incorporating them in the subsequent analysis. The approximation merely excludes the very small frequencies, and disregards eventual complicated interactions between the oscillations considered here and other low frequency mechanisms.

Let

$$(8) \qquad V_1(\underline{X},t) = \int W_1(\underline{K},\omega)\, e^{i(\underline{K}.\underline{X}-\omega t)} d\underline{K}\, d\omega$$

$$(9) \qquad V_2(\underline{X},t) = \int W_2(\underline{K},\omega)\, e^{i(\underline{K}.\underline{X}-\omega t)} d\underline{K}\, d\omega$$

$$(10) \qquad V_3(\underline{X},t) = \int W_3(\underline{K},\omega)\, e^{i(\underline{K}.\underline{X}-\omega t)} d\underline{K}\, d\omega$$

$$(11) \qquad V_4(\underline{X},t) = i\int W_4(\underline{K},\omega)\, e^{i(\underline{K}.\underline{X}-\omega t)} d\underline{K}\, d\omega \quad .$$

Four dimensional Fourier transforms of eq(3) to (7) yield, after eliminating the pressure :

$$(12) \qquad A_{\alpha\beta}W_{\beta} = \int C_{\alpha\beta}K_{\gamma}W_{\beta}(\underline{K}-\underline{K}',\omega-\omega')W_{\gamma}(\underline{K}',\omega')d\underline{K}'\, d\omega'$$

where the greek subscripts can take values from 1 to 4. (Note $K_4=0$) and where a sum is understood whenever a subscript is repeated.

The matrix elements $C_{\alpha\beta}$ and $A_{\alpha\beta}$ are given by

$$(13) \qquad C_{\alpha\beta} = (\delta_{\alpha\beta} - \frac{K_{\alpha}K_{\beta}}{K^2})$$

frequency. If N were not constant, there would be an extra term in the right hand side of (7) proportional to $\frac{d \ln N}{dX_3}$. Fig (1) shows a typical variation of ln N with depth.

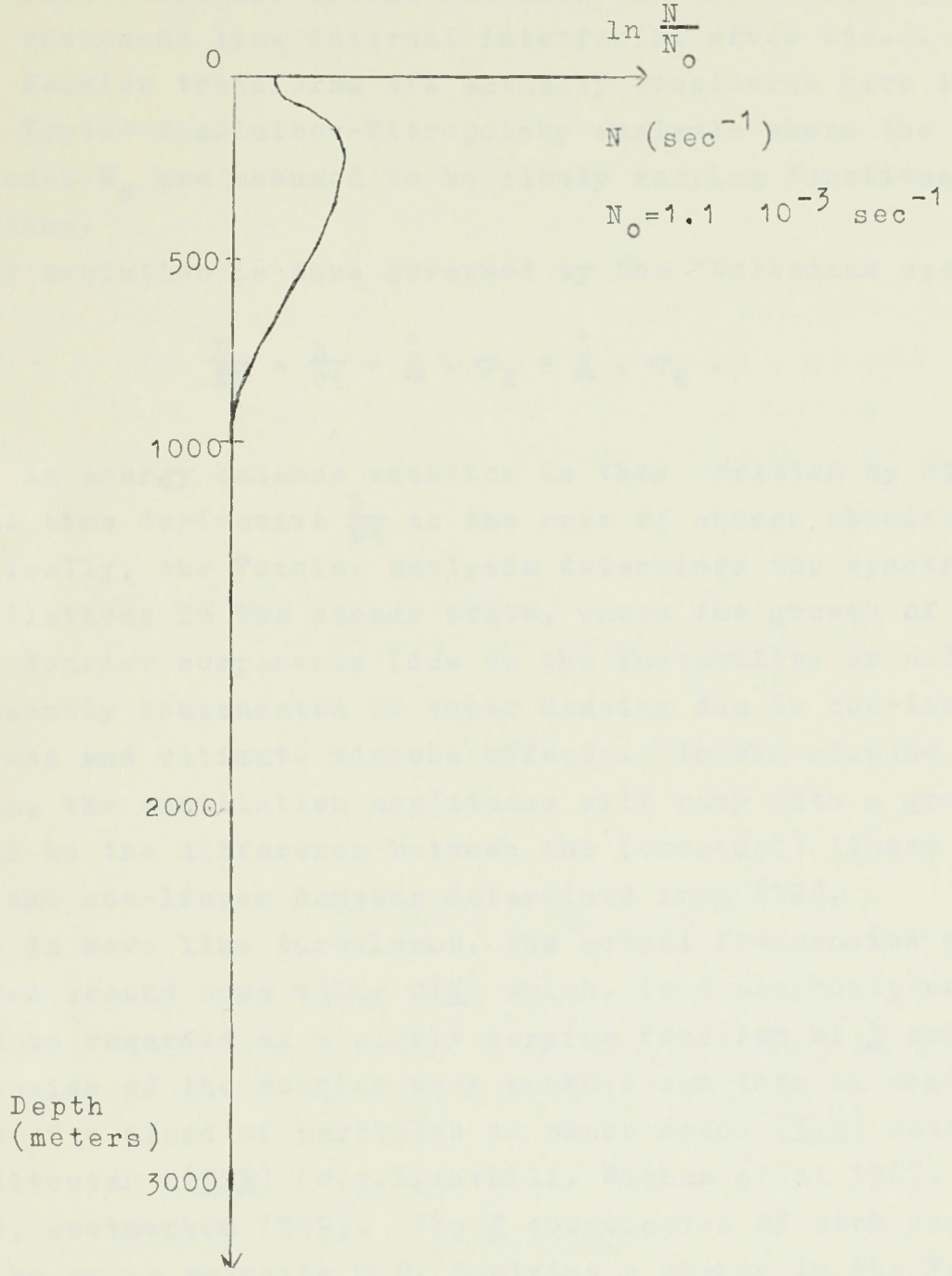

Clearly, the Brunt-Väisälä frequency is fairly constant in sufficiently deep ocean but varies in the thermocline. In addition, however, to the slow variations shown on fig.1, sharp changes in the Brunt-Väisälä profile have also been observed within narrow sheets. This fine structure is ignored here and the model neglects special phenomena like internal interfacial waves etc...

Fourier transforms are actually considered here in the scope of a Krylov-Bogoluibov-Mitropolsky analysis where the Fourier amplitudes W_α are assumed to be slowly varying functions of space and time.
Their evolution is thus governed by the "Boltzmann operator"

$$(19) \qquad \frac{D}{DT} = \frac{\partial}{\partial t} + \dot{\underline{X}} \cdot \nabla_X + \dot{\underline{K}} \cdot \nabla_K \ .$$

An energy balance equation is then written by equating the total time derivative $\frac{D}{Dt}$ to the rate of change obtained from (12). Physically, the Fourier analysis determines the spectrum of the oscillations in the steady state, where the growth of the different Fourier components (due to the instability or acting sources) is exactly compensated by their damping due to non-linear interactions and ultimate viscous effects. In the absence of equilibrium, the oscillation amplitudes will vary with a growth rate equal to the difference between the (eventual) linear growth rate and the non-linear damping determined from (12).

In wave like turbulence, the actual frequencies are concentrated around some value $\Omega(\underline{K})$ which, in a non-homogeneous medium, must be regarded as a slowly varying fonction of $\underline{X}$ and t. The evolution of the Fourier wave packets can then be assimilated to that of a cloud of particles in phase space $(\underline{X},\underline{K})$ under a Hamiltonian $\Omega(\underline{K},\underline{X})$ (e.g.Lighthill, Witham et al 1967, Hasselmann 1968, Bretherton 1969). The $\underline{X}$ coordinates of each packet change at the group velocity $\nabla_K\Omega$, implying a change in the Fourier amplitudes at a fixed point if their gradients in this direction are not zero. The "momenta" $(\underline{K})$ vary at the rate $\nabla_X\Omega$. This can

cause a flux through the wave number spectrum. The interaction coefficients must be calculated locally.

Thus

$$\frac{D}{DT} \equiv \frac{\partial}{\partial t} + \nabla_K \Omega . \nabla_X + \nabla_X \Omega \cdot \nabla_K \quad . \tag{20}$$

In stronger turbulence, at smaller scale, this would be a very crude description, but presumably slow variations of the medium will affect very little such motions whose scale is much smaller than its scale of inhomogeneity.
In fact, the part of the medium is played for these turbulent eddies by the wake-like weaker turbulence background and it will be shown below that adiabatic interactions with the background produce a much more important effect of inhomogeneity.

3. THE LINEAR APPROXIMATION.

If the non-linear terms are neglected in (12), one finds :

$$\omega^2 = N^2 \frac{K_1^2 + K_2^2}{K^2} \qquad \text{(dispersion relation)} \tag{21}$$

and

$$H_{11} + H_{22} + H_{33} = H_{44} \quad . \tag{22}$$

There is thus equipartition between kinetic and potential energy. This criterion may be used to investigate the limit of validity of the linear approximation (Fofonoff 1969).

4. THE WEAK COUPLING APPROXIMATION.

If the non-linear interactions are small but not negligible, it seems quite natural to seek a solution of the form $\underline{W} = {}^{o}\underline{W} + {}^{1}\underline{W}$

where $^1\underline{W}$ is a small perturbation which results from the non-linear beat interactions and is determined by eq.(12) where $\underline{W}$ in the right hand side is replaced by $^0\underline{W}$.

To take a global account of the action of higher order non-linear terms which are here neglected and which may produce a damping of the individual Fourier component, a term $D_{\alpha\beta}W_\beta$ is introduced in the left hand side of (12), the tensor $\underline{\underline{D}}$ being sofar unknown.

This artificial closure is very important as it incorporates the net non-linear contribution to irreversibility and permits the definition of a rate of change due to non-linear interactions and suitable for (22).

Thus

$$(23) \qquad [A_{\alpha\beta}+D_{\alpha\beta}]\,{}^1W_\beta = \int C_{\alpha\beta}\,{}^0W_\beta(\underline{K}-\underline{K}',\omega-\omega')\,{}^0W_j(\underline{K}',\omega')K_j\,d\underline{K}'d\omega \quad .$$

Solving (12) for W_β (after adding $D_{\alpha\beta}W_\beta$ to both sides) and introducing the matrices L and N by

$$(24) \qquad L_{\alpha\beta} = B_{\alpha\gamma}D_{\gamma\beta}$$

$$(25) \qquad N_{\alpha\beta} = B_{\alpha\gamma}C_{\gamma\beta}$$

with

$$(26) \qquad B_{\alpha\beta}(A_{\beta\gamma}+D_{\beta\gamma}) = \delta_{\alpha\gamma}$$

one gets, from (12) :

$$(27) \qquad \langle W_\alpha(\underline{K},\omega)W^*_\beta(\underline{\mu},\sigma)\rangle = L_{\alpha\gamma}\langle W_\gamma(\underline{K},\omega)W^*_\beta(\underline{\mu},\sigma)\rangle$$

$$+\int N_{\alpha\gamma}(\underline{K},\omega)\,\langle W_\gamma(\underline{K}-\underline{K}',\omega-\omega')W^*_\beta(\underline{\mu},\sigma)W_\gamma(\underline{K}',\omega')\rangle K_\gamma\,d\underline{K}'d\omega'.$$

In zero approximation, the oscillations are assumed uncorrelated with a Gaussian distribution (the random phase approximation). The integral in the right hand side of (27) in thus zero at this approximation. The next approximation is obtained by including successively in each of the three factors the first order correction $^1\underline{W}$ which leads to double integrals (over $\underline{K}'$ and $\underline{\mu}'$, ω' and σ', say) of fourth order correlations. These are split into sums of products of second order correlations which are expressed in terms of $H_{\alpha\beta}$ by (15). The integrations over $\underline{\mu}'$ and σ' may then be performed, taking the δ-functions into account. The result includes a linear part and an integral over $\underline{K}'$ and $\underline{\sigma}'$ of all <u>direct</u> non-linear interactions. If $D_{\alpha\beta}$ is chosen as to cancel the linear part (assuming that the global influence of the non linear higher interactions on the energy rate of change is the same at the zeroth and first order), the final result is of the form

$$(28)\quad D_{qs}=-J_{q\alpha\beta}\int K'_{\beta\gamma s}\, H_{\alpha\gamma}(\underline{K}-\underline{K}',\omega-\omega')\, d\underline{K}'\, d\omega'$$

where

$$(29)\quad J_{q\alpha\beta} = C_{q\alpha}(\underline{K},\omega)K_\beta + C_{q\beta}(\underline{K},\omega)\, K_\alpha$$

$$(30)\quad K'_{\beta\gamma s} = N_{\beta\gamma}(\underline{K}',\omega')\, K'_s + N_{\beta s}\,(\underline{K}',\omega')K_\gamma$$

and

$$(31)\quad H_{qs}=\int N_{q\alpha}K_\gamma[N^*_{s\beta}K_\delta+N^*_{s\delta}K_\beta]\, H_{\alpha\beta}(\underline{K}-\underline{K}',\omega-\omega')H_{\gamma\delta}(\underline{K}',\omega')d\underline{K}'\, d\omega' \quad .$$

Eq.(28) and (31) constitute a set of coupled integral equations which can be regarded as the generalization of Kraichnan's équations.

In the absence of stratification ($\nu_4=0$), assuming homogeneity and isotropy, on can write

$$(32) \qquad H_{\alpha\beta}(\underline{K},\omega) = G(K,\omega)\ (\delta_{\alpha\beta} - \frac{K_\alpha K_\beta}{K^2})$$

$$(33) \qquad B_{\alpha\beta} = (\omega + i\nu\ K^2 + \eta)^{-1}\ \delta_{\alpha\beta}.$$

Substituting in (31), one gets :

$$(34) \qquad \frac{1}{2} F_c(\underline{K},\omega) = \frac{1}{2}[H_{11}+H_{22}+H_{33}] = G(K,\omega) =$$

$$= |\omega + i\nu K^2 + \eta|^{-2} \int K^2\ S(\underline{K},\underline{K}')\ G(\underline{K}',\omega')\ G(\underline{K}-\underline{K}',\omega-\omega')d\underline{K}'d\omega'$$

where

$$(35) \qquad S(\underline{K},\underline{K}') = \frac{1}{2}\ [1 - 2\ \frac{(\underline{K}\cdot\underline{K}')^2(\underline{K}\cdot\underline{K}'')^2}{K^4K'^2K''^2} + \frac{(\underline{K}\cdot\underline{K}')(\underline{K}\cdot\underline{K}'')(\underline{K}'\cdot\underline{K}'')}{K^2K'^2K''^2}]$$

with $\underline{K}'' = \underline{K}-\underline{K}'$.

Eq (34) and (35) are identical to Kraichnan's equations. An important characteristic of eqs. (31) or (34) is that they retained only direct interactions in the energy exchanges; the interaction between the Fourier component $\underline{K},\omega$ and the component $\underline{K}'$, ω' appearing as a resonant imput of energy to $\underline{K},\omega$ from $\underline{K}''=\underline{K}-\underline{K}'$, $\omega''=\omega-\omega'$.

This result is obtained here as a consequence of the weak coupling approximation and indeed, turbulence being a mixing process which degrades information, one should expect that the indirect interaction of three modes through the turbulent motion as a whole should not convey phase information among them in the limit where the motion consists of the excitation of an infinitely large number of weakly dependent degrees of freedom.

5. THE LIMITED WEAK COUPLING APPROXIMATION.

A consequence of the weak coupling hypothesis is that an individual mode $\underline{K},\omega$ gains or loses energy only by triangular interactions with modes $\underline{K}',\omega'$; $\underline{K}"\omega"$ such that $\underline{K} = \underline{K}' + K"$, $\omega = \omega' + \omega"$.

Since the number of these modes is large and the amplitude of the oscillations of an individual mode is determined by the integral of its triangular interactions, it is not unreasonable to think that, even in stronger turbulence where the global non-linear interaction is O (1), the interaction of the Fourier component $\underline{K},\omega$ with each separate component $\underline{K}',\omega'$ is comparatively small.

It is thus tempting to extend the weak-coupling approximation to strong turbulence. One can object however that this approximation implicity allows only resonant interactions between Fourier components and that such a model does not seem to be appropriate for interactions between modes of very different wavelengths.

One visualizes, indeed, the non-linear effects as fostering the viscous decay and producing at every wave number an increased damping expressed by the imaginary part of D (or η). Let this damping be grossly described by an "eddy viscosity term" $\hat{\nu}K^2$ (which incorporates the ordinary viscosity). At moderate numbers, this effect (and also the contribution from the real part of D) may be regarded as small. Then, one should expect the energy to be concentrated on the frequency axis around the eigenfrequency (21) given by

$$\det |A| = 0 \tag{36}$$

and a wave like description to be valid.

In the region of wave numbers O(K), the "waves" will have a lifetime $\tau \sim \hat{\nu}^{-1} K^{-2}$ and although one given mode may initially be localised, it will spread out in general as time passes to

fill a region of space whose characteristic size L will be of the order of the distance through which the "wave" propagates during its lifetime i.e.

$$(37) \qquad l \sim \frac{N}{\hat{\nu} K^3} \quad .$$

Thus the state of turbulent motion must be regarded as a system of many wave packets. As long as the ratio (37) is large, these packets exist for a very long time and are almost unlocalised in space so that a wave-like description is appropriate. As the ratio increases, the packets tend to concentrate and appear more as turbulent eddies.

This suggests two apparently different descriptions of the random velocity field; the two descriptions overlapping in this region of wave-numbers where l, estimated from the turbulence concepts (i.e. $l=K^{-1}$) is equal to (37).

If, as a practical experimental situation, the observations made by Woods (1969) off Malta are used, the following estimations can be made (M.K.S units)

Eddy viscosity : $\hat{\nu} \sim 10^{-4}$

Brunt-Väisälä frequency : $N \sim 10^{-3}$

$$l^2 \sim \frac{\hat{\nu}}{N} \sim 10^{-1} \; ; \; l \sim 0.3.$$

The size of the largest eddy of the typically turbulent motion should thus be of the order of 30cm. This figure is in excellent agreement with Woods's observations (Woods 1969).

This suggests that typical turbulence is found within patches (of size ~ 30cm, in the exemple treated); these patches moving in the non-homogeneous background of the larger scales wave-like motions. One should expect then that, as in (20), wave packets move about in wave number space, leading to a strong

correlation between nearby Fourier components which now describe essentially one and the same wave packet.

In this interpretation, the interaction between the mode $\underline{K},\omega$ and a "distant" mode $\underline{K}',\omega'$ cannot be considered as the resonant input to $\underline{K},\omega$ from the nearby component $\underline{K}",\omega"$ because $\underline{W}$ and $\underline{W}"$ describe the same wave packet and cannot be considered independently of one another.

It is thus necessary to distinguish between two types of interactions and to bring in this distinction it is convenient to break up the region of integration with respect to $\underline{K}'$, ω' in the non-linear terms into three parts : the principal region where K and K', ω and ω' are comparable, the "long wave" region where the prime quantities are much smaller and the short wave region where they are much larger.

The weak coupling analysis can be applied to region (1) the contribution from region (3) is presumably small as little energy is contained in wave numbers $K' >> K$, $K" \sim K' >> K$. The contribution from region (2) can be taken into account by expanding in this region $\underline{W}(\underline{K}-\underline{K}')$ in Taylor series around K.

Limiting the treatment to the first approximation, one writes :

$$(38) \qquad \int_{(2)} C_{\alpha\beta} K_\gamma W_\beta(\underline{K}-\underline{K}',\omega-\omega') W_\gamma(\underline{K}',\omega') d\underline{K}' d\omega' \sim \omega_W \, W_\alpha(\underline{K},\omega)$$

where

$$(39) \qquad \omega_W = K_\gamma \int_{(2)} W_\gamma(\underline{K}',\omega') d\underline{K}' \, d\omega'$$

ω_W is a random quantity given by the sum of a large number of individually random and weakly correlated amplitudes and its distribution may be assumed Gaussian.

The contribution from region (2) may then be incorporated in the matrix A by changing the frequency ω to the relative frequency

(40) $$\tilde{\omega} = \omega - \omega_{\underline{W}} .$$

The final result is that one recovers eq.(31) with the difference that the range of integration in the non-linear term is restricted to cover the region (1) and that the energy spectrum tensor is now calculated in a system of coordinates moving with the long wave pulsations. The true spectral functions H_{qs} are obtained by averaging over $\omega_{\underline{W}}$ i.e.

(41) $$\underline{\underline{H}}(K,\omega) = \frac{1}{\pi\omega_o} \int H(\underline{K}, \omega - \omega_{\underline{W}})\, e^{-\frac{\omega_{\underline{W}}^2}{\omega_o^2}}\, d\omega_{\underline{W}}$$

where

(42) $$\omega_o^2 = 2\, K_\gamma K_\delta \int_{(2)} H_{\gamma\delta}(\underline{K}', \omega')\, d\underline{K}'\, d\omega' .$$

The application by Kraichnan of eq.(34) to ordinary homogeneous isotropic turbulence lead to a $K^{-3/2}$ spectral law instead of the well-known Kolmogorov $K^{-5/3}$ law. The present analysis suggests that this discrepancy might be due to Kraichnan overestimating the part played by the large-scale fluctuations, which is in fact no more than the convection of higher modes which are deformed adiabatically in the process.
Indeed, by setting the lower limit of the integration over $\underline{K}'$, ω' in (34) equal to $\xi\,\underline{K}$; $\xi\omega$ where ξ is a small constant number ($\xi \sim 1/3$), Kadomtsev (1965) has obtained the Kolmogorov spectrum.

6. PHENOMENOLOGICAL APPROACH.

At present, one has no rigorous method of performing the separation between resonant and adiabatic non-linear interactions and of reducing the integral equations. In considering strong turbulence the limited weak coupling approximation certainly opens new ways prolonging Kraichnan's ideas but, in the meantime,

phenomenological approaches like Kolmogorov's theory are still required to interpret the observations.

According to Kolmogorov, over a wide range of scales (if the Reynolds number is large enough) the viscosity plays a negligible role and, in the absence of a direct input or output of energy, a quasi equilibrium is established. The turbulence is there fairly homogeneous and there is a constant energy flux ε through the spectrum. The value of ε determines the local properties of the turbulence. This hypothesis is equivalent to the natural assumption that the energy transfer between modes is of a resonance character, in which the energy of a mode K can be transferred only to modes with nearly the same scale. Thus a portion of energy handed down from a given scale to another must pass through the entire range of intermediate scales of motion. One may assert therefore that for each K the value of ε is determined only by the fluctuation level at this scale, i.e by the value of the spectral function at the corresponding wave number. This means that ε must be expressible in terms of K and, say E(K) where E(K) is the average of $F_c(\underline{K})$ over a sphere of radius K. The only dimensionnally correct combination is then

$$\varepsilon \sim [K^3 E(K)]^{1/2} K E(K) \tag{43}$$

i.e.

$$E(K) \sim \varepsilon^{2/3} K^{-5/3} . \tag{44}$$

It is interesting to note that Kolmogorov's reasoning applies equally well to three-dimensional and two dimensional turbulence although the interpretation is different. In three-dimensional turbulence the cascade of energy is directed from the large scale eddies where presumably energy is being provided (or has been stored) by external stirring devices,

towards the small scale eddies where it is dissipated by viscosity.

As pointed out by Kraichnan (1967), in two dimensional turbulence, the $K^{-5/3}$ range entails backwards energy cascade from higher to lower wave numbers and can only be expected in eddies whose scale is larger than the scale of the energy reservoir.

Quasi-two-dimensional flow is not unrealistic in the ocean in view of the stratification.

In many cases, experimental data are obtained for the horizontal specific energy measured at a given point as a function of time. A Fourier analysis in time gives the distribution in frequency, often interpreted in terms of wave number by invoking Taylor's hypothesis.

According to Taylor's hypothesis, if there is a mean velocity field, large in comparison with the components of turbulent velocity fluctuations, which advects the turbulent cells past the point of measurements, spacial scales are observed as corresponding time scales, i.e. there is some linear relationship between ω and K. Now, from eq.(12), it is readily seen that $\omega[W_1W_1^*+W_2W_2^*]$ is the sum of two terms; the first of which is simply the right hand side of (12) multiplied by W_β^* with the summation on β and γ limited to 1 and 2 and the second of which is proportional to K_3 and contains terms in W_3 and W_4.
We may thus regard the first term as representing a cascade interaction between components of the horizontal energy of different scales while the second term describes interactions with the vertical and buoyancy fluctuations.

In a stably stratified medium, one may speculate that these interactions and the interactions between W_3 and W_4 result in a net transfer of energy from the horizontal kinetic energy to the potential energy. In this case, the second interaction term expresses an inhibition of the horizontal fluctuations. Since this term is proportional to K_3, it affects predominantly the

turbulent eddies whose wave number vector has an important K_3 component. It would be without influence on eddies with an horizontal wave number vector if the non-linear cascade did not redistribute energy over all directions as much as it transfers it from scale to scale.

In weak turbulence however, in the wave like region, this redistribution will presumably not work fast enough and horizontal energy will tend to be concentrated in horizontal wave number vectors while the strength of the inhibition term diminishes.

If this interpretation is correct, the agreement found by Webster (1969) between observational data at Site D and the $K^{-5/3}$ law might indicate, in this range of wave number where buoyancy effects are important, the existence of two-dimensional turbulence with a net energy transfer from the fluctuations at frequency of 1 cycle per hour(*) towards inertial frequencies.

Some evidence in support of the possibility of such a backward transfer in stratified fluids are given by Fjørtoft (1953).

7. REFERENCES.

BRETHERTON (1969), I.U.C.R.M. Colloquium on Spectra of Meteorological Variables, Stockholm.

FOFONOFF N.P.(1969), Deep Sea Res., Suppl. to vol.16,59.

FJØRTOFT R. (1953), Tellus 5, 225.

HASSELMANN K. (1962), J.Fluid Mech. 12, 481.

(1963), J.Fluid Mech. 15, 273 and 385.

(1966), Rev.Geophys 4, 1.

(1967), Proc. Prog Soc.(London)A 299, 71.

(1968), Basic Developments in Fluid Dynamics (M.Holt Editor), Academic Press.

(*) It is probably adventurous to imagine sources of energy in this range of frequency although it corresponds roughly to the Brunt-Väisälä frequency and the possibility of instabilities degenerating in turbulence but also losing energy to gravity waves has been mentionned by several authors (Woods 1969).

KADOMTSEV B.B. (1965), Plasma Turbulence, Academic Press.

KRAICHNAN R.H. (1959), J. Fluid Mech. 5, 497.

KRAICHNAN R.H. (1967), Phys. Fluids, 10, 1417.

LANDAHL M.T. (1967), J. Fluid Mech. 29, 441.

LIGHTHILL M.J., WHITHAM G.B. and al (1967), Proc. Roy. Soc. (London) A299, 1456.

NIHOUL J.C.J. (1969), Bull. Soc. Roy. Sc. Lg. 3-4, 73.

NIHOUL J.C.J. (1970), Physica, 42.

PEIERLS R.E. (1955), Quantum Theory of solids, Oxford University Press.

SAFFMAN P.G. (1968), Proc. Phys. Sess., Int. School of Non-linear Math and Phys., Munich 1966. Topics in Non-linear Physics, Springer Verlag.

TOWNSEND A.A. (1958), J. Fluid Mech., 5, 361.

WEBSTER F. (1969), Deep-Sea Res., Suppl. to Vol.16, 85.

WOODS J.D. (1969), Proc. First Coll. on Ocean Hydrodynamics, Liège, May 20-24, 1969 ; Cahiers de Mécanique Mathématique, A 22.

LECTURES BY FERRIS WEBSTER
UNIVERSITY OF LIEGE, MARCH 17-20, 1970

By Ferris Webster
Woods Hole Oceanographic Institution
Woods Hole, Mass.02543

I.-INTRODUCTION TO THE WOODS HOLE OCEANOGRAPHIC INSTITUTION

MOORED ARRAY EXPERIMENTS

Introductory remarks.

Since about 1959, first under the direction of Dr. William S. Richardson, and then of Dr. Nicholas P. Fofonoff, a sequence of experiments has been carried out at the Woods Hole Oceanographic Institution using moored current meters to observe the dynamics of deep-sea processes. The results to date have provided quantitative estimates of the spectrum of horizontal ocean currents over the range of time scales from a few seconds to several months. In addition, the studies have provided new information about oceanic phenomena such as tides, inertial oscillations, internal waves and turbulence. These results will be the principal subject of my lectures.

The scientific results which will be discussed are the work of many people, and would not have been possible without the support of the members of the engineering, sea operations, and data processing groups in the project at Woods Hole.

Because most of the work which will be discussed has already been reported in the oceanographic literature these notes will be brief and there will be extensive references to published reports.

There are a number of references of recent work which may not yet be published which should serve to complement the bibliography in the references.

Instrumentation and Techniques.

The original instrumentation and techniques were described by Richardson, et al (1963) and the results of early work were summarized by Fofonoff (1968a). Briefly, the observational technique consists of inserting recording oceanographic instruments, such as current meters, temperature, and pressure recorders, into the lines of deep-sea moorings having buoys at the ocean surface or below. Over the course of several years the mooring techniques have become highly developed (Berteaux and Walden, 1969; Berteaux, 1968) and losses of equipment have recently been significantly less than was the case a few years ago.

The present procedure is to set deep-sea moorings with instrumentation for periods of from two to four months. At the end of this time the mooring is retrieved and the data is recovered from inside the instruments for computer processing (Maltais, 1969).

The principal instrumentation used is current meters. These have evolved from Richardson's original design and are now manufactured in the United States by the Geodyne division of E.G. and G. Corporation. The response characteristics of the instrument have been studied by Fofonoff and Ercan (1967).

A few measurements have been made with temperature records (Fofonoff, 1969) and pressure recorders are used to monitor the depth of instruments on moorings having subsurface floats. Some measurements have also been made of mooring line parameters, such as line tension (Millard, 1969), principally for engineering studies of deep-sea moorings. Measurements of winds with anemometers mounted on surface buoys have beeb very useful for defining some air-sea interaction processes, and results from these will be discussed.

Measurement Procedures.

The questions of sampling (the time between observations) and of quantizing (the accuracy with which the measurements are made) are very important in setting up a systematic program of measurements. In any series of measurements of time series there is a danger that high-frequency noise components may appear in the form of low-frequency signal if the sampling rate is too infrequent. This process is called aliasing and is a well-known pitfall in time-series measurements. In the case of measurements collected with moored instruments it is possible for badly-designed sampling procedures to completely obscure the character of the oceanic phenomenon being studied (Webster, 1964).

A sampling procedure has been developed for moored current meters (Webster, 1967) which matches the conflicting requirements of data storage capacity, long-term operation, and frequent measurements. The procedure is based on prior knowledge of spectrum of ocean currents. Measurements have shown that the spectrum has a large concentration of kinetic energy at high frequencies (periods of about 5 to 10 seconds) but a minimum of energy below those frequencies down to the frequencies of principal oceanographic interest (periods of a few hours).

The sampling method used is one in which the current meter is regularly turned on at widely-spaced intervals, during each of which it collects a burst of rapidly-sampled measurements. By working with values averaged over the burst of samples, it is possible to obtain time series in which the high-frequency energy is essentially removed without serious distortion of the low-frequency signals of interest. A similar procedure for sampling winds for surface buoys has been developed by Millard (1968).

The problem of quantizing, or the accuracy with which the data are recorded is less insidious a problem than that of sampling. Nevertheless, care has to be taken that the roundoff error in a serie of measurements is not so great that processes having low

energy levels are not completely obscured by the "noise" generated by the coarseness of the recording.

Decisions about experimental design: duration of measurement, separation of samples in time and space, and precision of measurement, can be crucially important in deciding the effectiveness of a systematic program of time-series measurements in the ocean.

The Site D current measurement program.

Since 1965, the program of current measurements at the Woods Hole Oceanographic Institution has centered upon repeated measurements at a single location: Site D, 39° 20'N, 70°W. This location is about 50 km. south of the Continental Shelf south of Woods Hole and is about 175 km. north of the mean axis of the Gulf Stream. The advantages of using this location are that it is in deep water (about 2,600 m. depth) and is within easy overnight passage of ships from Woods Hole. There is also the advantage that successful mooring techniques have been developed for the Site D region that do not necessarily work in other regions of the Atlantic Ocean. Furthermore, it is useful to collect repeated measurements at a single site; such measurements can be used to examine those oceanographic properties that can only be identified using statistical procedures.

Disadvantages of Site D are that it is close to both the Continental Shelf and the Gulf Stream and that the currents are influenced by both. To an unknown extent then, Site D cannot be considered to be representative of true open-ocean conditions.

Other deep-sea mooring sites have been used from time to time. In particular, attempts have been made to set up a set of stations in the western North Atlantic along the 70° West meridian. Because of strong currents, fishbite, and possibly other factors, it has not yet been possible to establish a successful program of measurements at these sites.

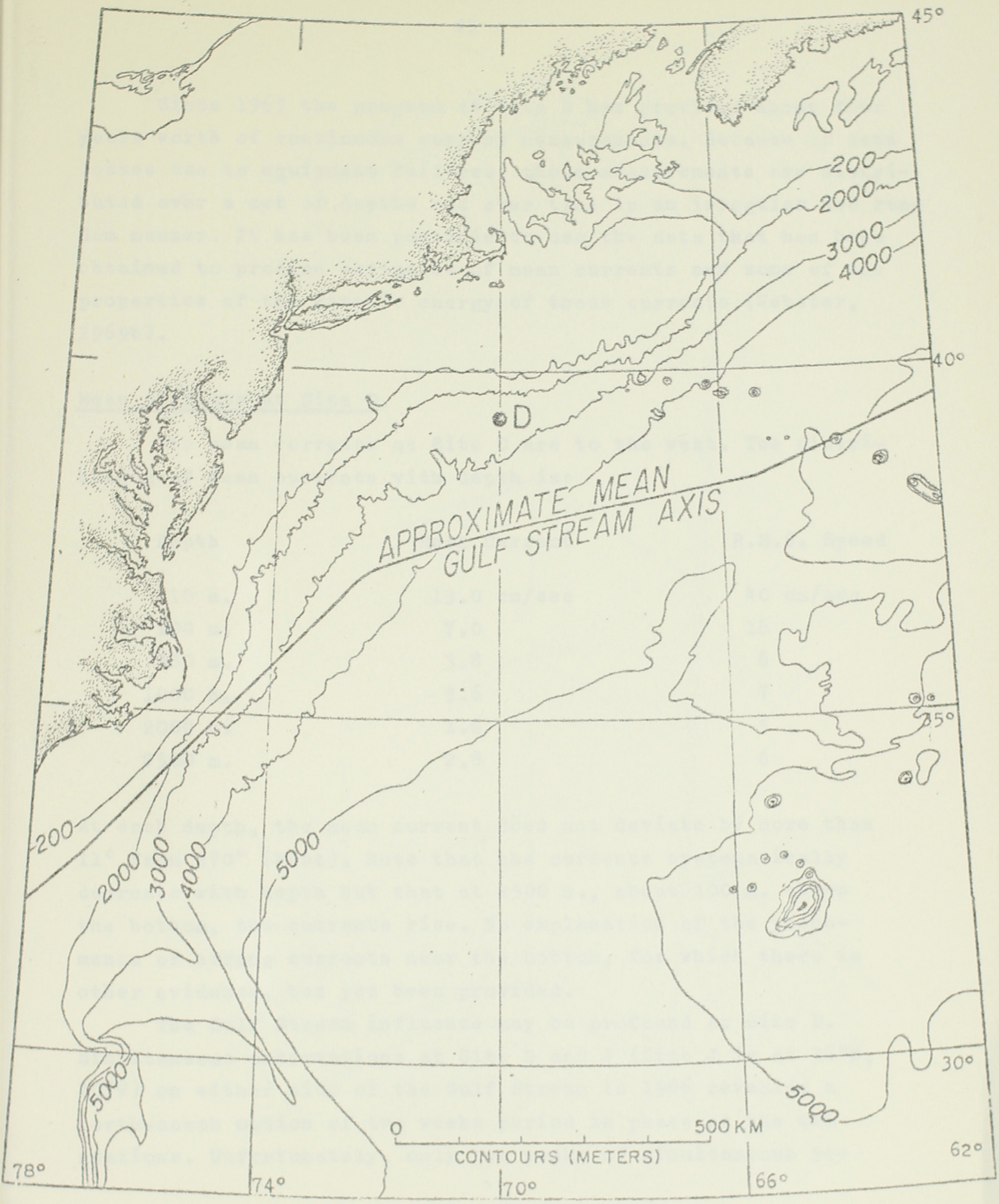

Fig. 1.- Chart showing the location of Site D in the western North Atlantic.

Since 1965 the program at Site D has provided about four years worth of continuous current measurements. Because of data losses due to equipment failures, these measurements are distributed over a set of depths and over time in an irregular and random manner. It has been possible to use the data that has been obtained to produce estimates of mean currents and some of the properties of the kinetic energy of those currents (Webster, 1969b).

Mean currents at Site D.

The mean currents at Site D are to the west. The distribution of mean currents with depth is:

Depth	Mean Current	R.M.S. Speed
10 m.	13.0 cm/sec	40 cm/sec
100 m.	7.0	18
500 m.	3.8	8
1000 m.	3.6	7
2000 m.	1.6	5
2500 m.	2.8	6

At each depth, the mean current does not deviate by more than 11° from 270° (West). Note that the currents systematically decrease with depth but that at 2500 m., about 100 m. above the bottom, the currents rise. No explanation of the phenomenon of strong currents near the bottom, for which there is other evidence, has yet been provided.

The Gulf Stream influence may be profound at Site D. Simultaneous observations at Site D and J (Site J is at 36°N, 70°W) on either side of the Gulf Stream in 1966 revealed a north-south motion of two weeks period in phase at the two stations. Unfortunately, only two weeks of simultaneous re-

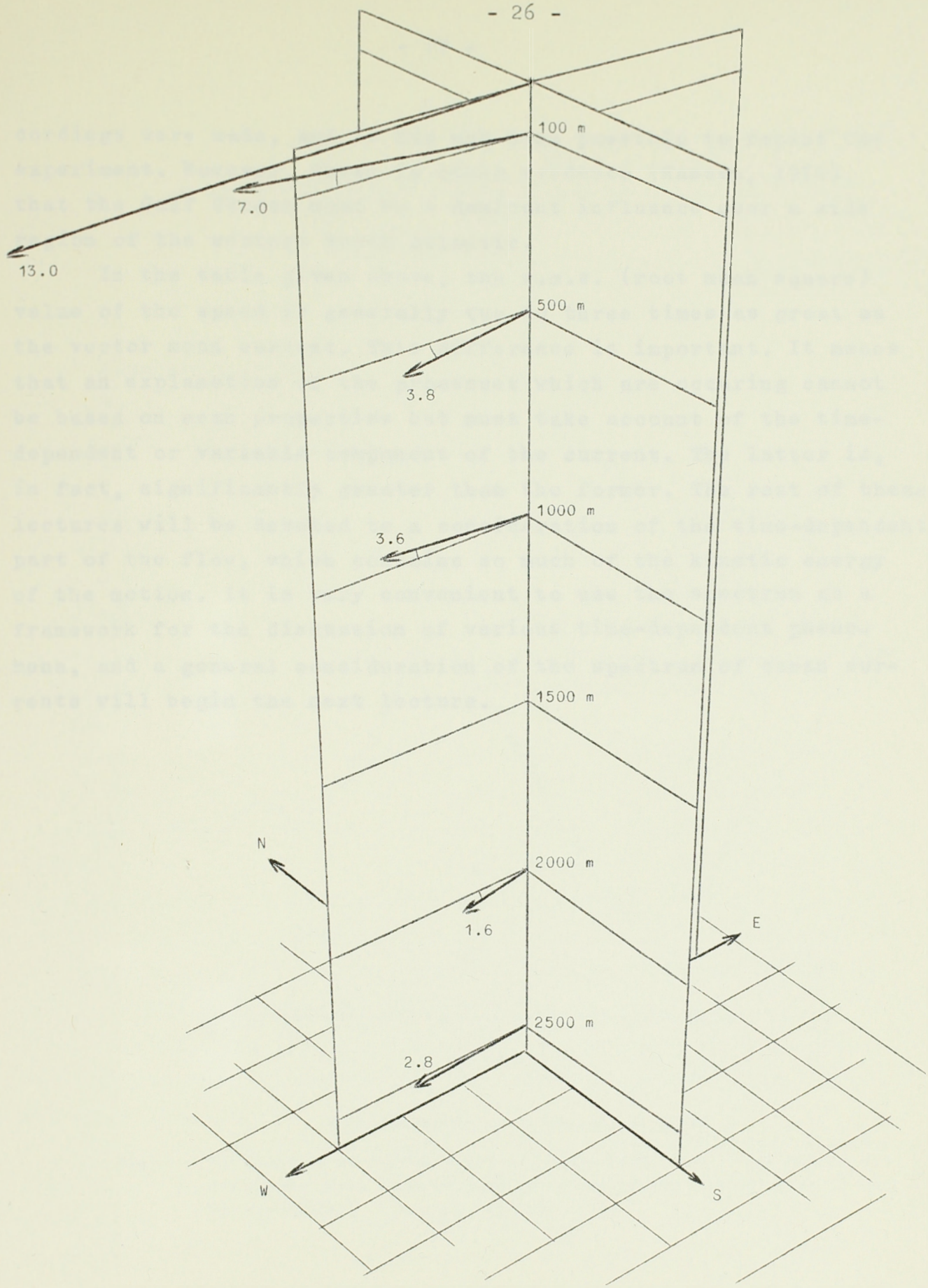

MEAN VELOCITY VECTORS AT SITE D

Fig. 2.- The profile of mean currents at Site D. Note that the currents decrease with depth but increase near the bottom.

cordings were made, and it has not been possible to repeat the experiment. However, there is other evidence (Hansen, 1970) that the Gulf Stream must be a dominant influence over a wide region of the western North Atlantic.

In the table given above, the r.m.s. (root mean square) value of the speed is generally two to three times as great as the vector mean current. This difference is important. It means that an explanation of the processes which are occuring cannot be based on mean properties but must take account of the time-dependent or variable component of the current. The latter is, in fact, significantly greater than the former. The rest of these lectures will be devoted to a consideration of the time-dependent part of the flow, which contains so much of the kinetic energy of the motion. It is very convenient to use the spectrum as a framework for the discussion of various time-dependent phenomena, and a general consideration of the spectrum of ocean currents will begin the next lecture.

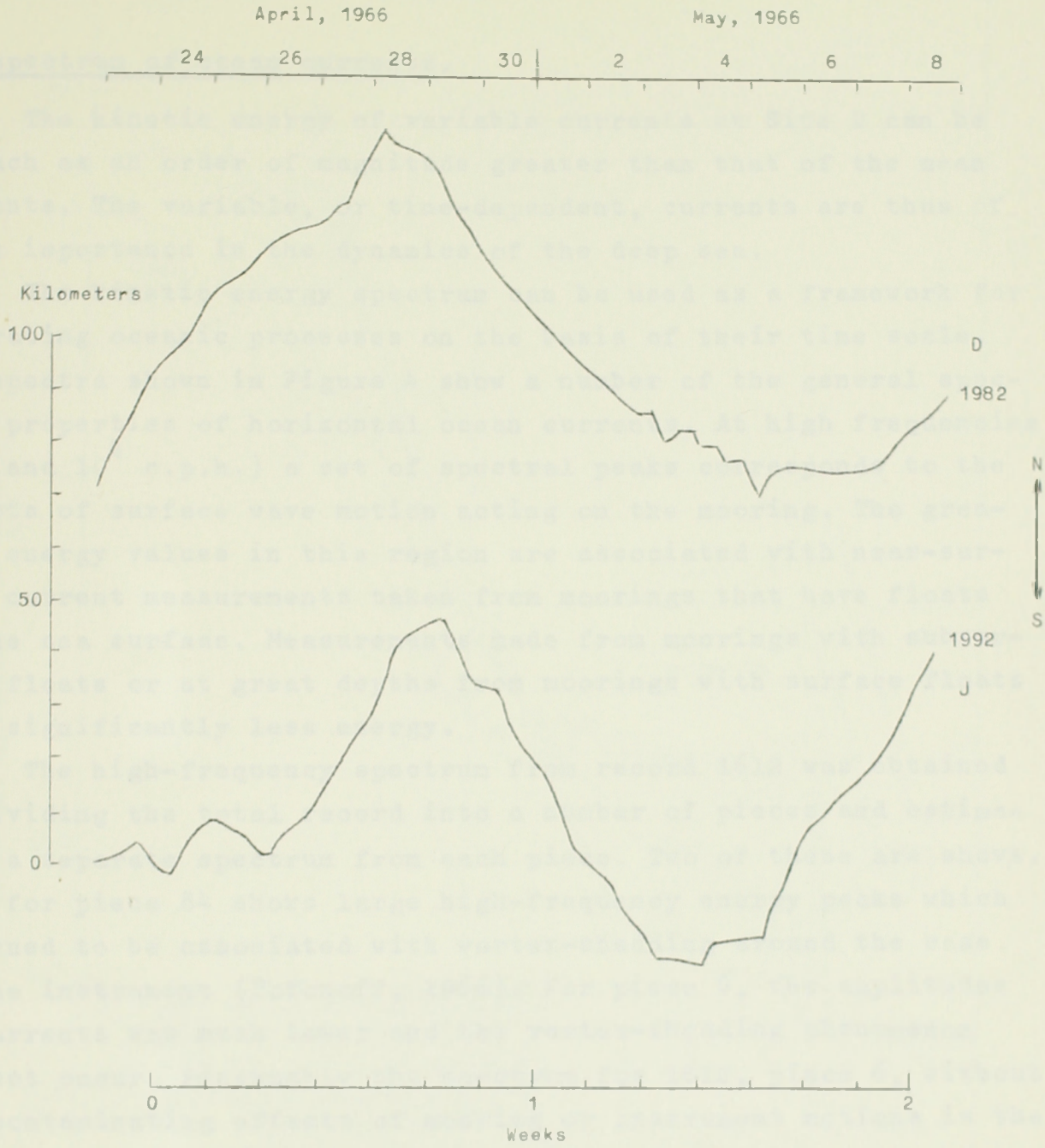

N-S EXCURSIONS OF INTEGRATED VELOCITY

Fig. 3.- Simultaneous current measurements from either side of the Gulf Stream. The curves shown were obtained by computing the time integral of the North-component of velocity at each time.

II.-VARIABILITY OF OCEAN CURRENTS

The spectrum of ocean currents.

The kinetic energy of variable currents at Site D can be as much as an order of magnitude greater than that of the mean currents. The variable, or time-dependent, currents are thus of great importance in the dynamics of the deep sea.

The kinetic energy spectrum can be used as a framework for separating oceanic processes on the basis of their time scale. The spectra shown in Figure 4 show a number of the general spectral properties of horizontal ocean currents. At high frequencies (10^2 and 10^4 c.p.h.) a set of spectral peaks corresponds to the effects of surface wave motion acting on the mooring. The greatest energy values in this region are associated with near-surface current measurements taken from moorings that have floats on the sea surface. Measurements made from moorings with subsurface floats or at great depths from moorings with surface floats show significantly less energy.

The high-frequency spectrum from record 1612 was obtained by dividing the total record into a number of pieces and estimating a separate spectrum from each piece. Two of these are shown. That for piece 84 shows large high-frequency energy peaks which happened to be associated with vortex-shedding around the case of the instrument (Fofonoff, 1966). For piece 6, the amplitudes of currents was much lower and the vortex-shedding phenomenon did not occur. Presumably the spectrum for 1612, piece 6, without the contaminating effects of mooring or instrument motions is the closest representation of the true high-frequency spectrum of horizontal currents.

For frequencies of about 10^{-1} c.p.h. and higher, the kinetic energy may drop proportional to $f^{-5/3}$. (A straight line with a slope of $-5/3$ on log-log graph paper). The similarity between this slope and that of homogeneous isotropic turbulence as postulated by Kolmogorov suggests that it might be fruitful to treat

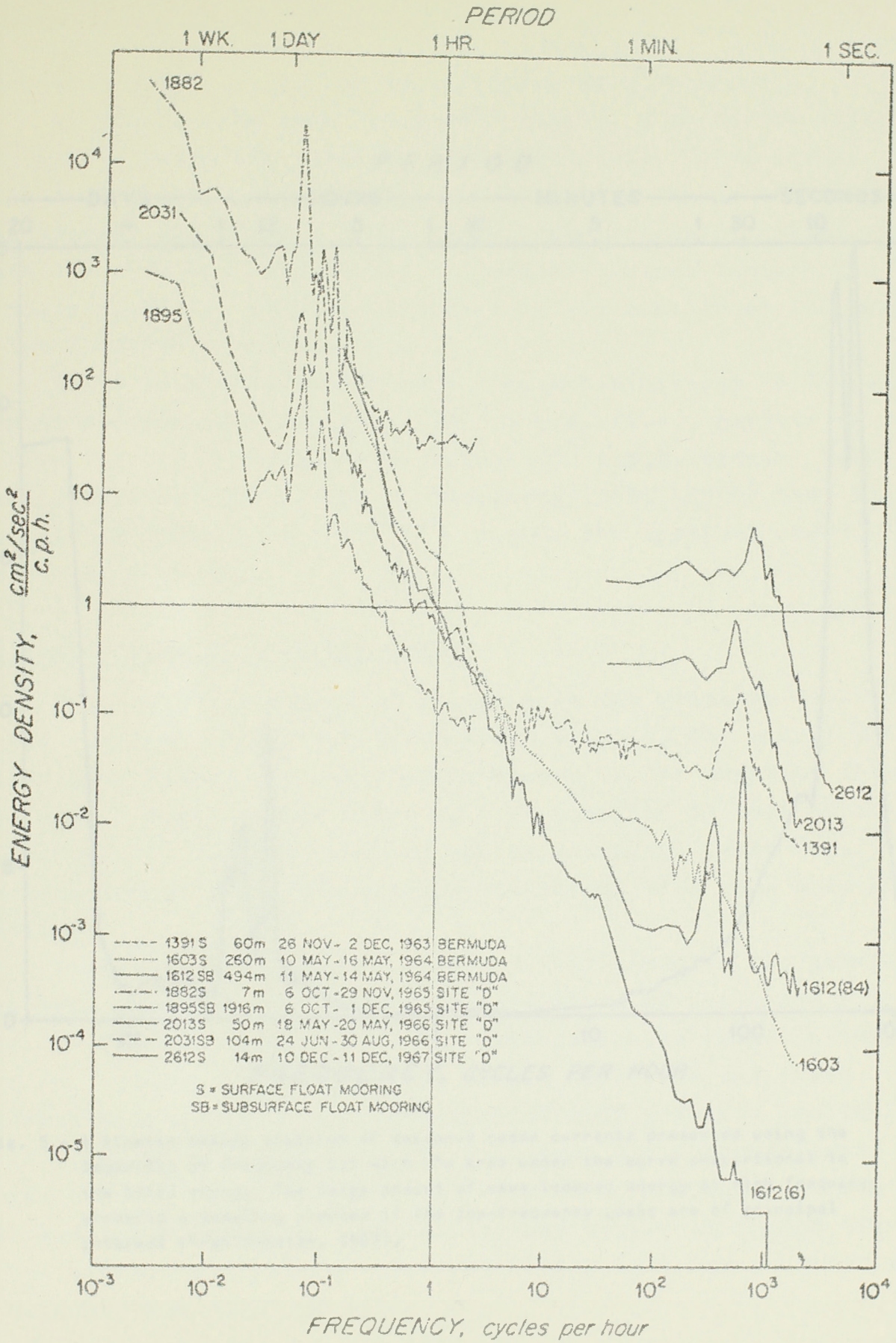

Fig. 4.- Examples of horizontal energy spectra of ocean currents collected under a variety of conditions (from Fofonoff, 1968b).

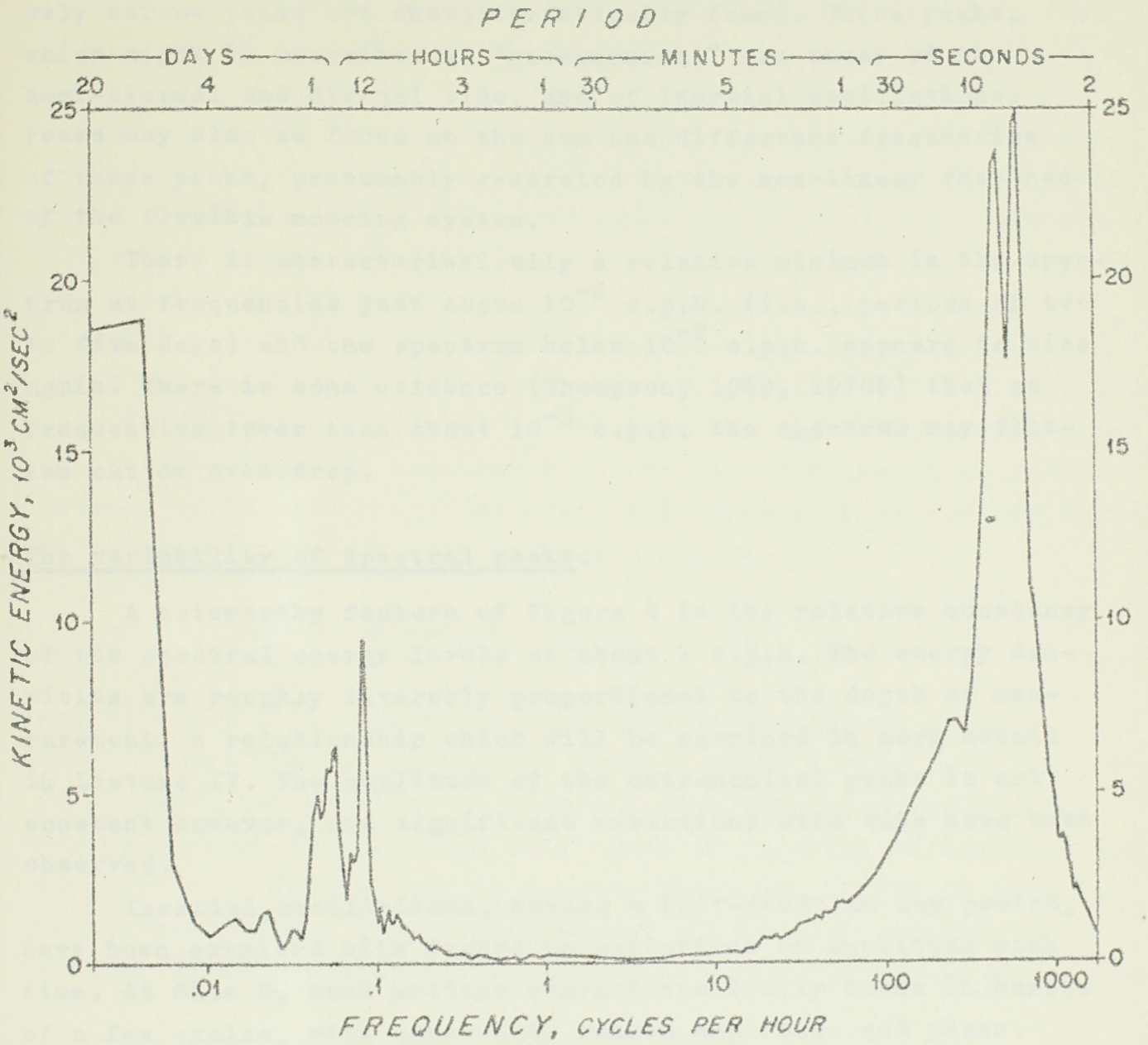

Fig. 5.- A kinetic energy spectrum of measured ocean currents presented using the logarithm of frequency but with the area under the curve proportional to the total energy. The large amount of wave-induced energy at high frequency presents a sampling problem if the low-frequency peaks are of principal interest (from Webster, 1967).

processes in this region of the spectrum as turbulence.

At frequencies just below 10^{-1} c.p.h., a number of relatively narrow peaks are characteristically found. These peaks, which might be described as "astronomical" are those of the semi-diurnal and diurnal tide, and of inertial oscillations. Peaks may also be found at the sum and difference frequencies of these peaks, presumably generated by the non-linear response of the flexible mooring system.

There is characteristically a relative minimum in the spectrum at frequencies just above 10^{-2} c.p.h. (i.e., periods of two to five days) and the spectrum below 10^{-2} c.p.h. appears to rise again. There is some evidence (Thompson, 1969, 1970b) that at frequencies lower than about 10^{-3} c.p.h. the spectrum may flatten out or even drop.

The variability of spectral peaks.

A noteworthy feature of Figure 4 is the relative constancy of the spectral energy levels at about 1 c.p.h. The energy densities are roughly inversely proportional to the depth of measurement, a relationship which will be examined in more detail in Lecture IV. The amplitude of the astronomical peaks is not constant however, and significant variations with time have been observed.

Inertial oscillations, having a half-pendulum day period, have been examined with regard to variations of amplitude with time. At Site D, such motions characteristically occur in bursts of a few cycles, with apparently random amplitude and phase. Treating motions of this kind quantitatively presents problems, since from one point of view the processes are not stationary. It may be more accurate to regard them as non-Gaussian in that both tides and inertial oscillations may appear at random times in the manner of a Poisson process. Little work has yet been done to explore this point of view.

For describing time-varying quasi-periodic processes, the method of complex demodulation (Tukey, 1961, Granger and Hatanaka, 1964, Perkins, 1970), has proven effective. With this method, a frequency band of interest is shifted to zero frequency, and the result is run through a low-pass filter. The resultant complex-valued series gives the phase and amplitude of the frequency of interest. If one chooses the local inertial frequency at latitude Φ (sin Φ /12 hours) as the frequency for complex demodulation, time variations in amplitude and phase can be detected. More importantly, departures from local inertial frequency can easily be detected by the existence of slow systematic phase change.

It would be of inteterest to measure the generation and decay times associated with each burst of inertial or tidal motions. This is extremely difficult in practice. To separate such motions of other time scales requires a record having a length of several periods of the motion of interest. The "frequency window" through which complex demodulation defines a signal is

$$W(f) = \frac{\sin \omega T/2}{\omega T/2} \quad \text{where } \omega = 2\pi f$$

and T is the time over which each complex demodulate estimate is made. Such a window can only be sharply tuned for large T. However, it is often not possible to obtain enough data to provide sharp tuning because the duration of a burst of inertial or tidal energy may only be a few periods in length. Since the length of data needed to resolve the motions may exceed the natural lifetime of the motion, it is often impossible to resolve generation and decay times.

Coherence of currents over spatial separations.

The spatial variability of ocean currents is more difficult to measure than time variability. It is relatively easy to collect a time series of measurements at a fixed point. The corresponding

problem of collecting a spatial series at a fixed time is extremely difficult in the deep sea and has not yet been accomplished on an extensive scale.

In order to explore spatial variability the coherence between simultaneous time series at a pair of points is often used. By such means an elementary picture of the extent of spatial coherent motions can be built up. However, the ultimate results fall short of the information which a full spatial spectrum might provide.

For a pair of vector time series, such as a pair of current meter records, the full description of the cross spectrum between them must take account of each combination of component pairs. The full specification of a complete cross-spectrum between two vector series can be expressed as a 16-term matrix (Webster, 1968a). An alternative formulation, in which the cross-spectrum is expressed as the sum of two counter-rotating components has been used by Mooers (1969), and is particularly well suited for treating rotating phenomena such as inertial oscillations.

At low frequencies, there can be apparent coherence over several thousand meters vertically and many kilometers horizontally (Webster, 1969a) and Figure 6 shows a set of progressive vector diagrams showing vertical coherence between 500 m. and 2000 m. at Site D.

A simple experiment examining the horizontal and vertical coherence of currents at inertial frequency is summarized in Figure 7 (Webster, 1968a). These results were interpreted as showing a generally low vertical coherence as contrasted with a relatively high horizontal coherence for inertial motions. Later investigations, for example by Schott, have shown that factors such as stratification and water depth can be important in controlling the scales of coherence, and that caution must be exercised in interpreting the results from Site D generally.

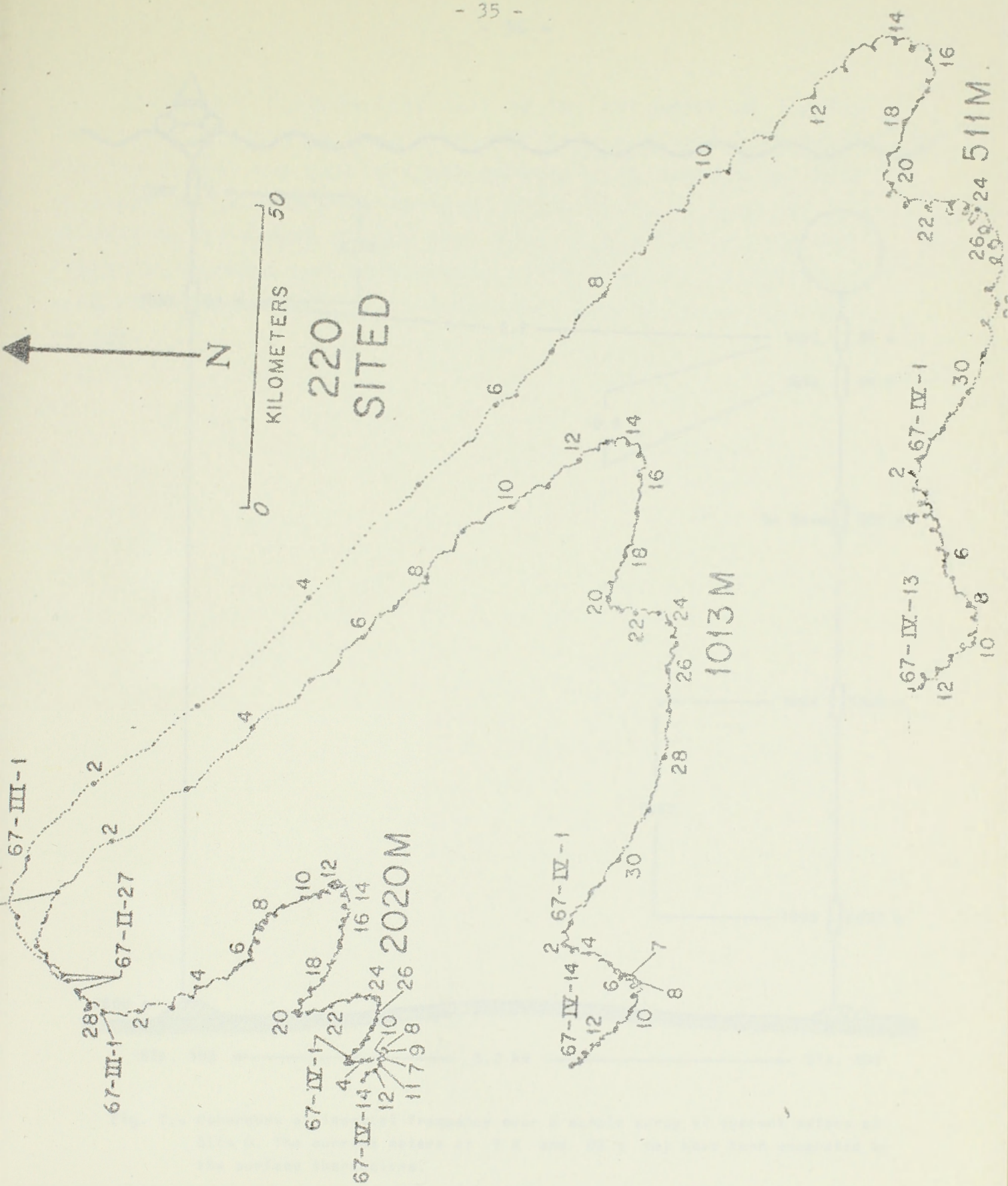

Fig. 6.- Progressive vector diagrams for simultaneous current measurements at nominal depths of 100, 500, 1000 and 2000 m depth. The near-surface observations are apparently not coherent with those at depth, but there is an obvious coherence in low-frequency motions between 500 and 2000 m (from Webster, 1968b).

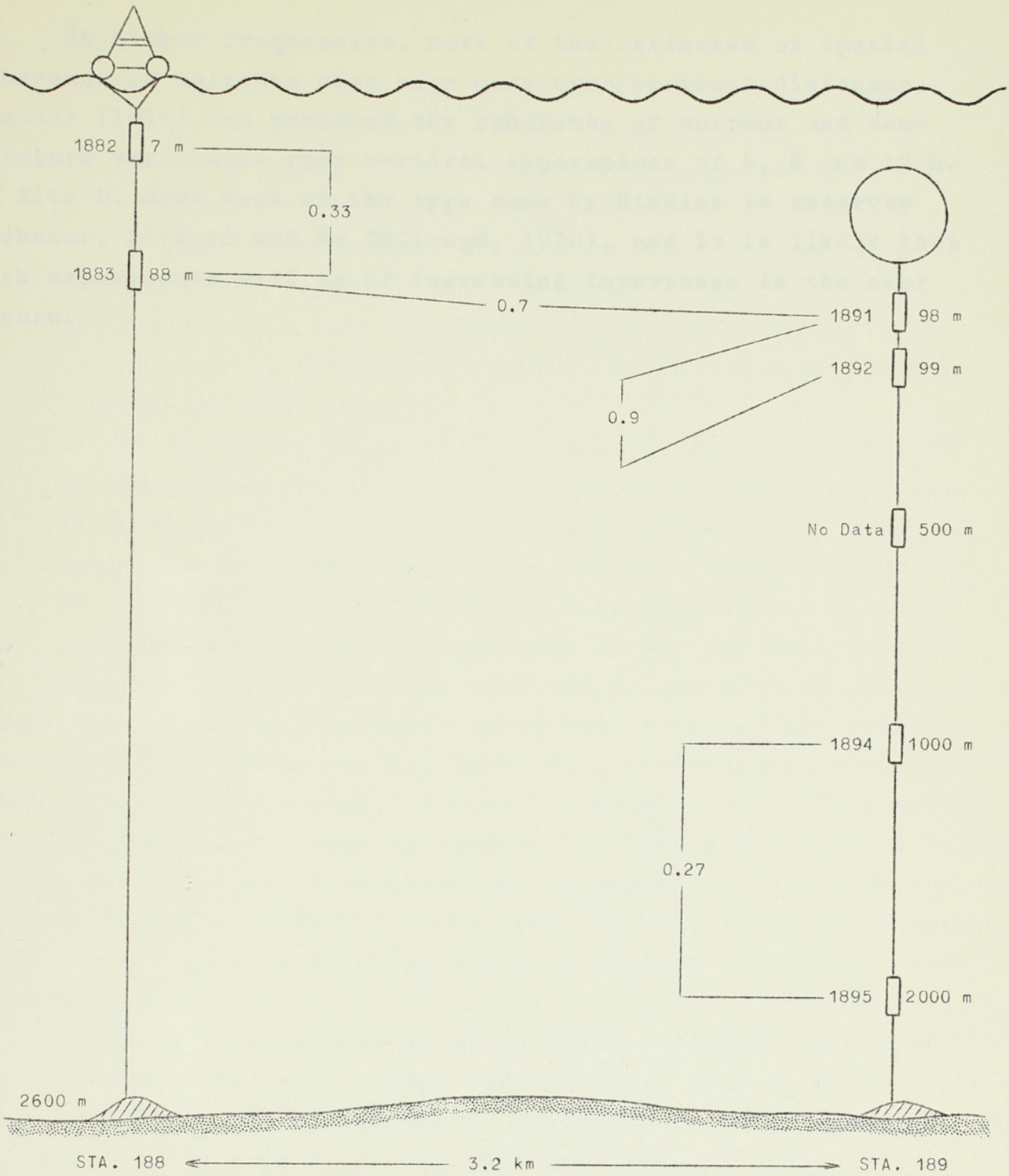

Fig. 7.- Coherence at inertial frequency over a simple array of current meters at Site D. The current meters at 7 m and 88 m may have been separated by the surface thermocline.

At higher frequencies, most of the estimates of spatial coherence of currents have been made over vertical distances. Siedler (1970) has examined the coherence of current and temperature variations over vertical separations of 4, 8 and 12 m. at Site D. More work of the type done by Siedler is underway (Webster, Rickard and Mc Cullough, 1970), and it is likely that such experiments will be of increasing importance in the near future.

III.-INERTIAL MOTIONS

. Inertial oscillations are found in direct ocean currents wherever current measurements are made systematically over an extended period of time. Figure 8 shows an example of currents at Site D showing intermittently strong inertial oscillations. A review of their occurence in oceans, enclosed seas and lakes was made by Webster (1968a). Since the date of that paper, abundant new observations have been made over a wide range of oceanic conditions with both direct and indirect current measuring techniques (Rooth and Düing, 1970).

An intriguing property of inertial oscillations, which is particularly well marked at Site D, is their intermittence. For the data shown in Figure 8, the amplitude determined by complex demodulation is shown in Figure 9. It has been suggested (Saelen, 1963; Day and Webster, 1965) that the intermittence is due to their generation by winds. The question of the generation mechanism has recently been examined from two points of view. Pollard (1970) and Pollard and Millard (1970) have modelled the response of a homogeneous Ekman surface layer to a time-varying wind stress. Their results, even though not exact in detail, are sufficiently realistic for major events to suggest that the model must be relevant to surface-layer intermittency. An example of computed and observed currents at Site D, using their model, is shown in Figure 10. Recent work by Gonella, reported at this colloquium, supports this view.

Inertial oscillations at great depth also show an intermittent character. So far no model has explained either their intermittent character or the mechanism of energy transfer into the deep sea. It has been suggested that inertial oscillations are the manifestation of globally generated waves which are amplified at their critical or turning latitude (Blandford, 1966). In such a process, it would be expected that energy should be propagated along known ray paths. This possibility has recently been investigated by Perkins (1970).

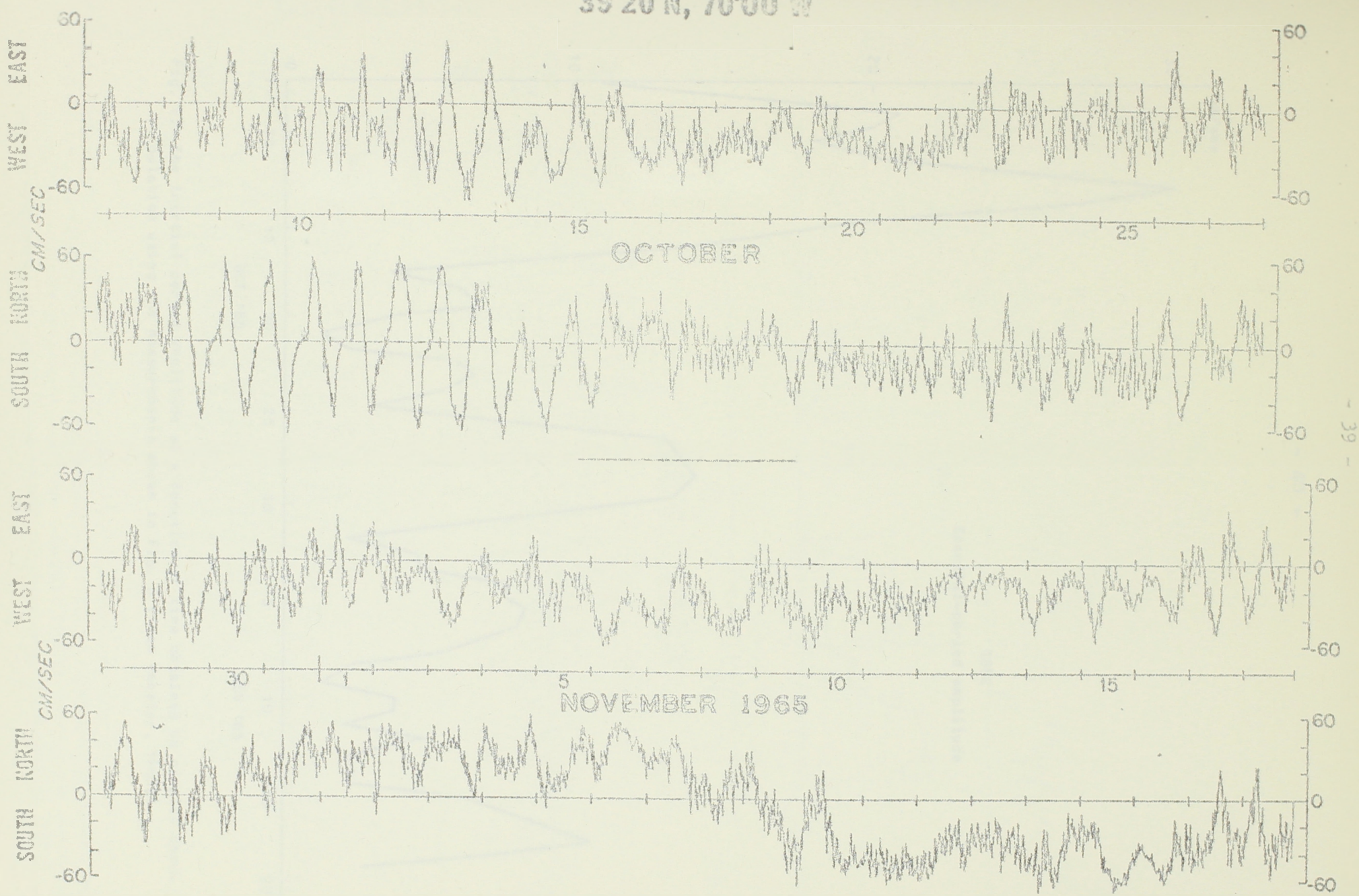

Fig. 8.- An example of currents measured at a depth of 7 m at Site D (1882). The first several days show large-amplitude inertial oscillations. Note the intermittency of occurrence of inertial oscillations (from Webster, 1968a).

Fig. 9.- The inertial period amplitude as a function of time obtained by complex demodulation using the measurements shown in Fig. 8 (from Webster, 1968a).

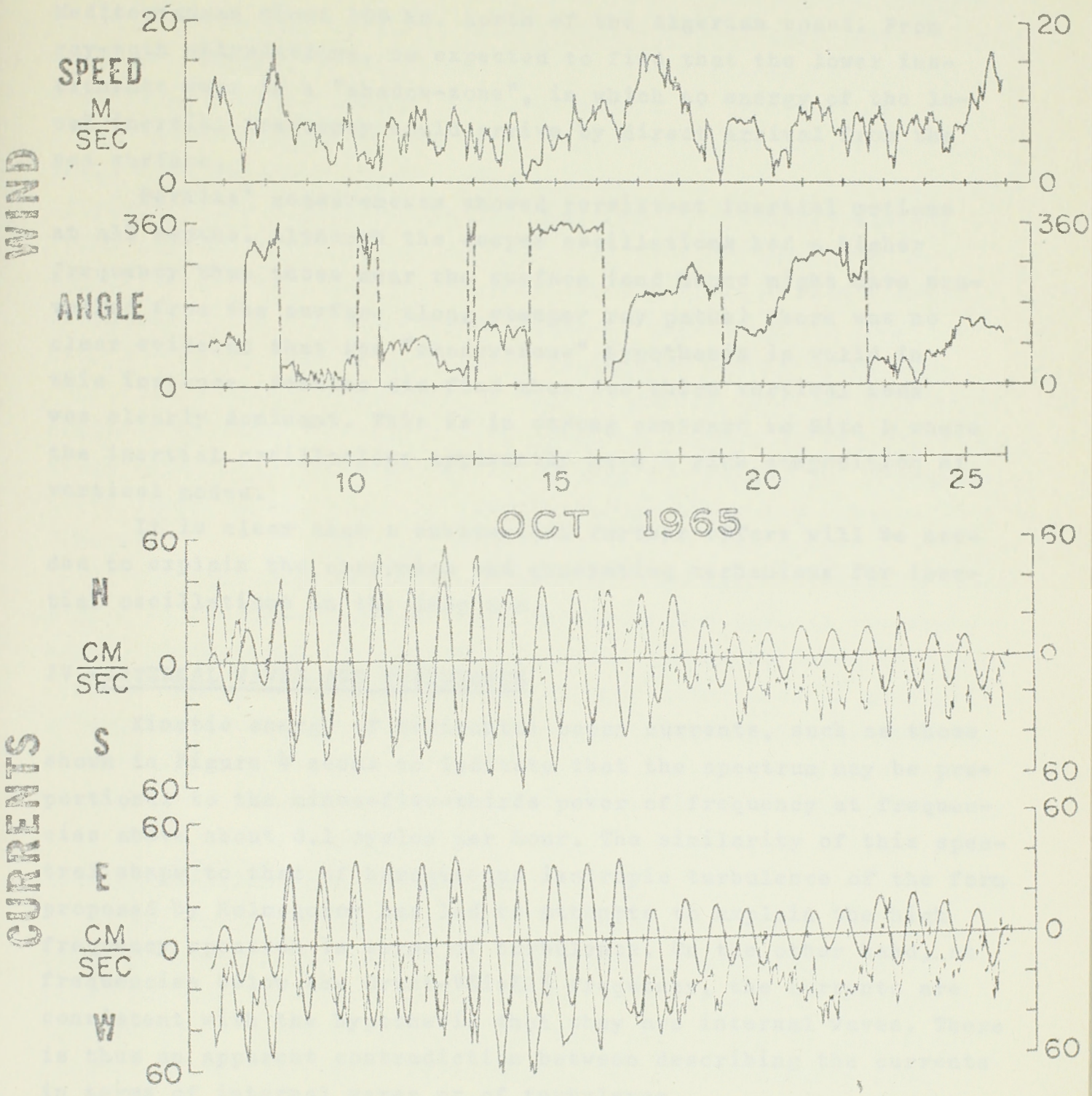

Fig. 10.- The data of figure 8 modelled using Pollard and Millard's model with eight-day damping. In the lower part of the figure, the light irregular line is the observed current and the heavy smoother line is the computed current (from Pollard and Millard, 1970).

Perkins collected two-month-long simultaneous current measurements at depths of 200, 700, 1200, 1700 and 2200 m. in the Mediterranean about 100 km. north of the Algerian coast. From ray-path calculations, he expected to find that the lower instruments were in a "shadow-zone", in which no energy of the local inertial frequency could arrive by direct arrival from the sea surface.

Perkins' measurements showed persistent inertial motions at all depths. Although the deeper oscillations had a higher frequency than those near the surface (and hence might have travelled from the surface along steeper ray paths) there was no clear evidence that the "shadow-zone" hypothesis is valid in this instance. Perkins did find that the third vertical mode was clearly dominant. This is in strong contrast to Site D where the inertial oscillations apparently have a rich composition of vertical modes.

It is clear that a substantial further effort will be needed to explain the occurence and generating mechanisms for inertial oscillations in the deep sea.

IV.-INTERNAL WAVES AND TURBULENCE

Kinetic energy of horizontal ocean currents, such as those shown in Figure 4 seems to indicate that the spectrum may be proportional to the minus-five-thirds power of frequency at frequencies above about 0.1 cycles per hour. The similarity of this spectral shape to that of homogeneous isotropic turbulence of the form proposed by Kolmogorov has led to attempts to explain the high frequency spectrum in terms of turbulence. On the other hand, at frequencies below the Brunt-Väisälä frequency, the currents are consistent with the hypothesis that they are internal waves. There is thus an apparent contradiction between describing the currents in terms of internal waves or of turbulence.

Vertical profiles.

Vertical profiles of horizontal kinetic energy are proportional to vertical profiles of the Brunt-Väisälä frequency (Webster, 1969b). A comparison between the vertical profile of horizontal kinetic energy, shown in Figure 11 with that of Brunt-Väisälä frequency, shown in Figure 12 shows this relationship. (The straight lines having a slope of $z^{-0.7}$ on both are arbitrary). Such a result might be expected for wavelike motions (Munk and Phillips, 1968). On the other hand, recent work by Rooth (unpublished so far) suggests that a similar result would be obtained for either internal waves or turbulence if conservation of energy flux is maintained throughout the water column.

The relative constancy of kinetic energy level at any given depth is striking in view of the large variations in surface winds which presumably are a principal driving mechanism. The mechanism which controls the level of kinetic energy has not yet been discovered.

The time-dependent motion at Site D is not horizontally isotropic at frequencies lower than one cycle per day. In the surface layer, north-south (V) components have a larger variance than east-west (u) components ; at mid-depths, the u-variance is greater ; at greater depths the variances are approximately equal. This pattern may be due to the interaction of low-frequency processes with the continental shelf, which is about 50 km. north of Site D.

Homogeneous isotropic turbulence.

The interpretation of the $f^{-5/3}$ region of the spectrum in terms of homogeneous isotropic turbulence is unsatisfactory. Below the Brunt-Väisälä frequency, the stratification imposes a constraint on vertical movement so that the motion is not three-dimensionally isotropic. Furthermore, the transformation from wavenumber, in which Kolmogorov's hypothesis is stated, to frequency in which the observed spectra are expressed, is only possible if there is a large mean advecting velocity past the point

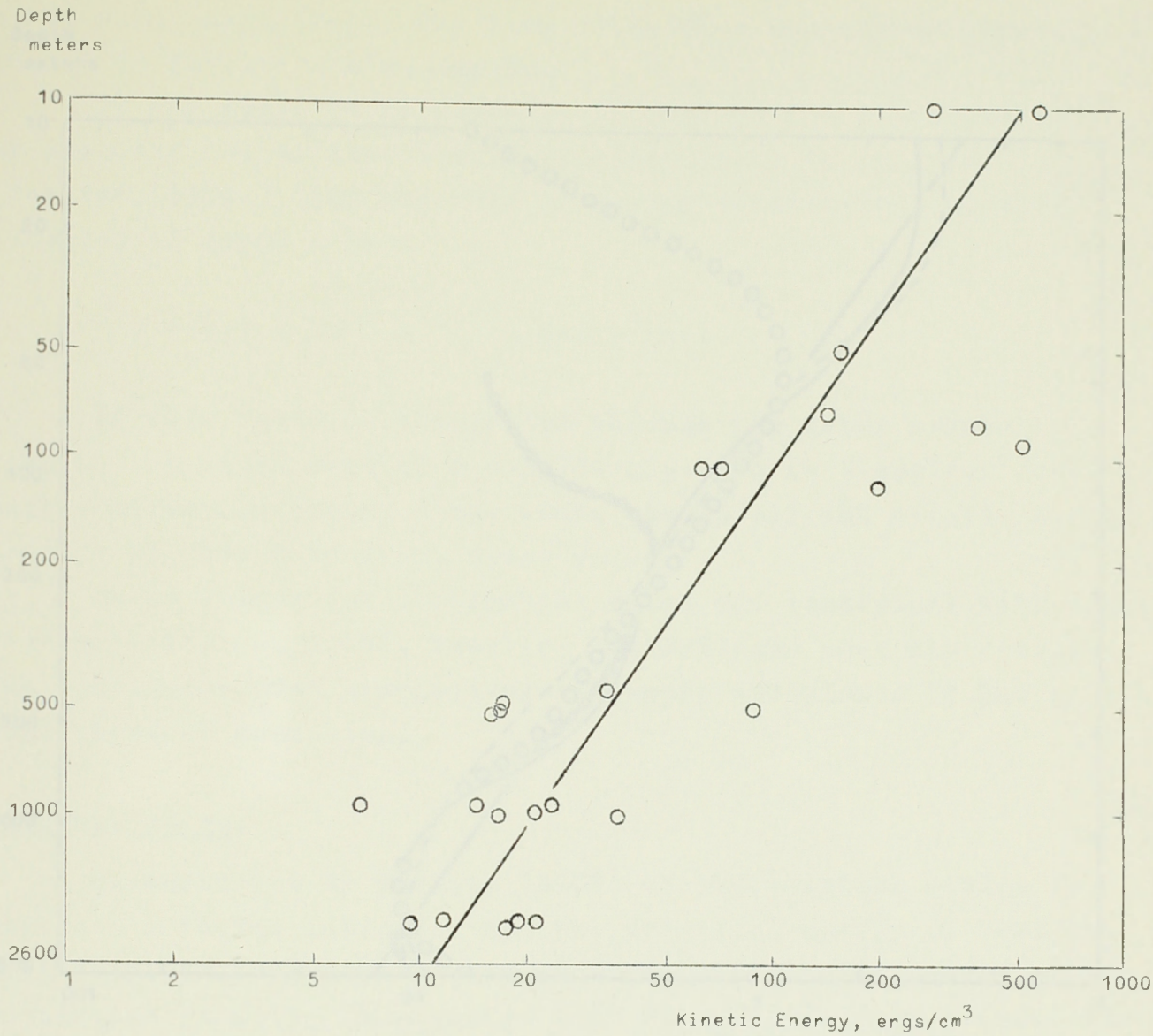

Fig. 11.- Measurements of horizontal kinetic energy vs. depth at Site D. Each point is the average obtained from one current meter record, usually from 6 to 8 weeks duration. The line fitted through the points is proportional to $Z^{-0.7}$ (from Webster, 1969b).

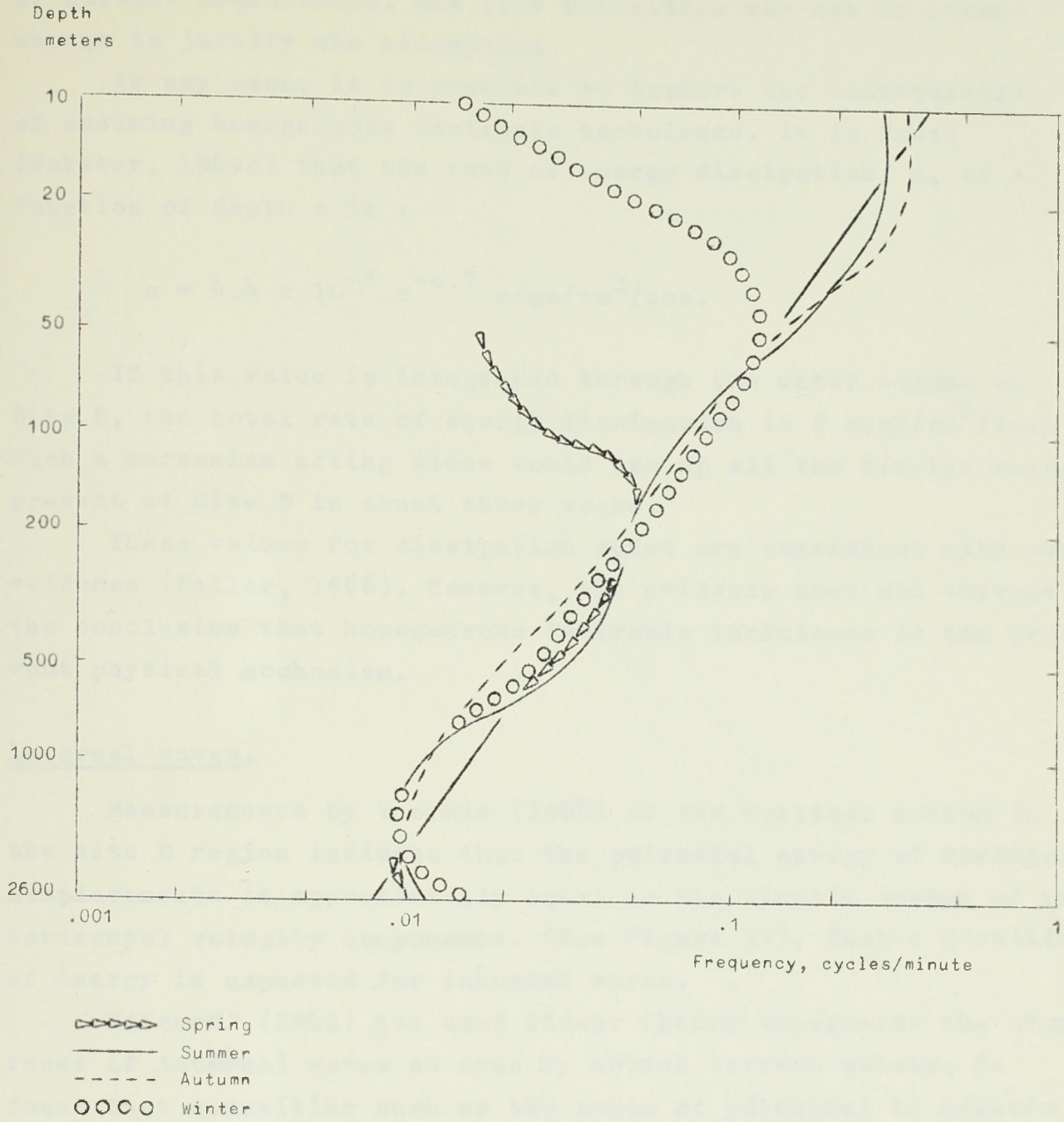

Fig. 12.- Profiles of the Brunt-Vaisala frequency at Site D at four seasons. A line proportional to $Z^{-0.7}$ has been drawn across the figure (from Webster, 1969b).

of current measurement. The true velocities may not be large enough to justify the assumption.

In any case, it is possible to explore the consequences of assuming homogeneous isotropic turbulence. It is found (Webster, 1969c) that the rate of energy dissipation, e, as a function of depth z is :

$$e = 4.4 \times 10^{-2} z^{-0.7} \text{ ergs/cm}^3\text{/sec.}$$

If this value is integrated through the water column at Site D, the total rate of energy dissipation is 5 ergs/cm^2/sec. Such a mechanism acting alone would use up all the kinetic energy present at Site D in about three weeks.

These values for dissipation rates are consistent with other evidence (Faller, 1966). However, the evidence does not warrant the conclusion that homogeneous isotropic turbulence is the relevant physical mechanism.

Internal waves.

Measurements by Voorhis (1968) of the vertical motion in the site D region indicate that the potential energy of vertical displacements is approximately equal to the kinetic energy of the horizontal velocity components. (See Figure 13). Such a partition of energy is expected for internal waves.

Fofonoff (1969) has used linear theory to examine the occurence of internal waves as seen by moored current meters. He found that quantities such as the ratio of potential to kinetic energy and the coherence between velocity components do not involve amplitudes explicitly and can be compared with similar ratios computed from observations. On the basis of measured temperature and current fluctuations Fofonoff concluded that the observed spectra between inertial and Brunt-Väisälä frequencies are

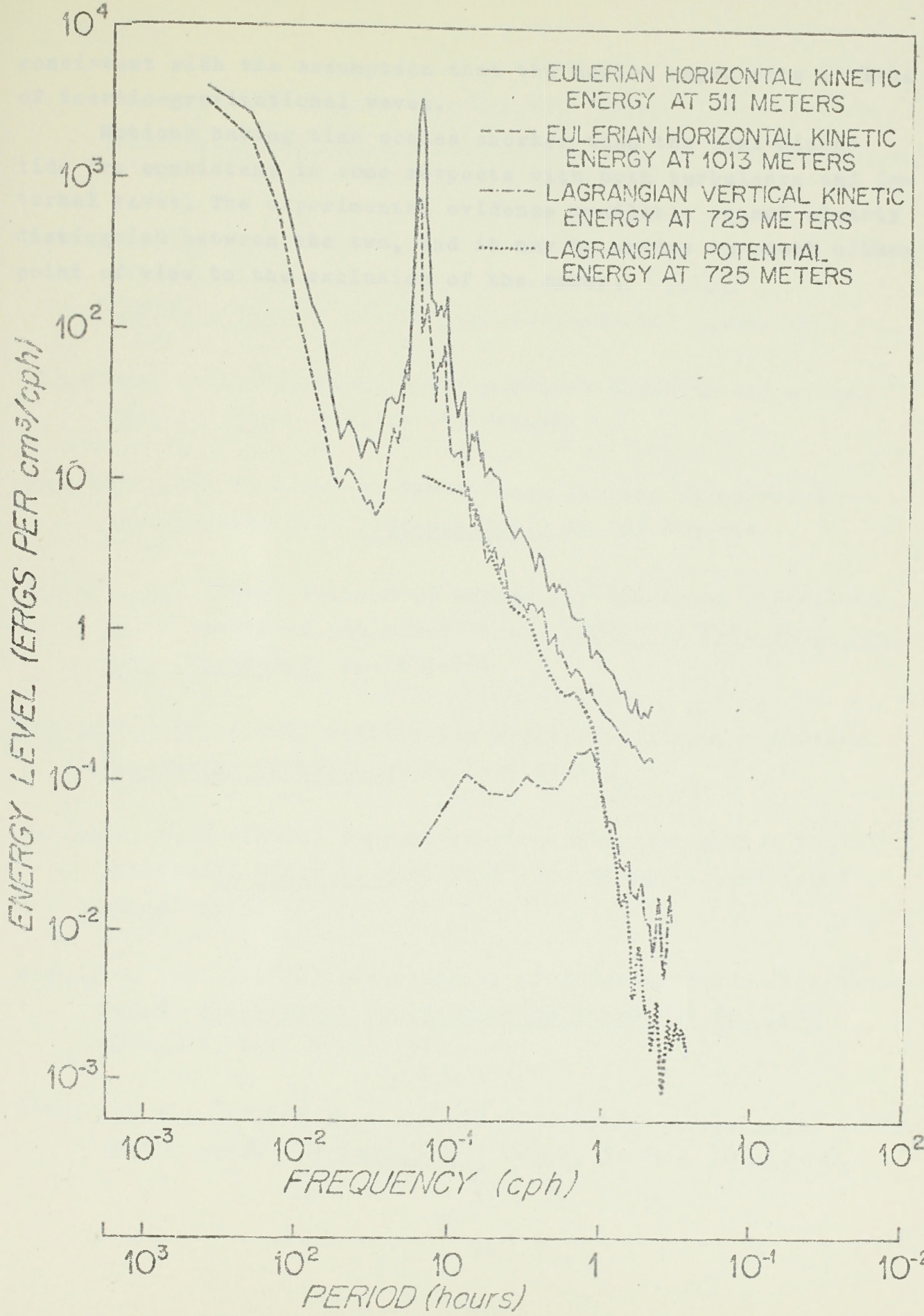

Fig. 13.- Spectra of horizontal and vertical kinetic energy and of vertical potential energy. Over the range of frequencies from the inertial frequency to the Brunt-Väisälä frequency, there is an approximate equipartition of energy (from Voorhis, 1968).

consistent with the assumption that the motion represents a field of inertio-gravitational waves.

Motions having time scales shorter than the semi-diurnal tide are consistent in some respects with both turbulence and internal waves. The experimental evidence available cannot clearly distinguish between the two, and it may be unwise to adopt either point of view to the exclusion of the other.

REFERENCES

Berteaux, H.O. (1968) Surface moorings, review of performance. W.H.O.I. (Woods Hole Oceanographic Institution) Reference N° 68-20, 41 pp. (Unpublished manuscript).

Berteaux, H.O., and R.G. Walden. (1969) Analysis and experimental evaluation of single point moored buoy systems. W.H.O.I. Ref. 69-36, 100 pp. (Unpublished manuscript).

Blandford, R. (1966) Mixed gravity-Rossby waves in the ocean. Deep-Sea Res., Vol. 13 (5) 941-961.

Day, C.G., and F. Webster. (1965) Some current measurements in the Sargasso Sea. Deep-Sea Res., 12 (6) 805-814.

Faller, A.J. (1966) Sources of energy for the ocean circulation and a theory of the mixed layer. Proc. 5th U.S. Natl. Cong. Appl. Mechanics, pp. 651-669.

Fofonoff, N.P. (1966) Oscillation modes of a deep-sea mooring. Geo-Marine Technology, 2, (9), 13-17.

Fofonoff, N.P. (1968a) Current measurements from moored buoys 1959-1965. W.H.O.I. Ref. N° 68-30, 36 pp. (Unpublished manuscript).

Fofonoff, N.P. (1968b) Measurements of internal waves from moored buoys. Geophysical Fluid Dynamics Course Notes, 1968. (W.H.O.I. Ref. N° 68-72).

Fofonoff, N.P. (1969) Spectral characteristics of internal waves in the ocean. Deep-Sea Res., Suppl. to Vol. 16, 59-71.

Fofonoff, N.P., and Y. Ercan. (1967) Response characteristics of a Savonius rotor current meter. W.H.O.I. Ref.N° 67-33, 46 pp. (Unpublished manuscript).

Granger, C.W.J., and Hatanaka. (1964) Spectral analysis of economic time series.-299 pp., Princeton Univ. Press, Princeton, N.J.

Hansen, D.V. (1970) Correlation of movements in the Western North Atlantic. (in preparation, ESSA Laboratory, Miami, Florida).

Maltais, J.A. (1969) A nine channel digital magnetic tape format for storing oceanographic data. W.H.O.I. Ref. N° 69-55, 13 pp. (Unpublished manuscript).

Millard, R.C. Jr. (1968) Wind measurements from buoys : a sampling scheme. W.H.O.I. Ref. N° 68-68, 34 pp. (Unpublished manuscript).

Millard, R.C. Jr. (1969) Observations of static and dynamic tension variation from surface moorings. W.H.O.I. Ref. N° 69-29, 43 pp. (Unpublished manuscript).

Moooers, C.N.K. (1969) The interaction of an internal tide with the frontal zone in a coastal upwelling region. Ph. D. Thesis, Oregon State Univ. 480 pp.

Munk, W., and N. Phillips. (1968) Coherence and band-structure of inertial motion in the sea. Rev. Geophys. Vol. 6 (4), 447-472.

Perkins, H.T. (1970) Inertial Oscillations in the Mediterranean. Ph. D. Thesis, Massachussetts Institute of Technology, and Woods Hole Oceanographic Institution.

Pollard, R.T. (1970) On the Generation by winds of inertial waves in the ocean. Deep-Sea Res., (in press).

Pollard, R.T., and R.C. Millard, Jr. (1970) Comparison between observed and simulated wind-generated inertial oscillations. Deep-Sea Res., (in press).

Richardson, W.S., P.B. Stimson, and C.H. Wilkins (1963). Current measurements from moored buoys. Deep-Sea Res. 10, (4), 369-388.

Rooth, C., and W. Düing. (1970) On the detection of "inertial" waves with pynocline followers. Scientific Report, ML 70006 Univ. of Miami, Rosenstiel School of marine and atmospheric sciences, 17 pp.

Saelen, O.H. (1963) Studies in the Norwegian Atlantic current. Geofys. Publikasjoner Norske Videnskaps-Akad., Oslo, Vol. 23, (6), 1-82.

Siedler, G. (1970) Vertical coherence of short-periodic current variations (in preparation).

Thompson, R. (1969) The search for topographic Rossby waves in the gappy current records at Site D. W.H.O.I. Ref. N° 69-67. (Unpublished manuscript)

Thompson, R. (1970b) Topographic Rossby waves at a site north of the Gulf Stream. (Submitted for publication).

Tukey, J.W. (1961) Discussion, emphasizing the connection between analysis of variance and spectrum analysis. Technometrics, 3, (2) 191-234.

Voorhis, A.D. (1968) Measurements of vertical motion and the partition of energy in the New England slope water. Deep-Sea Res., Vol. 15, (5), 599-608.

Webster, F. (1964) Some perils of measurement from moored ocean buoys. Trans., 1964 Buoy Tech. Symp., Marine Tech. Soc. Washington, D.C., pp. 33-48.

Webster, F. (1967) A scheme for sampling deep-sea currents from moored buoys. Trans., 2nd Int. Buoy Tech. Symp., Marine Tech. Soc., Washington, D.C. pp. 419-431.

Webster, F. (1968a) Observations of inertial-period motions in the deep sea. Rev. of Geophys., Vol. 6 (4) 473-490.

Webster, F. (1969a) On the representativeness of direct deep-sea current measurements. Progress in Oceanography, Vol. 5, M. Sears, ed. Pergamon Press, Oxford, pp. 3-15.

Webster, F. (1968b) Observations of time dependent currents. Geophysical Fluid Dynamics Course Notes, 1968, (W.H.O.I. Ref. 68-72).

Webster, F. (1969b) Vertical profiles of horizontal ocean currents. Deep-Sea Res., 16, (1), 85-98.

Webster, F. (1969c) Turbulence spectra in the ocean. Deep-Sea Res., Suppl. to Vol. 16, 357-368.

Webster, F., J.R. Rickard, and J.R. Mc Cullough (1970) Estimates of the coherence of ocean currents over vertical distances. W.H.O.I. Ref. (in preparation).

PROGRAMME DE RECHERCHE EN OCEANOGRAPHIE DYNAMIQUE A BORD DE LA BOUEE-LABORATOIRE*

Par J. Gonella

Laboratoire d'Océanographie Physique
Muséum National d'Histoire Naturelle
Paris Vème

SOMMAIRE

*Ce programme de recherche se poursuit avec le support du Centre National pour l'Exploitation des Océans (C.N.E.X.O.)

1ère Conférence

LE PROGRAMME ET LES MOYENS

Au cours de ce cycle de conférences, nous vous exposerons les grandes lignes du programme de recherche poursuivi en Océanographie Dynamique à bord de la Bouée-Laboratoire. Le premier exposé sera ensuite consacré au site d'expérimentation, la Méditerranée Occidentale Nord, et à l'engin-support des capteurs, la Bouée-Laboratoire. L'exposé suivant s'attachera davantage aux résultats théoriques et expérimentaux obtenus.

LES INTERACTIONS AIR-MER.

Si l'on excepte les forces gravitationnelles, l'essentiel de l'énergie responsable des mouvements fluides de notre planète provient du rayonnement solaire. Par une série de transformations et de rebonds entre l'air et l'eau, cette énergie est à l'origine de multiples phénomènes observés dans les océans : phénomènes d'ordre thermique comme la congélation, l'évaporation, la stratification thermique, ou phénomène d'ordre dynamique : vagues, courants, ondes internes... L'interface air-eau revêt une importance fondamentale car c'est à son niveau que se font les transformations et les transferts les plus importants. Les études poursuivies à bord de la Bouée-Laboratoire s'appuient essentiellement sur le thème de ces interactions océan-atmosphère. Le programme de travail s'attache plus particulièrement à l'étude des répercussions de ces interactions sur les caractéristiques physiques et sur les mouvements des masses d'eau.

LA MEDITERRANEE OCCIDENTALE : MODELE REDUIT D'OCEAN.

Il ne suffit pas de se fixer une orientation de recherche, encore faut-il choisir un champ d'expérimentation. Pour des raisons faciles à comprendre, l'étude de l'océan mondial ne peut

être entreprise raisonnablement sans moyens considérables. Une analyse des masses d'eau, appliquée à l'échelle du globe, montre que l'essentiel des eaux océaniques profondes résulte d'un mélange d'eaux formées dans deux régions seulement : l'Atlantique Nord, au Sud du Groenland, et le pourtour de l'Antarctide. Ces "sources" alimentent 75°/° des eaux des océans, plus d'un milliard de km^3 d'eau ! Cette proportion contraste avec l'exéguité relative des aires de ces sources qui sont de l'ordre de 2 à 3°/° seulement de la surface liquide. Ainsi transits et échanges d'énergie, à travers de surfaces d'étendue minime, retentissent sur les caractères des 3/4 du contenu océanique. Ces eaux profondes "respirent" sur l'atmosphère par les seuls petits "hublots" que sont leurs "sources". Mais la formation des eaux profondes n'est pas un privilège des océans et de telles "zones polaires" se rencontrent dans des mers à des latitudes beaucoup plus basses. Bien sûr, à ces latitudes, la congélation qui augmente la salinité des eaux de surface n'existe pas, mais l'évaporation y joue le même rôle. Tel est le cas de la Méditerranée qui est un bassin de "concentration" alimenté en eau atlantique (salinité 36°/°°) par le détroit de Gibraltar. La "constance du sel" dans le bassin est assurée par de la sortie d'eau méditerranéenne (salinité 38°/°°) sur le fond du détroit. A quel moment et où l'eau de surface plonge-t-elle pour boucler le circuit ?

Le Nord de la Méditerranée Occidentale est caractérisé en toute saison par une circulation marine cyclonique (fig. 1). Dans la région centrale, la stratification verticale de densité est, du fait de la rotation terrestre, moins stable que sur les bords.

Au début de l'hiver, après disparition de la thermocline superficielle, on peut y distinguer la présence de 3 couches :

- la couche superficielle d'eau froide toute récente et relativement douce ($T < 13°00$ et $S \simeq 38°/°°$);

CAMPAGNE HYDROLOGIQUE DE L' "ELIE MONNIER" EN MEDITERRANEE OCCIDENTALE

FEVRIER - MARS 1960

ISOPYCNES DE SURFACE

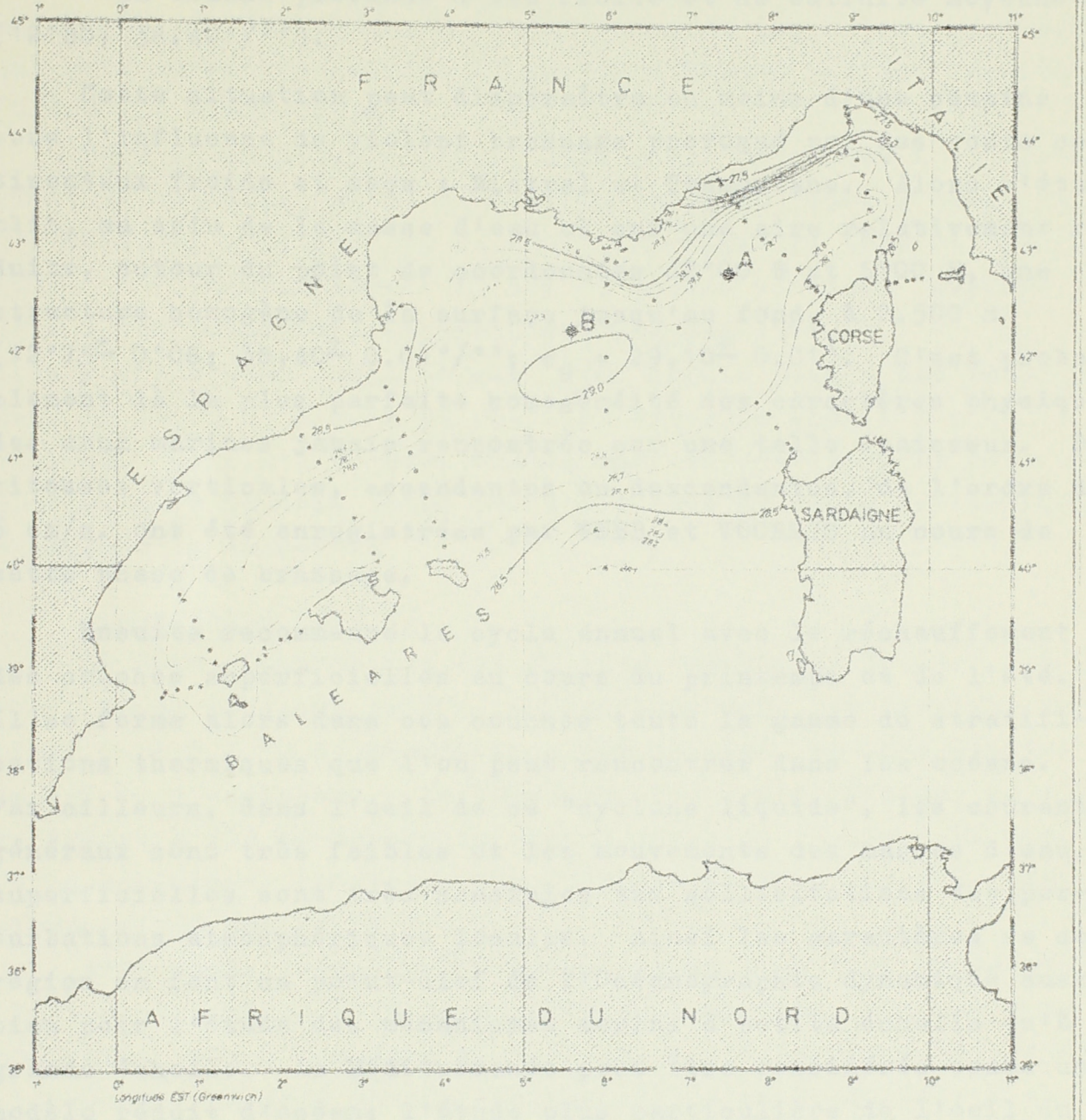

Fig: 1

- la couche intermédiaire d'eau chaude et salée provenant de la Méditerranée Orientale (maximum vers 500m : 13°40; 38.50°/°°);

- la couche profonde d'eau froide et de salinité moyenne (12°80; 38.40°/°°).

Cette situation peut disparaître en moins d'une semaine sous l'influence du violent brassage provoqué par des vents continentaux froids et secs : Mistral et Tramontane. Alors s'établit, au sein de la masse d'eau et sur une aire relativement réduite, autour du point de coordonnées 42°00 N et 5°00 E, une structure homogène de la surface jusqu'au fond, à 2.500 m ($12°75 \pm 0°08$; $38,40 \pm 0.01$°/°°; $\sigma_\theta = 29,10 \pm 0.01$). C'est probablement là la plus parfaite homogénéité des caractères physiques des eaux marines jamais rencontrée sur une telle épaisseur. Des vitesses verticales, ascendantes ou descendantes, de l'ordre de 6 cm/s. ont été enregistrées par WEBB et VOORHIS au cours de cette phase de brassage.

Ensuite recommence le cycle annuel avec le réchauffement des couches superficielles au cours du printemps et de l'été. Il se forme alors dans ces couches toute la gamme de stratifications thermiques que l'on peut rencontrer dans les océans. Par ailleurs, dans l'oeil de ce "cyclone liquide", les courants généraux sont très faibles et les mouvements des masses d'eau superficielles sont très sensibles aux sollicitations des perturbations atmosphériques locales. Ainsi les caractères de cette région en font un point-clef de l'Océanographie dynamique aussi bien pour l'étude des mécanismes marins à petite échelle qu'à grande échelle. La Méditerranée peut être considérée comme un modèle réduit d'océan; l'étude plus particulière de l'oeil du cyclone a motivé la construction et la mise en place de la Bouée-Laboratoire.

LA BOUEE-LABORATOIRE.

La Bouée-Laboratoire est une bouée habitée, construite sur l'initiative du Cdt. COUSTEAU avec le support financier du Gouvernement Français. Son fonctionnement est assuré actuellement par le Centre National pour l'Exploitation des Océans (C.N.E.X.O) qui en a confié la gestion au Centre d'Etudes Marines Avancées (C.E.M.A.) à Marseille.

Mise en chantier en 1962, elle a été remorquée à son premier point de mouillage entre Nice et la Corse en janvier 1964 (Point A : 42°47'N, 7°29'E). Un incendie détruisit la tête en février 1965. Fort heureusement, il n'y eu aucune victime. Réparée, elle a été replacée à la position A en mai 1966.
Elle y est restée jusqu'en mai 1968; depuis elle a été remorquée dans le Golfe du Lion à la position actuelle (point B : 42°14 N, 5°35 E). Elle n'a pu être placée dans le centre de la zone cyclonique; le mauvais temps qui s'est levé en cours de remorquage a empêché la manoeuvre.

Description (fig.2)

La Bouée-Laboratoire est du type "perche de Froude". Le tube, d'une longueur de 60m, cylindrique avec des sections variant de 1,8 à 3m de diamètre, a été réalisé en tôle d'acier de 1,5 cm d'épaisseur. La tête comporte trois niveaux; sa base se trouve à 10m au-dessus du niveau moyen de la mer. La plateforme supérieure constitue une terrasse de 10 m sur 6 m. Le tirant d'eau est de 50 m.

D'un poids total de 250 tonnes, elle a un lest solide de 110 tonnes environ à la base inférieure du tube. Le câble de mouillage, d'une longueur de 3.500 m, a été fabriqué tout spécialement d'un seul tenant (polypropylène en profondeur Ø 45mm; nylon en surface Ø 35mm). Le corps mort est une masse d'acier de 6 tonnes. Avec une profondeur de 2.500 m, cette longueur de mouillage confère à l'engin un cercle d'évitage de l'ordre de 5 km de diamètre.

Son grand tirant d'eau et son col mince lui assurent une

BOUEE LABORATOIRE

C. N. E. X. O.

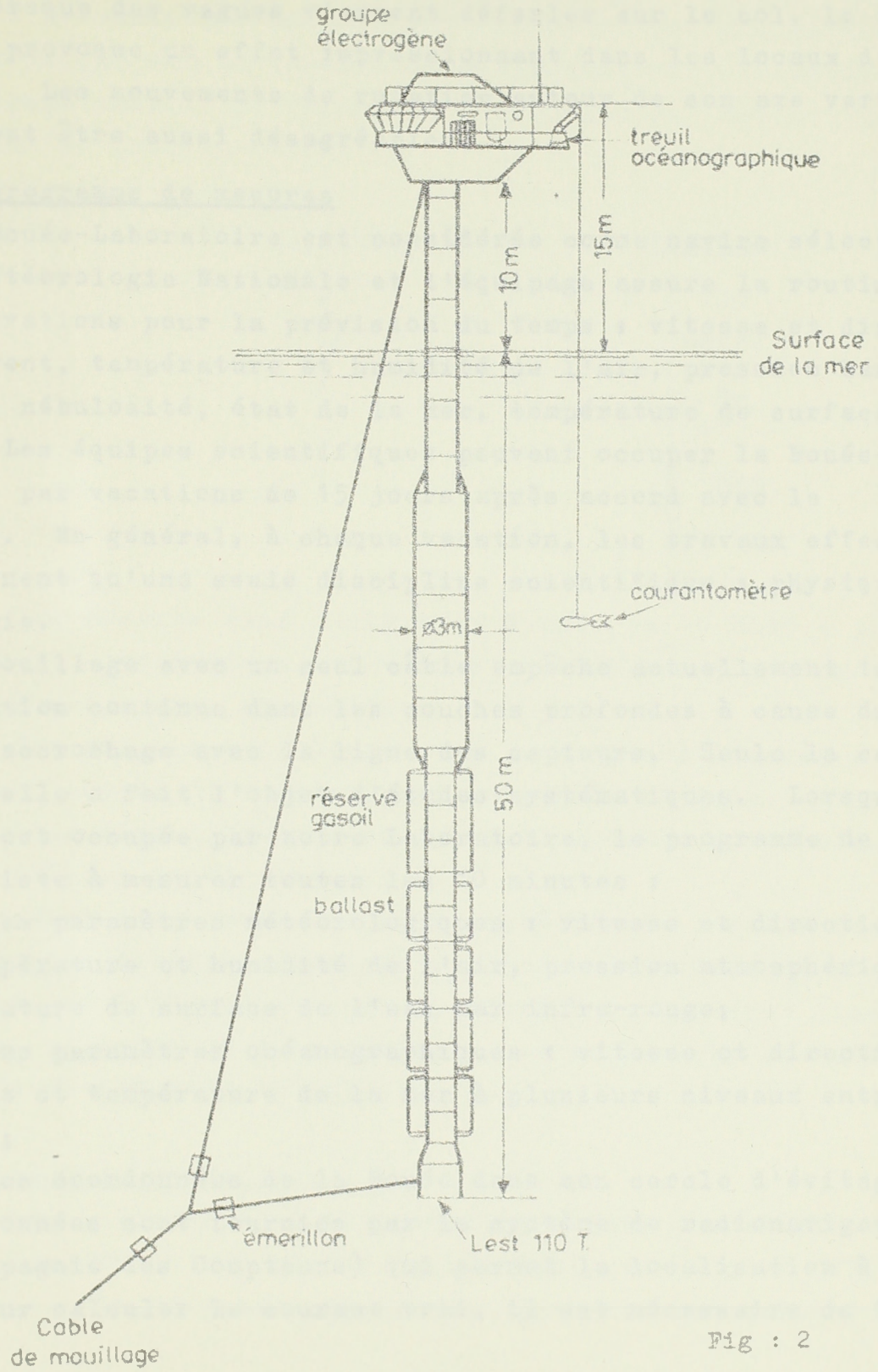

Fig : 2

très bonne stabilité. Toutefois, par mauvais temps, de brusques mouvements de rappel apparaissent surtout lorsque la Bouée se trouve sollicitée par son câble en limite d'évitage. Par ailleurs, lorsque des vagues viennent déferler sur le col, le tube vibre et provoque un effet impressionnant dans les locaux d'habitation. Les mouvements de rotation autour de son axe vertical peuvent être aussi désagréables.

Le programme de mesures

La Bouée-Laboratoire est considérée comme navire sélectionné par la Météorologie Nationale et l'équipage assure la routine des observations pour la prévision du temps : vitesse et direction du vent, température et humidité de l'air, pression barométrique, nébulosité, état de la mer, température de surface de la mer. Les équipes scientifiques peuvent occuper la Bouée-Laboratoire par vacations de 15 jours après accord avec le C.N.E.X.O. En général, à chaque vacation, les travaux effectués ne concernent qu'une seule discipline scientifique : physique ou biologie.

Le mouillage avec un seul câble empêche actuellement toute investigation continue dans les couches profondes à cause du risque d'accrochage avec la ligne des capteurs. Seule la couche superficielle a fait l'objet d'études systématiques. Lorsque la Bouée est occupée par notre Laboratoire, le programme de travail consiste à mesurer toutes les 10 minutes :

1/ Les paramètres météorologiques : vitesse et direction du vent, température et humidité de l'air, pression atmosphérique et température de surface de l'eau par infra-rouge;

2/ les paramètres océanographiques : vitesse et direction du courant et température de la mer à plusieurs niveaux entre 5 - 60 m ;

3/ les coordonnées de la Bouée dans son cercle d'évitage. Ces coordonnées sont fournies par le système de radionavigation RANA (Compagnie des Compteurs) qui permet la localisation à 5m près. Pour calculer le courant vrai, il est nécessaire de tenir

compte de la vitesse de déplacement de la Bouée qui peut atteindre 25 cm/s.

A l'exception des coordonnées RANA et de la température de surface, l'ensemble des données est recueilli par une centrale de mesure conçue par un ingénieur du Laboratoire : Ph.GAUDILLERE.

Le cycle complet de mesure se fait selon la séquence représentée dans le tableau suivant :

Minutes	Capteurs	Niveaux
0	Météo	
1	"	15m
2	CM	entre
3	"	
4	"	-5m
5	"	et
6	"	
7	"	-60m
8	"	
9	"	

Pour les mesures dans l'air on a 8 mots de 10 bits : pression, vitesse, température, référence, différence psychrométrique, cap de la Bouée, zéro, girouette.

Pour les mesures dans la mer, on a, à chaque niveau, 6 mots de 10 bits : compas 1, température, compas 2, vitesse, compas 3, référence. Au dépouillement, on prend la moyenne géométrique des trois mesures de direction.

La transmission entre les courantomètres et l'unité centrale est assurée par liaison acoustique. L'enregistrement de chaque mot se fait sur 2 lignes de ruban perforé 8 canaux avec bits d'imparité, d'erreur et de référence. Le traitement se fait sur ordinateur IBM 1130 au Laboratoire.

Avantages et servitudes :

La Bouée-Laboratoire a été construite pour accueillir 6 personnes au maximum : 2 places pour l'équipage, 4 pour l'équipe scientifique. La réduction d'effectif présente des avantages

certains mais demande beaucoup de qualités de la part de l'équipage qui doit être : observateur météo, opérateur radio, mécanicien, cuisinier, intendant, marin, plongeur, peintre, électricien... Il est nécessaire de faire preuve de beaucoup de tolérance pour vivre longtemps dans un espace aussi réduit. Tout le monde, personnel scientifique compris, participe aux diverses tâches quotidiennes : cuisine en particulier !

Les liaisons radio avec la terre sont excellentes par l'intermédiaire de Grasse-Radio ou de Marseille Radio. Les conditions météorologiques sont transmises en phonie à ces stations pour être diffusées dans le bulletin régional pour les navigateurs.

De Marseille, le ravitaillement en matériel, vivre, eau douce et fuel a lieu toutes les deux semaines avec un navire de la taille d'un petit chalutier : l' "ESPADON". La relève du personnel est aussi effectuée au cours de ces liaisons. Le mauvais temps (vent supérieur à 30 nds.) peut provoquer un retard pouvant atteindre deux à trois semaines.

2ème Conférence

L'ACTION DU VENT SUR LES COURANTS SUPERFICIELS DE L'OCEAN

- Le modèle d'EKMAN en régime impulsionnel : une approche théorique simple.
- Confrontation avec les observations recueillies à la BOUEE LABORATOIRE.
- Conclusion.

-:-

Depuis 1964, les résultats les plus intéressants, dans le programme d'interactions air-mer poursuivi à la Bouée-Laboratoire, ont été obtenus dans le domaine de l'action du vent sur les courants marins superficiels (0-100m). Le modèle d'EKMAN en régime impulsionnel est un modèle assez simple sur lequel nous pouvons baser notre discussion après avoir examiné quelques résultats d'observations recueillies à la Bouée-Laboratoire.

LE MODELE D'EKMAN EN REGIME IMPULSIONNEL.

Les hypothèses de départ sont les mêmes que celles d'EKMAN (1905) dans sa théorie des courants induits par le vent : océan homogène, visqueux (hypothèse de Boussinesq : ν = Cte), illimité et de profondeur infinie. La tension du vent en surface est $\underline{\tau}(t)$ pour $t > 0$.

Nous supposerons en outre qu'à l'instant $t = 0$, il existe une distribution de vitesse $\underline{u}_o(z)$. Dans ces conditions, l'équation du mouvement prise au sens des distributions est :

$$\frac{\partial \underline{u}}{\partial t} + 2\underline{\Omega} \wedge \underline{u} - \nu \Delta \underline{u} = \frac{2\underline{\tau}(t)}{\rho} + \underline{u}_o(z)\, \delta(t)$$

où δ est la distribution de Dirac.

En prenant comme unité de base la période d'inertie T_I à la latitude donnée (considérée comme constante) et la profondeur D égale à deux fois la profondeur d'Ekman D_E, l'équation s'écrit avec des grandeurs sans dimension : ($D^2 = 4\pi\nu T_I = 4D_E^2$)

$$\frac{\partial u}{\partial t} + 2i\pi u - \frac{1}{4\pi}\frac{\partial^2 u}{\partial z^2} = 2\tau(t)\,\delta(z) + u_o(z)\,\delta(t). \quad (1)$$

Le symbole "-" est supprimé, mais u et τ restent des grandeurs complexes. Cette équation est, au terme $2i\pi u$ près, analogue à l'équation de la chaleur dans une tige infinie avec une source de chaleur à l'origine et une distribution initiale de température. La solution élémentaire est :

$$E(z,t) = Y(t)\; e^{-2i\pi t}\; e^{-\pi z^2/t}\; t^{-1/2}\,.$$

Avec cette notation, la solution satisfaisant au problème d'Ekman est donc :

$$u(z,t) = 2\tau(t) \underset{(t)}{*} E(z,t) + u_o(z) \underset{(z)}{*} E(z,t) \quad (2)$$

où le symbole "*" représente le produit de convolution en z ou en t : $f(t) * g(t) = \int_{-\infty}^{+\infty} f(\theta)g(t-\theta)d\theta$. Cette expression donne la solution générale mais il est intéressant d'examiner quelques cas particuliers.

1) <u>$\tau = 0$ mais $u_o(z) \neq 0$</u>. Ceci correspond à un mouvement sur lequel toute action cesse d'agir à t = 0. Si R_o désigne la résultante des vitesses ($R_o = \int u_o(\zeta)d\zeta$), on montre que pour t assez grand : $u_o(z,t) \rightarrow Y(t)\; t^{-1/2}\; R_o e^{-2i\pi t}$. C'est-à-dire que le courant tend à décroître en $t^{-1/2}$ et à se mettre en phase avec $R_o e^{-2i\pi t}$. Ainsi, suivant que le courant initial est, à un niveau déterminé, en avance ou en retard par rapport à la

résultante R_o sa période tendra théoriquement vers la période d'inertie (terme en $e^{-2i\pi t}$) par valeur supérieure ou inférieure (fig.1).

2) $\underline{\tau \neq 0 \text{ mais } u_o(z)} = 0$. En général $\tau(t)$ est une fonction quelconque du temps t.

Le cas examiné par Ekman est celui où $\tau(t) = Y(t)\ \tau_o$ où τ_o est une constante complexe. Dans ce cas :

$$u(z,t) = 2\ \tau_o Y(t) \underset{(t)}{*} E(z,t) = 2\ \tau_o \int_o^{\infty} E(z,\theta)d\theta \quad (3),$$

c'est la solution donnée par Fredholm. Une autre expression de $u(z,t)$ peut être obtenue dans ce cas en considérant le régime permanent pour $t > 0$ comme la superposition d'une distribution initiale égale à la Spirale d'Ekman $u_o(z)$ avec une tension $Y(t)\ \tau_o$. Dans ces conditions :

$$u(z,t)=u_o(z)-u_o(z) \underset{(z)}{*} E(z,t) \text{ avec } u_o(z)=\sqrt{2}\ \tau_o\ e^{-i\pi/4} e^{-2\pi(1+i)|z|}.$$

Ainsi, quand t devient grand, le deuxième terme de cette dernière équation tend vers zéro et, à chaque niveau, le vecteur courant tend vers la Solution d'Ekman en régime permanent.

Le modèle d'Ekman en régime impulsionnel est celui où la tension τ a la forme d'une impulsion rectangle τ_o de durée d. Dans ce cas, la solution peut avoir plusieurs expressions :

- en prenant l'origine des temps à la fin du coup de vent, alors $u_d(z,t) = u(z,d) \underset{(z)}{*} E(z,t)$
  où $u(z,d)$ est donnée par (3) en faisant $t = d$.
- en prenant l'origine des temps au début du coup de vent, la tension peut s'écrire $\tau = Y(t)\ \tau_o - Y(t-d)\tau_o$
  d'où $u_d(z,t)=u(z,t)-u(z,t-d)$ pour $t>d$.

On montre ici que pour t assez grand, on a :

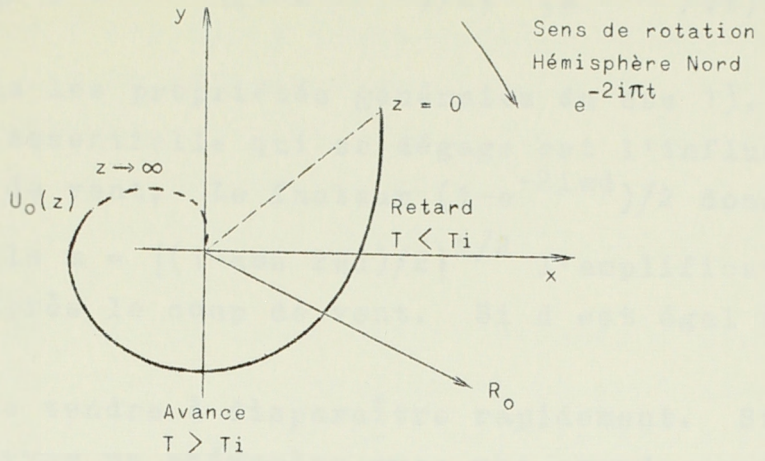

Fig. 1.- Distribution initiale des vitesses $U_o(z)$

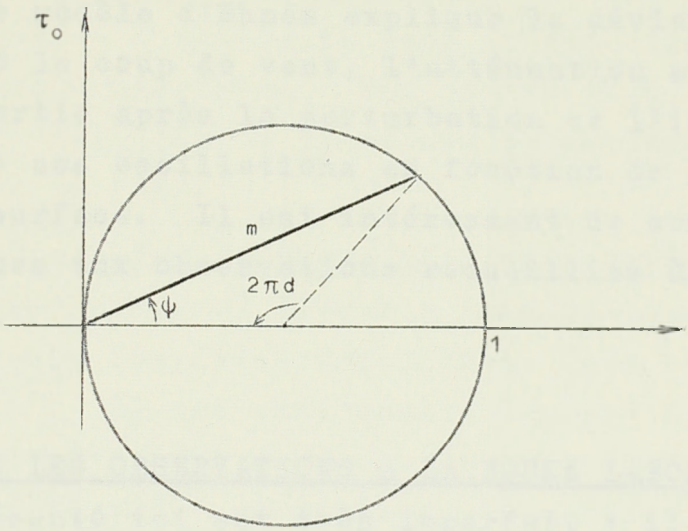

Fig. 2.- Influence de la durée d du coup de vent sur le module m de l'amplification et sur la phase ψ du courant d'inertie

$$\frac{1 - e^{-2i\pi d}}{2}$$

$$u_d(z,t) \rightarrow (2\tau_o/\pi)\ e^{-i\pi/2}\{(1-e^{-2i\pi d})/2\}\ \ (e^{-2i\pi t}/\sqrt{t}).$$

Nous retrouvons les propriétés générales du cas 1), mais la caractéristique essentielle qui se dégage est l'influence de la durée d du coup de vent. Le facteur $(1-e^{-2i\pi d})/2$ donne :

- par son module $m = \{(1-\cos 2\pi d)/2\}^{1/2}$ l'amplification du courant d'inertie après le coup de vent. Si d est égal à un entier n, m = 0

et le phénomène tendra à disparaître rapidement. Si d=n+1/2, m=1, on pourra observer un phénomène avec une grande amplitude d'inertie.

- par son argument ϕ la phase du courant par rapport à

$$(2\tau_o/\pi)\ e^{-i\pi/2}\ e^{-2i\pi t}\ :\ tg\phi = (\sin 2\pi d)/(1-\cos 2\pi d).\ \text{(fig.2)}$$

En résumé, le modèle d'Ekman explique la déviation à droite du courant pendant le coup de vent, l'atténuation en $t^{-1/2}$ des oscillations d'inertie après la perturbation et l'intensité plus ou moins grande de ces oscillations en fonction de la durée d de la tension en surface. Il est intéressant de confronter ces résultats théoriques aux observations recueillies à bord de la Bouée-Laboratoire.

CONFRONTATION AVEC LES OBSERVATIONS A LA BOUEE LABORATOIRE.

Le modèle présenté ici est très imparfait : il ne tient compte ni de la limite du champ de vent dans l'espace ni de la stratification de l'océan. Aussi, il n'a pas la prétention d'expliquer tous les phénomènes observés d'autant plus que les gradients horizontaux de pression sont négligés.

Parmi les campagnes de mesures effectuées à bord de la Bouée Laboratoire, il y en a trois qui ont bénéficié de conditions météorologiques particulières : juillet 1964, décembre 1964, juillet 1968. Chaque fois une accalmie relativement longue

a suivi un coup de vent qui peut être assimilé à une impulsion rectangle. La figure 3 visualise d'une manière extrêmement nette la génération par le vent de l'oscillation d'inertie et son atténuation ultérieure (juillet 1968 : 10m.). Les mesures effectuées en 1969 ne sont pas toutes dépouillées : les planches exposées au cours de la conférence représentent les résultats de février et de juillet 1969.

Nous allons examiner les trois sujets d'intérêt particulier : la déviation du courant moyen en fonction de la profondeur pendant le coup de vent, l'atténuation de l'oscillation d'inertie après la perturbation atmosphérique et l'influence de la durée du coup de vent.

1) Déviation du courant moyen en fonction de la profondeur pendant la durée du coup de vent. En mai 1966, nous avions déjà observé ce phénomène qui nous donne une spirale analogue à celle d'Ekman (GONELLA, 1968). En juillet 1969, le même phénomène a été observé : déviation à droite du vent et rotation à droite avec les profondeurs croissantes. Par contre rien d'analogue ne s'observe en février 1969 où l'eau est parfaitement homogène de la surface jusqu'au fond.

2) Atténuation des oscillations d'inertie après la perturbation. Le graphique (fig. 4) à double échelle logarithmique montre que dans chaque cas, l'atténuation se fait selon une loi plus forte que $t^{-1/2}$. Il est remarquable de constater que la décroissance est sensiblement la même pour les deux mois de juillet (1964,1968) en $t^{-2/3}$ et beaucoup plus forte en décembre en $t^{-6/5}$. Par ailleurs, aucune oscillation nette n'apparaît dans les observations de février 1969. Il est évident que la déviation du courant en fonction de la profondeur et l'atténuation des oscillations d'inertie doivent être directement liées à la stratification en densité. En juillet, la stratification est continue; en décembre, l'eau est homogène jusqu'à 70 m.; en février, l'homogénéité se fait jusqu'au fond.

Ainsi, il est curieux de voir que plus l'océan est stratifié, plus il a tendance à être en accord avec le modèle d'Ekman conçu pour un océan homogène. En réalité cet accord vient du fait que l'hypothèse du coefficient de Boussinesq constant n'est pas représentatif d'un océan entièrement homogène où les phénomènes de turbulence verticale sont extrêmement important : WEBB et VOORHIS ont enregistré des vitesses verticales de 6cm/sec.

Toutefois, la stratification ne suffit pas à expliquer toute l'atténuation des oscillations d'inertie observées; il est nécessaire de tenir compte aussi du champ de vent. Ce modèle doit être complété avec celui de POLLARD et MILLARD. Ces deux auteurs font intervenir dans l'équation du mouvement un facteur de dissipation proportionnel à la vitesse et une tension constante en module et direction dans toute la couche de mélange. Leur modèle ne peut rendre compte des écarts angulaires et de l'atténuation des vecteurs courants dans la couche de mélange elle-même. Par contre, à une profondeur déterminée, l'atténuation du courant dans le temps est exponentielle et son coefficient d'atténuation peut être ajusté avec le champ de vent.

3) La durée du coup de vent. La loi concernant l'influence de la durée du coup de vent sur l'amplitude de la composante d'inertie se trouve assez bien vérifiée. En effet, la mesure à 20m. en juillet 1964 montre que le courant est nettement plus important qu'en juillet 1968, alors que la force du vent était du même ordre de grandeur : 14 à 15 cm/sec en 1964 et 13 à 14cm/sec en 1968. Par contre $d(1964) \simeq 2T_I$ et $d(1968) \simeq 1,5\ T_I$.

D'autres caractéristiques peuvent être mises en évidence, en particulier l'effet d'écran de la thermocline au transfert de quantité de mouvement. En juillet 1969, les oscillations d'inertie au-dessous de la thermocline n'apparaissent qu'après le coup de vent. Le transfert d'énergie n'a pu se faire que par un effet de frontière et non par viscosité : CREPON explique la genèse de l'onde interne d'inertie dans un milieu à deux couches

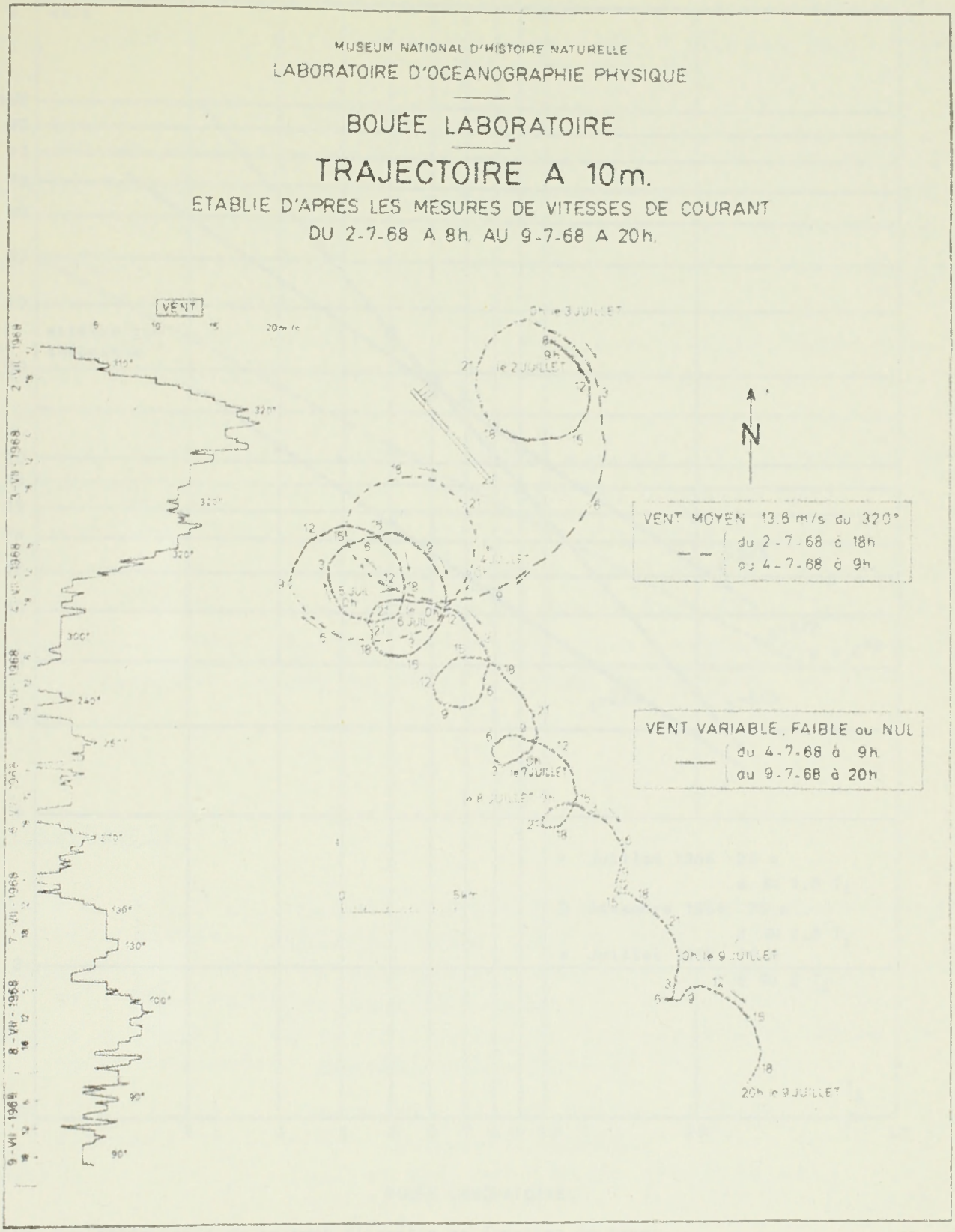
MUSEUM NATIONAL D'HISTOIRE NATURELLE
LABORATOIRE D'OCEANOGRAPHIE PHYSIQUE
BOUÉE LABORATOIRE
TRAJECTOIRE A 10m.
ETABLIE D'APRES LES MESURES DE VITESSES DE COURANT
DU 2-7-68 A 8h AU 9-7-68 A 20h
VENT
N
VENT MOYEN 13.8 m/s du 320°
du 2-7-68 à 18h
au 4-7-68 à 9h
VENT VARIABLE, FAIBLE ou NUL
du 4-7-68 à 9h
au 9-7-68 à 20h
0h le 3 JUILLET
9h le 2 JUILLET
20h le 9 JUILLET
2-VII-1968
3-VII-1968
4-VII-1968
5-VII-1968
6-VII-1968
7-VII-1968
8-VII-1968
9-VII-1968

Fig : 3

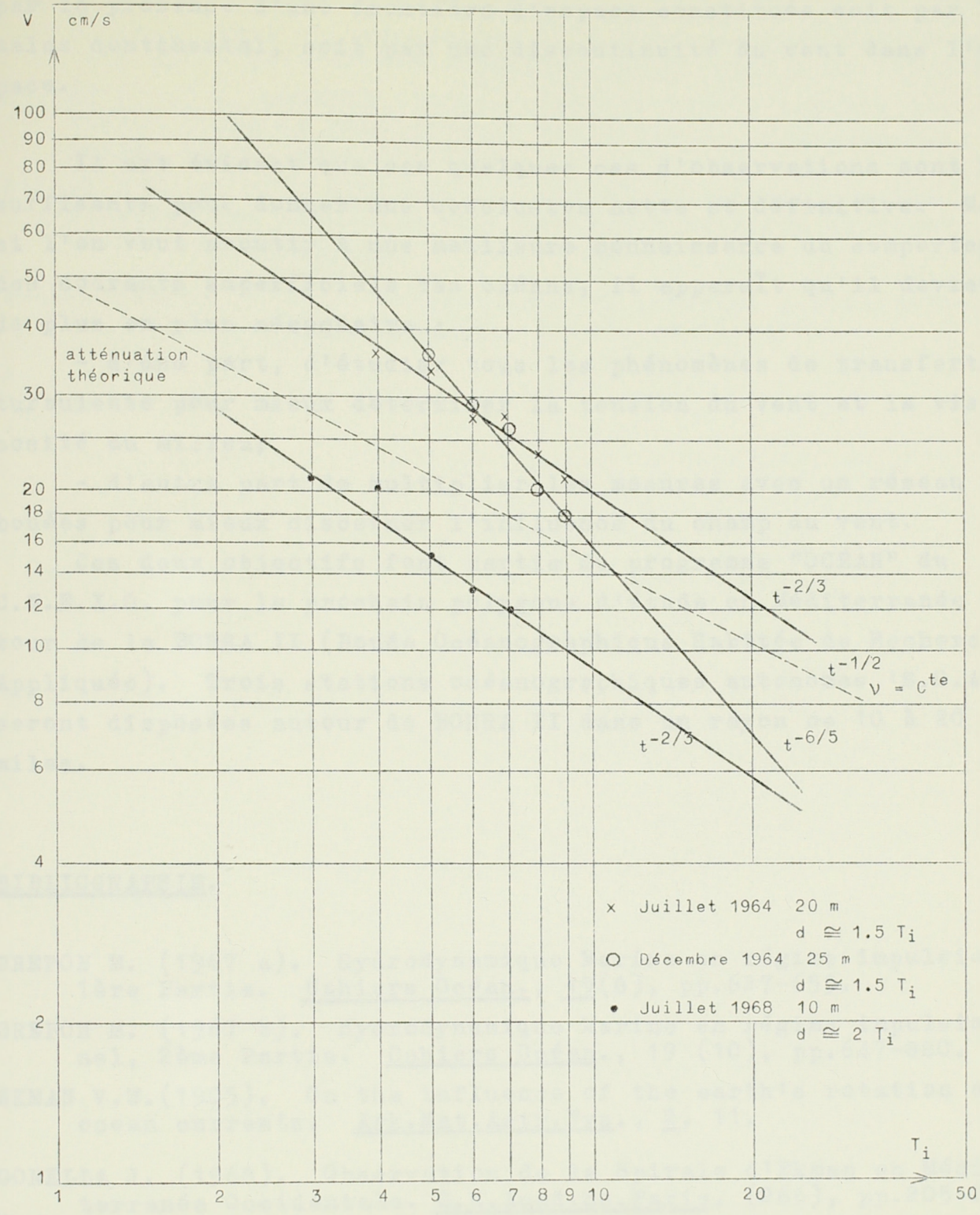

Fig. 4.- Atténuation du courant d'inertie en fonction du temps.
Origine des temps : début du coup de vent.
Unité de temps = une période d'inertie T_i .

par la présence d'une frontière d'espace constituée soit par le talus continental, soit par une discontinuité du vent dans l'espace.

Il est évident que ces quelques cas d'observations sont insuffisants pour donner une conclusion nette et définitive. Mais, si l'on veut aboutir à une meilleure connaissance du comportement des courants superficiels des océans, il apparaît qu'il devient de plus en plus nécessaire :

- d'une part, d'étudier tous les phénomènes de transferts turbulents pour mieux déterminer la tension du vent et la viscosité du milieu;
- d'autre part de multiplier les mesures avec un réseau de bouées pour mieux discerner l'influence du champ du vent.

Ces deux objectifs font partie du programme "OCEAN" du C.N.E.X.O. pour le prochain polygone d'étude en Méditerranée autour de la BOHRA II (Bouée Océanographique Habitée de Recherche Appliquée). Trois stations océanographiques autonomes 'S.O.A.) seront disposées autour de BOHRA II dans un rayon de 10 à 20 miles.

BIBLIOGRAPHIE.

CREPON M. (1967 a). Hydrodynamique Marine en régime impulsionnel, 1ère Partie. Cahiers Océan., 19(8), pp.627-655.

CREPON M. (1967 b). Hydrodynamique Marine en régime impulsionnel, 2ème Partie. Cahiers Océan., 19 (10), pp.647-880.

EKMAN V.W.(1905). On the influence of the earth's rotation on ocean currents. Ark.Mat.Astr.Fys., 2, 11.

GONELLA J. (1968). Observation de la Spirale d'Ekman en Méditerranée Occidentale. C.R.Acad.Sc.Paris, (266), pp.205-208.

GONELLA J. (1969). Analyse des mesures de courants et de vent à la Bouée Laboratoire (Position B). Juillet 68. Cahiers Océan. 21(9), pp.855-862.

GONELLA J., M. CREPON et F. MADELAIN(1969). Observations de courant, vent et température à la Bouée Laboratoire (Position A). Sept.-Oct.1966. Cahiers Océan, 21(9), pp.195-218.

LACOMBE H. et J. GONELLA (1964). Oscillations d'inertie des masses d'eau en Méditerranée Occidentale. C.R.Acad.Sc. Paris, (259), pp.2487-2490.

POLLARD R.T. et R.C. MILLARD, Jr. (1970). Comparison between observed and simulated wind-generated inertial oscillations. Deep-Sea Res. (sous presse).

WEBSTER Ferris (1968). Observations of inertial period motions in deep sea. Rev. Geophys., 6 (4), pp.473-490.

ON THE FINE STRUCTURE OF OCEAN VARIABLES AND ITS CORRELATION WITH THE FIELD OF MOTION (SUMMARY AND REFERENCES).

By G. Siedler

Institut für Meereskunde
an der Universität Kiel
23 Kiel

1.-INTRODUCTION

The intention of this summary is to select some profiles showing typical features of the oceanic fine structure, to discuss some ideas concerning the generation of this structure, and to present results which indicate a weak correlation of temperature fine structure and current variability at small time scales.

2.-METHODS OF MEASUREMENTS

The state of instrumental techniques and the limitations in financial support will always imply that a sufficiently dense net of sensor packages can only be approximated, and similar restrictions apply to the resolution in time and the duration of the measurements. The most important methods allow a very high spatial resolution in either vertical or horizontal direction of a high resolution in time at selected depth levels.

The first type of measurement is achieved by lowered sensor packages like the Bathysonde (Hinkelmann, 1957, Siedler, 1963) or other salinity-temperature-depth (STD) measuring instruments, or by an underwater winch system (Siedler, Krause, 1964). The second type of measurement is obtained by instrumented moorings (Fofonoff, 1967, Siedler, 1967). In addition, there are dye techniques (Woods, 1968) and methods using towed temperature and hot film probes (Grant, et al., 1968).

3.-TYPICAL VERTICAL PROFILES OF TEMPERATURE AND SALINITY

Some typical features of the vertical profiles of temperature and salinity can be found. A few references to results obtained at Kiel University are given in the following text. There are regions like the deep Mediterranean or the deep Red Sea where there is usually no fine structure which can be detected by Bathysonde measurements. Near the surface, fine structure occurs mainly in and below the thermocline. The spatial variability is especially high in shallow areas like the Baltic (Siedler, 1961), but there is also a considerable structure in deep regions where the water is renewed by vertical convection (Holzkamm et al., 1964) or where water from adjacent seas is spreading in the open ocean (Krause, 1968, Zenk, 1970).

Detailed discussions of certain features of vertical temperature and salinity profiles obtained by STD lowerings have been given by Stommel and Fedorov, 1967.

4.-GENERATION OF FINE STRUCTURE IN THE OCEAN

There are three groups of processes which probably generate most of the temperature and salinity fine structure observed in the ocean: Air-sea interaction at the surface, shear instability and molecular diffusion in the interior of the ocean.

Air-Sea Interaction: Recent measurements obtained by an underwater winch system in the Baltic made it possible to determine the types of fine structure which are generated during certain weather conditions and the time scales of the variability of this structure (Münzer, 1969). At low wind speeds, slowly growing homogeneous surface layers with a few decimeters thickness are generated during the day-time. At most times, however, heat from the atmosphere is transferred to surface layers with varying thickness in certain time intervals. The generated irregular structures often migrate downwards. When the atmospheric conditions change rapidly, e.g.

when a front passes the position of measurement, the water is mixed down to at least 15 m within a few hours. Step-like structures are also observed from time to time.

Very thin surface layers with a vertical extension of 10 to 30 cm occur frequently, their typical duration is half an hour to a few hours. Fine structure is frequently removed by vertical convection caused by surface cooling during the night.

Possibly, most of the fine structure is generated by air-sea interaction. Stern (1968) discussed a model which assumes that all fine structure is generated at the sea surface.

Shear instability in the interior of the ocean: The generation of fine structure by shear instability due to internal waves was shown by Woods (1968). By using dye techniques he found that thin layers with large vertical gradients of density and current velocity existed in the seasonal thermocline. Internal waves at these layers change the current shear, and frequently shear instability is observed at the crest or the trough of the wave. The resulting transition from laminar to turbulent motion leads to the generation of temperature fine structure. A patchiness of the fine structure results from these processes. Apparently, this patchiness is a common feature of the ocean. This has been demonstrated by measurements with temperature and hot film probes which were towed or mounted on a submarine (Grant et al., 1968).

Shear instability may also be caused by the thenohaline circulation. In straits connecting the oceans and adjacent seas, very small Richardson Numbers are found which apparently explain the occurence of a strong variability in time and space of vertical temperature and salinity profiles (Siedler, 1968).

The variations of mixing processes with tidal periods in such areas lead to two peaks in the frequency distribution of water types and to a resulting structure with two main maxima in the deep ocean (Siedler, 1969).

Differences in the molecular diffusion of heat and salt in the interior of ocean: As heat is transferred much faster than salt by molecular diffusion, the temperature-salinity patterns is unstable under certain conditions (Stern, 1960, Turner, Stommel, 1964). It has been shown by tank experiments (Turner, 1967) that salt fingers can be formed at such interfaces, and step-like structures are generated if warm salty water is layered above cold, less salty water (Stern, Turner, 1969). Such step-like structures have been observed in certain areas below the "Mediterranean Water" in the Eastern North Atlantic (Tait et al., 1968, Zenk, 1970).

5.-CORRELATION OF THE TEMPERATURE AND CURRENT VARIABILITY

Recent measurements at deep-sea moorings indicate that high frequency variations of currents in the deep ocean are weakly correlated with the corresponding variation of temperature (Siedler, 1970). Probably, this is caused by the superposition of a rapidly changing temperature and salinity fine structure to a mean temperature and salinity field which controls the internal waves in the ocean.

REFERENCES

FOFONOFF, N.P. (1967), Current measurements from moored buoys. Transactions of the 1967 Buoy Technology Symposium, Marine Technology Society, Washington, D.C., 409-418.

GRANT, H.L., MOILLET, A. and W.M. VOGEL (1968), Some observations of the occurence of turbulence in and above the thermocline. Journal Fluid Mechanics, 34, 443-448.

HINKELMANN, H. (1957), Gerät zur Schnellregistrierung in der Ozeanographie. Zeitschrift für Angewandte Physik, 9, 505-513.

HOLZKAMM, F., KRAUSE, G. and G. SIEDLER (1964), On the processes of renewal of the North Atlantic deep water in the Irminger Sea. Deep-Sea Research, 11, 881-890.

KRAUSE, G. (1968), Struktur und Verteilung des Wassers aus dem Roten Meer in Nordwesten des Indischen Ozeans. "Meteor" Forschungsergebnisse, Reihe A, Heft 4, Berlin, 77-100.

MÜNZER, W. (1969), Das Eindringen des täglichen Temperaturganges in das Meer aus Messungen in der Eckernförder Bucht. Dissertation, Universität Kiel (unpublished manuscript).

SIEDLER, G. (1961), Über die kurzfristige Veränderlichkeit von Temperatur- und Salzgehaltsschichtung in der östlichen und mittleren Ostsee im Sommer 1960. Kieler Meeresforschungen, 17, 148-153.

SIEDLER, G. (1963), On the in situ measurement of temperature and electrical conductivity of sea-water. Deep-Sea Research, 10, 269-277.

SIEDLER, G. and G. KRAUSE (1964), An anchored vertically moving instrument and its application as parameter follower. Transactions of the 1964 Buoy Technology Symposium, Marine Technology Society, Washington, D.C., 483-488.

SIEDLER, G. (1967), Mooring Systems used in the Eastern Atlantic. Transactions of the Buoy Technology Symposium, Marine Technology Society, Washington, D.C., 77-83.

SIEDLER, G. (1968), Schichtungs- und Bewegungsverhältnisse am Südausgang des Roten Meeres."Meteor" Forschungsergebnisse, Reihe A, Heft 4, Berlin, 1-76.

SIEDLER, G. (1969), Die Häufigkeitsverteilung von Wasserarten im Ausstrombereich von MeeresstraBen. Kieler Meeresforschungen, 24, 59-65.

SIEDLER, G. (1970), Vertical coherence of short-periodic current variations. Deep-Sea Research (in preparation).

STERN, M.E. (1960), The "salt-formation" and thermohaline convection. Tellus, 12, 172-175.

STERN, M.E. (1968), T-S gradients on the micro-scale. Deep-Sea Research, 15, 245-250.

STERN, M.E. and J.S. TURNER (1969), Salt fingers and convecting layers. Deep-Sea Research, 16, 497-511.

STOMMEL, H. and K.N. FEDOROV (1967), Small scale structure in temperature and salinity near Timor and Mindanao. Tellus, 19, 306-325.

TAIT, R.J. and M.R. HOWE (1968), Some observations of the thermohaline stratification in the deep ocean. Deep-Sea Research, 15, 275-280.

TURNER, J.S. and H. STOMMEL (1964), A new case of convection in the presence of combined vertical salinity and temperature gradients. Proceedings National Academy Sciences, 52, 49-53.

TURNER, J.S. (1967), Salt fingers across a density interface. Deep-Sea Research, 14, 599-611.

WOODS, J.D. (1968), Wave-induced shear instability in the summer thermocline. Journal Fluid Mechanics, 32, 791-800.

ZENK, W. (1970), On the temperature and salinity structure of the Mediterranean water in the Northeast Atlantic. Deep-Sea Research, (in print).

SOME NEW IDEAS ABOUT THE FORMATION OF ANTARCTIC BOTTOM WATER

By A.E. Gill and J.S. Turner

Department of Applied Mathematics and Theoretical Physics, University of Cambridge.

In this communication, we point out two things : first, the existence of a convection process which is active when the surface water is considerably less dense than the deeper water, and, second, the importance of variations of depth on any convection which may occur. Previous theories (Brennecke, 1921 ; Mosby, 1934 ; Mosby, 1966 ; Fofonoff, 1956 ; Munk, 1966) all require the production of denser water near the surface by freezing during the winter ; in contrast, the process discussed here can be driven by melting of surface ice, and can also be active in the summer. It can explain in a natural way the measured characteristics of Antarctic bottom water, and it is supported by observations of a simple laboratory model.

In Antarctic waters south of the Antarctic convergence, the great bulk of the water, called "warm deep water", has a salinity close to $34.7^{o}/_{oo}$ and temperature close to $+0.5^{\circ}C$. The surface water above and bottom water below are presumably formed by modification of this basic water mass. The surface water is found to be fresher, colder and lighter than the deep water, its temperature is usually near the freezing point (about $-2^{\circ}C$), and salinities cover a fairly wide range. The freshness can be ascribed to an excess of precipitation over evaporation and the discharge of ice and melt water from the Antarctic Continent. The bottom water, whose properties we seek to explain, is also cooler and fresher, but also denser, than deep water (see Fig.1).

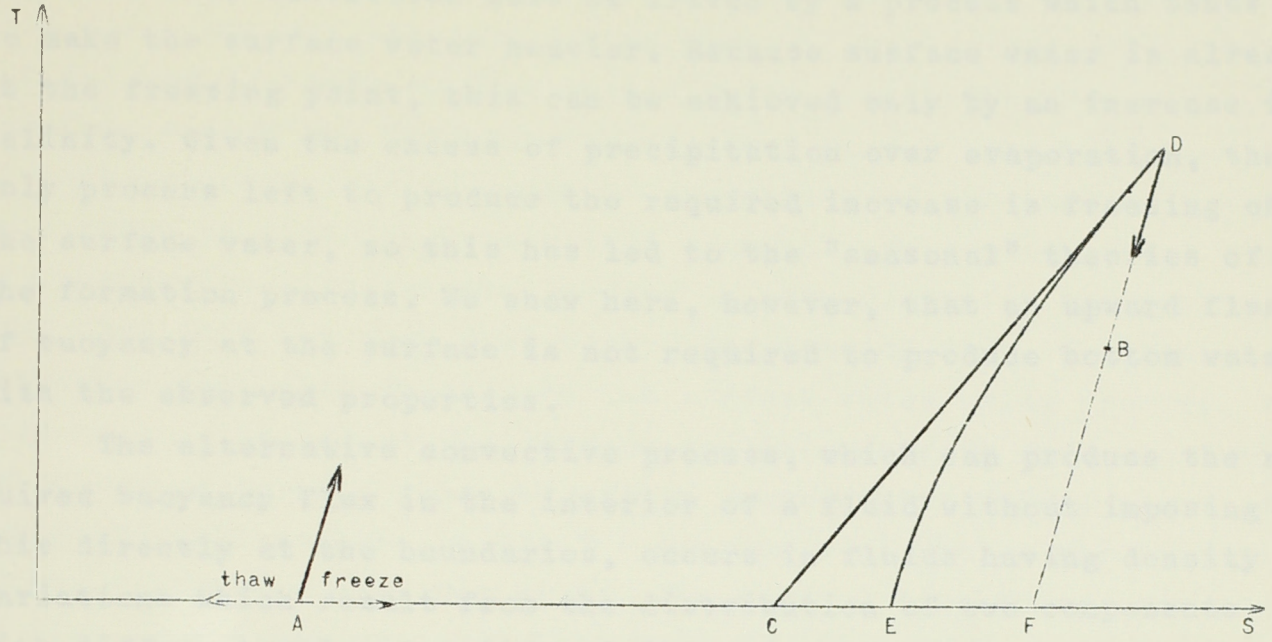

Fig. 1.- A temperature-salinity diagram showing the effect (solid arrows) of thermohaline processes on the properties of surface water (A) and warm deep water (D). The point B represents bottom water. In conditions of rapid thaw or of freezing, the properties of surface water change in the direction of the appropriate broken arrow. The line ACEF is not precisely one of constant temperature but is the freezing curve. The curved line DE is one of constant density and CD is tangent to it at D .

The old arguments about bottom water formation are based on the idea that convection must be driven by a process which tends to make the surface water heavier. Because surface water is already at the freezing point, this can be achieved only by an increase in salinity. Given the excess of precipitation over evaporation, the only process left to produce the required increase is freezing of the surface water, so this has led to the "seasonal" theories of the formation process. We show here, however, that an upward flux of buoyancy at the surface is not required to produce bottom water with the observed properties.

The alternative convective process, which can produce the required buoyancy flux in the interior of a fluid without imposing this directly at the boundaries, occurs in fluids having density variations which result from the distribution of two components with different molecular diffusivities (for example, salt and heat). If one of the components (in this case heat) has a destabilizing gradient, motions can be driven by drawing on the potential energy in the field of that component, even though the overall density distribution is statically stable. This thermohaline convection mechanism has been well documented by laboratory experiment (Turner, 1964 ; Turner, 1956), and it has been used to interpret various small scale features in lakes (Hoare, 1966) and the ocean (Tait, 1968 ; Cooper, 1968). We now suggest that there can also be important larger scale consequences of the process.

The upward flux of heat (in density units) is only partly compensated by a flux of salt, and so the density of the upper layers will decrease and that of the lower layers will increase. If a layer of shelf water with properties A overlies deep water with properties D (Fig.1), the fluxes across the interface cause the temperature and salinity to change in the directions indicated by the solid arrows. Energy considerations show that the arrow at D must always li lie between the direction AD and the vertical ; and, in fact, the relative rates of change of temperature and salinity have been determinated quantitatively in the laboratory (Turner, 1956).

A significant feature of the thermohaline process (Stommel, 1962) is that the resulting properties need not lie on the line AD, as they must after an ordinary mixing process. The modification of the deep water would produce bottom water B with the observed properties, colder and slightly fresher than D, and this will continue to hold true over a wide range of properties of the surface water. To sustain an unstable temperature gradient, of course, there must be continued cooling at the surface to compensate for the upward heat flux from the warm deep water. The special form of convection discussed here also depends on the surface water being fresher, so that melting of ice at the surface can indeed drive such convection by providing both of these necessary ingredients. Taking the surface processes into account on the T-S diagram will change the direction of the arrow at A (but not at D). The surface temperature will tend to stay near freezing, while the salinity changes in either direction along the freezing curve ; to the left in conditions of rapid thaw, and to the right in freezing conditions (with no net thawing or freezing, the arrow will point to the right because of the salinity flux from below).

The explanation of the properties of bottom water in terms of non-linear mixing effects (Fofonoff, 1956) seems, however, to put undue emphasis on surface water with the properties F (which is heavier than D), and we do not believe this to be physically sound. We agree that, in winter conditions, the surface salinity will tend to increase at least to the point C where some mixtures with deep water will be heavier than either water mass, and that this effect can cause a flow down the slope when surface salinities lie in the range between C and E. The maximum salinities produced by this kind of direct mixing, however, while still maintaining static stability, will lie on the straight line joining D and E. Before overturning occurs, therefore, only the thermohaline mechanism can produce sufficiently saline bottom water, with properties which are at the same time consistent with the observations and insensitive to the surface salinity. When the surface water reaches salinities to the right

of E and it (as well as the mixtures) becomes heavier than D, mixing will take place rapidly throughout the depth, and non-linearity will play a minor part. There can certainly be an important contribution to bottom water formation at this stage, as discussed by earlier workers. The convection must then be driven entirely by a buoyancy flux at the surface, because there is no longer an "interface" across which a compensating interior flux can occur.

Our argument is not yet complete, for if conditions were uniform horizontally, no distinct bottom water would be formed ; the deep water D would merely undergo a slow change of properties (in the direction of the arrow in Fig.2, when the thermohaline process is important). Our second main point concerns the effect of variations in depth on the convection, and is independent of how this is driven, whether by an interior or a surface flux of buoyancy. Consider, for example, the situation shown in Fig.2, where a cold fresh layer overlies a warmer salty one in a container with a sloping bottom. The thermohaline process initially produces an uniform upward flux of buoyancy through the interface, but the result of this is that fluid at H becomes heavier faster than at L, because mixing occurs through a smaller depth of fluid. The fluid at H therefore sinks and gives rise to a circulation in the sense shown, an important feature of which is the current down the slope carrying colder fresher water right to the bottom under the warm salty layer. The existence of this bottom current in the summer is a definite prediction arising from the thermohaline mechanism, which seems worth testing by direct observation.

A variation of the above argument shows that in the corner G, where there is only a single layer, a uniform downward flux of salt through the surface would produce the heaviest water in the corner, leading to a current down the slope towards H. If it is sufficiently heavy it will penetrate the interface and add to the flow below H. Note that although this water may be saltier than deep water on formation (such water has been observed on the shelf), it will continually mix with fresher surface water as it runs down the slope and need not be as salty as the warm deep water when it flows underneath it.

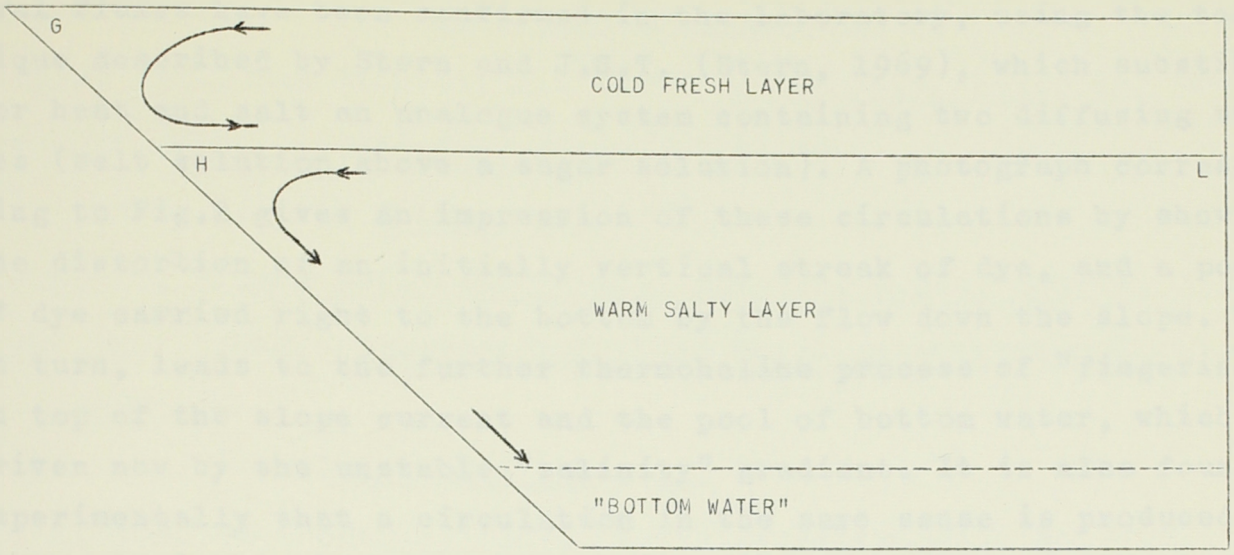

Fig. 2.- Sketch of the circulations set up by convection in a container with a sloping boundary.

The main features of the circulation driven by the interfacial fluxes have been confirmed in the laboratory, using the technique described by Stern and J.S.T. (Stern, 1969), which substitutes for heat and salt an analogue system containing two diffusing solutes (salt solution above a sugar solution). A photograph corresponding to Fig.2 gives an impression of these circulations by showing the distortion of an initially vertical streak of dye, and a pool of dye carried right to the bottom by the flow down the slope. This, in turn, leads to the further thermohaline process of "fingering" on top of the slope current and the pool of bottom water, which is driven now by the unstable "salinity" gradient. It is also found experimentally that a circulation in the same sense is produced in the upper layer, because the density difference between the layers is altered at different rates in different positions. This results in a strong shear at the interface, especially in the corner and out to the position where the layers are comparable in depth.

The sugar-salt technique is useful when it is important to avoid complications due to irrelevant heating or cooling from the room, but it is possible to illustrate the effect more simply and directly. If ice cubes are dropped into salty water at room temperature in a tilted container, a current down the slope will soon be set up, and can be made visible by adding a few drops of dye at the shallow end. This circulation is driven by the cooling and freshening caused by melting, while a thin lighter layer of melt water remains floating on the top.

This work has been supported by a grant from the British Admiralty.

References

Brennecke, W., (1921) Arch. Deut. Seewarte, 39, 1.

Cooper, J.W., and Stommel, H., (1968) J. Geophys. Res., 73, 5849.

Fofonoff, N.P., (1956) Deep-Sea Res., 4, 32.

Hoare, R.A., (1966) Nature, 210, 787.

Mosby, H., (1934) Sci. Res. Norweg. Antarct. Exped. 1927-8, 1, N°11.

Mosby, H., (1966) SCAR/SCOR/IAPO/IUBS Symp. on Antarctic Oceanography, 47.

Munk, W.H., (1966) Deep-Sea Res., 13, 707.

Stern, M.E., and Turner, J.S., (1969) Deep-Sea Res., 16, 497.

Stommel, H., (1962) Okeanologia, 2, 205.

Tait, R.I., and Howe, M.R., (1968) Deep-Sea Res., 15, 275.

Turner, J.S., and Stommel, H., (1964) Proc. US Nat. Acad. Sci., 52, 49.

Turner, J.S., (1956) Int. J. Heat Mass Transfer, 8, 759.

Acknowledgments :

The courtesy of the journal "Nature" in granting permission to reproduce material from a recent paper by A.E. Gill and J.S. Turner is gratefully acknowledged. The original paper has been published in Nature, Vol. 224, N° 5226, pp. 1287-1288, December 27, 1969.

LONG THERMOCLINE WAVES IN THE NORTH SEA

By Friedrich Schott
Institut für Meereskunde, Kiel.

In September 1968, near 56°20'N, 1°E (northern North Sea) four moorings of temperature and current recorders were set out in a triangle 4.5 km on a side, with one in the middle. The water depth at the array position was 82 m, the density was two-layered with the thermocline in 35 m depth.

The vertical amplitude of the semidiurnal internal tidal wave was about 2 m, only the first mode was of significance. To determine the direction of propagation and wave-length of the internal tidal wave the co- and quadrature spectral functions were computed from the temperature fluctuations in the thermoclines.

The directional energy spectrum can be written in the form

$$E(\varkappa,\eta,\omega)=\int\!\!\int_{-\infty}^{\infty}[C(\zeta,\mu,\omega)-iQ(\zeta,\mu,\omega)]e^{-i(\varkappa\zeta+\eta\mu)}\,d\zeta\,d\mu$$

with $\varkappa,\eta$ horizontal wave-numbers, ω frequency, ζ,μ horizontal spacings. For p discrete points of measurement (p = 4 in our case) the real part of the integral-treating all unknown values of the co-and quadr.spectral functions C and Q as zero - is :

$$\tilde{E}(\varkappa,\eta,\omega)=\frac{1}{2N+1}\Big[C_o+2\sum_{i=1}^{N}C_i\cos(\varkappa\zeta_i+\eta\mu_i)-2\sum_{i=1}^{N}Q_i\sin(\varkappa\zeta_i+\eta\mu_i)\Big].$$

With $N=\frac{1}{2}\,p\,(p-1)$. An approximation is determined for the set of the measured C_i, Q_i by a sine-wave of amplitude a_o and wave-numbers $\varkappa_o,\eta_o$ with infinite long crests. The directional spectrum

$\tilde{E}_o$ for this sine-wave has the coefficients :

$$C_{oo}=a_o^2;\ C_{io}=a_o^2\cos(\varkappa_o\zeta_i+\eta_o\mu_i);\ Q_{io}=a_o^2\sin(\varkappa_o\zeta_i+\eta_o\mu_i)\ .$$

A best fit - in the least squares sense - of these coefficients to the C_i, Q_i is determined by a minimum of $(\tilde{E} - \tilde{E}_o)^2$. For the internal tidal wave the best fit was a wave-length of 38 km and a propagational direction of 3°. So the internal tidal wave travels almost against the surface tide at the observation site (propagation of the surface tide towards 210°). The wave-length fitted well in between the values of 36 km at the beginning and of 45 km at the end of the registration time which were determined from the changing density distribution. The same procedure was applied to the 4th harmonic of the internal tidal wave for a part of the registration time with almost constant density distribution. The result was a similar propagational direction (10°) and a wave-length of 5.2 km close to the value of 5.9 km as calculated by help of the eigen value. The area of generation of the internal tidal waves observed in this area should be the slopes of the Doggerbank region.

The inertial period currents derived from the experiment show antiphase between upper an lower layer, the coherence between both layers is high. The temperature oscillations are in phase throughout the thermocline.

The interpretation is that by wind action at the sea surface internal waves are generated with frequencies above the inertial frequency, and that these frequencies approach the inertial frequency in the course of time.

During this frequency variation the vertical elevation declines quickly compared with the horizontal currents. So the current oscillations contain more energy for the very small wave-numbers than the temperature fluctuations. This is demonstrated by horizontal phase differences.

From the current records the free oscillations are eliminated, and the time series of the remaining forced oscillations are shown to depend upon variations of local winds.

The horizontal wave-lengths and propagation of the forced oscillations for different weather situations are determined by help of directional spectra. The wave-lengths were about 50 km, the direction of propagation could not satisfactorily be related to the motions of the wind fields.

WAVE DRIVEN INERTIAL OSCILLATIONS

By K. Hasselmann

Geophysikalisches Institut
University of Hamburg, Germany

1. INTRODUCTION.

The spectra of ocean currents usually show a sharp peak at the inertial frequency. Within the peak, the two components of horizontal velocity are found to be highly coherent, in quadrature, and of equal amplitude, as expected for the rotating current vector of an inertial oscillation of large wave length.

Inertial oscillations have been observed in the open ocean and in enclosed basins, at all latitudes and depths. Typically, the amplitudes are $\sim$ 0 (10 cm/sec) (but sometimes considerably larger), the vertical coherence scale of $\sim$ 0(10 m); estimates of the horizontal scale vary from 5 to 100 km. All records show a characteristic intermittency of the oscillations, each distinct burst of 5 to 20 oscillations long. There is evidence that the bursts near the surface are correlated with high local winds.

At greater depths, no clear dependence on surface conditions has been found. Surveys of inertial current observations and various hypotheses of their origin have been given by Webster (1968; this issue).

In a recent paper (Hasselmann, 1970[+]), a mechanism has been investigated in which the driving forces are attributed to non-linear interactions between high-frequency gravity waves. The apparent "damping" of the inertial oscillations is interpreted as the diffusion due to phase-mixing of a large ensemble of modes with closely neighbouring frequencies. Thus the generation process is regarded as weakly non-linear and the decay process as linear.

[+]Reference to this paper will be indicated in the following by(I).

The approach is in accordance with the "weak-interaction" interpretation of oceanic turbulence which suggests that a broad range of the ocean-current spectrum can be regarded as a superposition of linear wave motions, rather than strongly non-linear fluctuations. The non-linear Reynolds stresses driving low-frequency currents in the ocean may then be interpreted as interactions between higher-frequency wave fields, rather than turbulent stresses. The total stress can be divided into a mean term, arising from quadratic self interactions of the waves, and a fluctuating term, arising from difference interactions between pairs of waves. Only the mean term has been considered.

The response of the ocean to the mean stress exerted by the waves is closely related to the mass transport of a wave field.

In a non-rotating system, the shear components of the Reynolds stress tensor vanishes, since the horizontal and vertical components of the orbital velocity are exactly in quadrature. The mass transport reduces then to the Stokes current which is the difference between the local Lagrangian and Eulerian currents.

In a rotating system, the Lagrangian current cannot remain constant but rotates with the local inertial frequency (Ursell, 1950). Here, it is shown that the wave-induced shear stresses are non zero, which is equivalent. It is also shown that the mass transport currents are not simply a property of the local wave field but represente the cumulative low-frequency response of the ocean to a variable, wave induced force field.

The solution can be represented formally as a superposition of normal modes. The prominence of the inertial peak in the low-frequency spectrum is due to the degeneracy of the modes at zero wave number (in the f-plane approximation, the frequency ω of all modes converges to f, the horizontal Coriolis component, as the wave number k approaches zero).

If the driving wave field is homogeneous in the horizontal, corresponding to excitation at zero wave number, the current vectors of all modes rotate with the same frequency f and their

superposition yields an inertial oscillation which keeps rotating infinitely with its initial vertical distribution. If the scale of the driving field is large but finite, the initial horizontal and vertical distribution is gradually modified by the phase mixing of modes rotating with slightly different frequencies, inducing a dispersion of the oscillation in the horizontal and vertical directions.

The same dispersion-type behaviour is yielded by any effect which removes the degeneracy at zero wave number and introduces mode-dependent frequency shifts : horizontal inhomogeneities of the wave guide, the horizontal component of the Coriolis vector, non-linear interactions with geostrophic flows, planetary variations of the Coriolis parameters.

Instead of the standart normal mode approach (not practicable for all stratifications), the Green function representation is used to expand the solution about the degenerate state, yielding a characteristic operator for each phase-mixing process. The operators can be obtained directly from the equations of motion using eigenvalue formulae from the perturbation theory of linear operators.

Computations have been made for phase-mixing due to wave field inhomogeneities in a continuously stratified model representative of the Baltic. The orders of magnitude of the amplitude response and decay time are in reasonable agreement with observations.

2. EQUATIONS OF MOTION.

It is assumed that the motions are of a horizontal scale small compared with the radius of the earth or the lateral dimension of the ocean. The ocean can thus be described, to the first order, as an incompressible, stratified fluid of infinite horizontal extent. The equations of motion are given in the Boussinesq approximation by

$$\frac{\partial u_1}{\partial t} - fu_2 + \frac{\partial}{\partial x_1} p = - \frac{\partial}{\partial x_j} (u_1 u_j) \qquad (1)$$

$$\frac{\partial u_2}{\partial t} + fu_1 + \frac{\partial}{\partial x_2} p = - \frac{\partial}{\partial x_j} (u_2 u_j) \qquad (2)$$

$$\frac{\partial u_3}{\partial t} - b + \frac{\partial p}{\partial x_3} = - \frac{\partial}{\partial x_j} (u_3 u_j) \qquad (3)$$

$$\frac{\partial b}{\partial t} + N^2 u_3 = - \frac{\partial}{\partial x_j} (b u_j) \qquad (4)$$

$$\frac{\partial u_j}{\partial x_j} = 0 \ . \qquad (5)$$

where $\underline{u} = (u_1, u_2, u_3)$ is the current velocity, p is the deviation of pressure from equilibrium /ρ, (x_1, x_2, x_3) are the Cartesian coordinates, x_1 Eastwards, x_2 Northwards, x_3 upwards, b is the buoyancy field, N^2 the Brunt-Väisälä frequency. At the free surface $x_3 = 0$, the solution must satisfy the dynamical and kinematical boundary conditions

$$\frac{\partial}{\partial t} p - g u_3 = - \frac{\partial}{\partial t} [\zeta (\frac{\partial}{\partial x_3} p + \frac{N^2 \zeta}{2})] - g \frac{\partial}{\partial x_\alpha} (u_\alpha \zeta) \ ; \ x_3 = 0; \ (\alpha = 1,2) \qquad (6)$$

ζ being the vertical displacement, g the gravitational acceleration. At the bottom,

$$u_3 = 0 \ , \quad x_3 = - h \ . \qquad (7)$$

Gradual variation of f, h and N^2 will be considered as perturbations of the homogeneous state; the inclusion of $\hat{f}$, the horizontal Coriolis component will be also incorporated in the per-

turbation scheme.

The low-frequency response of the linear system on the left hand side of (1) - (7) to the non-linear forcing terms on the right is of interest. It is assumed that the components in the non-linear terms can be represented to first order as wave solutions which satisfy the linearised equations of motion and which are of "high" frequency $\omega >> f$. The response is determined for "low" frequencies $\omega << N$. In practice, the two frequency ranges are well separated.

The linearised equations (1) - (7) have normal-mode solutions $\underline{\varphi} \sim e^{i(\underline{k}\underline{x}-\omega t)}$, $k = (k_1, k_2, 0)$.

For the low-frequency modes ($\omega << N$), the hydrostatic approximation is used. By elimination, the linearised equation of motion can be written

$$\frac{\partial}{\partial t} \underline{\varphi}_c - i H_c \underline{\varphi}_c = 0 \qquad (8)$$

where $\underline{\varphi}_c = \begin{pmatrix} u_1 \\ u_2 \\ p \end{pmatrix}$ and the linear operator H_c is

$$H_c = \begin{pmatrix} 0 & -if & i \frac{\partial}{\partial x_1} \\ if & 0 & i \frac{\partial}{\partial x_2} \\ iI \frac{\partial}{\partial x_1} & iI \frac{\partial}{\partial x_2} & 0 \end{pmatrix} \qquad (9)$$

with

$$I = \int_{x_3}^{0} N^2 dx_3' \int_{h}^{x_3'} dx_3'' + g \int_{h}^{0} dx_3' . \qquad (10)$$

For small wave numbers, the dominant part of H_c is the 2×2 rotation matrix in the top left of the matrix. It is convenient to diagonalise this submatrix by transforming to rotary velocity components

$$\begin{aligned} u_+ &= u_1 + iu_2 \\ u_- &= u_1 - iu_2 \,. \end{aligned} \tag{11}$$

Defining

$$\partial_{\pm} = \frac{\partial}{\partial x_1} \pm i \frac{\partial}{\partial x_2}, \quad k_{\pm} = k_1 \pm ik_2 \tag{12}$$

(8) reads

$$\frac{\partial}{\partial t} \Psi - i H \Psi = 0 \tag{13}$$

where $\varphi = \begin{pmatrix} u_+ \\ u_- \\ p \end{pmatrix}$ and

$$H = \begin{pmatrix} -f & 0 & i\partial_+ \\ 0 & f & i\partial_- \\ \frac{iI\partial_-}{2} & \frac{iI\partial_+}{2} & 0 \end{pmatrix}. \tag{14}$$

The operator H has separable eigenfunctions

$$H \Psi^s_{n\underline{k}} + \omega \Psi^s_{n\underline{k}} = 0$$

where

$$\underline{\varphi}^{s}_{n\underline{k}} = \underline{\beta}^{s}\ \psi_n(x_3)\ e^{i(\underline{k}\cdot\underline{x}-\omega t)}\ . \qquad (15)$$

Solution of the eigenvalue problem gives the eigenfrequencies

$$\omega^{\pm} = \pm\ (f^2+\lambda_n k^2)^{\frac{1}{2}} \qquad \text{(gravity waves)} \qquad (16)$$

$$\omega^{o} = 0 \qquad \text{(geostrophic flow)} \qquad (17)$$

and the associated eigenvectors

$$\underline{\beta}^{s} = \begin{pmatrix} (\omega^s+f)k_+ \\ (\omega^s-f)k_- \\ \lambda_n k^2 \end{pmatrix}\ ,\quad s = \pm\ ;\quad \underline{\beta}^{o} = \begin{pmatrix} -k_+/f \\ k_-/f \\ 1 \end{pmatrix}\ . \qquad (18)$$

The sequence of eigenvalues λ_n (λ_n being a constant) decreases monotonically, the eigenvalue of the barotropic mode (λ_o) standing out several orders of magnitude above the eigenvalue of the internal modes ($n = 1,2,\ldots$).

To construct the general solution of (13), we shall involve only a partial decomposition of the solution into the three normal mode branches $s = \pm\ 0$, leaving the horizontal and vertical mode structure unresolved. To do this, $\underline{\beta}^{s}$ is interpreted in (15) as an operator, independent of the wavenumber and vertical mode index. This is achieved simply by replacing ik_i by $\frac{\partial}{\partial x_i}$ and λ_n by I. Introducing

$$\Omega^{s} = s(f^2-I\nabla^2)^{1/2} = sf\left(1-\frac{I\nabla^2}{2f^2}-\frac{I^2\nabla^4}{8f^4}-\ldots\right) \qquad (19)$$

$$\equiv s\ \Omega\ ;\quad \nabla^2 \equiv \frac{\partial^2}{\partial x_1^2}+\frac{\partial^2}{\partial x_2^2}$$

(15) can be written

$$H\ \underline{\beta}^s = -\underline{\beta}^s\ \Omega^s \qquad (20)$$

and defining the orthogonal projection operators $\tilde{\underline{\beta}}_s$, the general solution of (13) may be written

$$\underline{\varphi} = \sum_{s=\pm,0} \underline{\beta}^s\ \varphi^s \quad , \text{ where } \varphi^s = \tilde{\underline{\beta}}^s \cdot\ \underline{\varphi}.$$

The equation for the scalar field φ^s follows by multiplying (13) from the left with $\tilde{\underline{\beta}}_s$

$$\frac{\partial}{\partial t}\ \varphi^s + i\ s\ \Omega\ \ \varphi^s = 0\ . \qquad (21)$$

The equation of motion

$$\frac{\partial}{\partial t}\ \underline{\varphi} - i\ H\ \underline{\varphi} = \underline{q} \qquad (22)$$

in the presence of a forcing field $\underline{q} = \begin{pmatrix} q_+ \\ q_- \\ q_o \end{pmatrix}$ reduces similarly to

$$\frac{\partial}{\partial t}\ \varphi^s + i\ s\ \Omega\ \varphi^s = q^s \qquad (s=\pm,0) \qquad (23)$$

where

$$q^s = \tilde{\underline{\beta}}^s \cdot\ \underline{q}\ \ . \qquad (24)$$

3. THE HOMOGENEOUS PROBLEM.

The low frequency response for the forcing field $\underline{q}$ arising from quadratic interactions between high frequency waves is investigated. The correct solution for a rotating system is obtained by allowing for first order Coriolis effects in the high - frequency wave field which is treated as strictly homogeneous, but is allowed to vary slowly with time.

If the frequencies of the wave field are high compared with the inertial period, we can presumably take the mean value of the quadratic terms in (1) - (6), in considering the low - frequency response; this contribution arises from quadratic self interactions of waves with their complex conjugates. A rough estimation of the fluctuating term indicates that its contribution is comparatively negligible for low - frequency response.

Since the wave - field is statistically homogeneous, the mean forcing terms are independent of x_1, x_2 and the resulting velocity field must then be horizontal. Hence, equations (1) and (2) need only to be considered. Provided the wave - field is homogeneous and stationnary, (1) and (2) reduce to :

$$\frac{\partial}{\partial t}\,\underline{u} + \underline{f} \wedge \underline{u} = - \underline{f} \wedge \underline{u}^{st} \qquad (25)$$

$\underline{u}$ and $\underline{u}^{st}$ being horizontal. The Stokes current $\underline{u}^{st}$ is the difference between the mean Lagrangian and Eulerian currents;
$f = (0,0,f)$

$$\underline{u}^{st} = \underline{u}^{l} - \underline{u}^{e} \,. \qquad (26)$$

To quadratic order, one has

$$\langle u_i^l(\underline{r})\rangle = \langle u_i^e(\underline{r})\rangle + \langle \frac{\partial}{\partial x_j}\, u_i(\underline{r})\ \zeta_j(\underline{r})\rangle \qquad (27)$$

where $\underline{\zeta}$ is the displacement of a particle from its position of rest $\underline{r}$; $\underline{u}^e(\underline{x}) = \underline{u}^e(\underline{r})$ is the fluid velocity at the particle position $\underline{x}(\underline{r}) = \underline{r} + \underline{\zeta}(\underline{r})$.

For constant $\underline{u}^{st}$, the general solution of (27), (28) is

$$\underline{u} = \underline{u}^e = -\underline{u}^{st} + \underline{U} \cos ft - (\underline{z}_o \times \underline{U}) \sin ft \qquad (28)$$

where $\underline{z}_o$ is the unit vector upwards and $\underline{U}$ is a constant amplitude dependent on the initial value of u^e. The Lagrangian current, given by (26) is a purely rotary current.

If $\underline{u}^e = 0$ at $t = 0$, the solution corresponds to a step function onset of the high frequency wave field in a previously calm ocean. It is easy to show that the earth's rotation must usually be taken into account in considering the wave induced mass transport in the ocean.

By relaxing the condition of stationary of the wave field, it is found that a free undamped inertial oscillation remains in the fluid indefinitely, after the excitation has died away. The amplitude of the residual oscillation depends stronly on the detailed time history of the excitation, which might help to explain the observed variability of inertial oscillations generated by different storms. The order of magnitude of the response is comparable with observed inertial currents for generation by both surface and internal wave fields.

4. PHASE-MIXING.

In order to explain the observed damping of inertial oscillations, various idealisations of the model are relaxed, yielding a serie of phase-mixing processes which produce damping by vertical and horizontal dispersion.

An obvious idealisation in the present model is the statistical homogeneity of the driving wave field, an assumption which greatly simplified the analysis in the previous section. The

system was excited at zero wave number, a point of degeneracy at which all gravity modes have the same frequency $\pm$ f. Consequently, the vertical coordinate entered only as a parameter and there was no need for decomposition into modes.

If the fields are allowed to vary horizontally, the source function excites an ensemble of low - frequency modes of finite wave number, each of which rotates with a slightly different frequency. Velocity components of neighbouring modes which were originally excited in phase therefore gradually loose their phase relation; the field becomes "randomised". In the present problem, the essential dynamical features of the oscillations are governed by the transition from an initially coherent mode ensemble to the asymptotic random state.

The time scale of the phase - mixing process depends on the frequency separation between neighbouring modes. For large spatial scale of the driving wave field, the frequencies of the excited modes are close to f and the time scale T of the phase-mixing is large compared with f. The solution is hence expanded with respect to the parameter $\frac{t}{T}$ which avoids mode decomposition and is applicable for arbitrary stratification.

PHASE-MIXING DUE TO INHOMOGENEOUS FIELDS.

For a weakly inhomogeneous wave field, the source vector of the field equation (22) takes the form

$$\underline{q} = f \begin{pmatrix} -iu_+^{st} \\ i\,u_-^{st} \\ 0 \end{pmatrix} + \begin{pmatrix} \frac{\partial}{\partial x_\alpha} & T_{\alpha+} \\ \frac{\partial}{\partial x_\alpha} & T_{\alpha-} \end{pmatrix} \qquad \alpha = 1,2. \qquad (29)$$

The second vector represents the divergence of the interaction stress tensor, $T_{\alpha\beta} = \langle u_\beta^2 \rangle\, \delta_{\alpha\beta} - \langle u_\alpha u_\beta \rangle$ which vanished before on account to the homogeneity, but is non zero for slowly

varying field (Hasselmann,1970). The third component of $\underline{q}$ is irrelevant for the generation of inertial oscillations.

Using (29), equation (23) can be integrated to yield the inertial current response

$$\varphi^s(\underline{x},t) = e^{-is\Omega t}\ \varphi^s_{t=0} + \int_o^t e^{-is\Omega(t-t')} q^s(\underline{x},t')dt' \ . \quad (30)$$

A convergent serie is then obtained by expanding (30) with respect to the perturbed frequency operator X_w

$$\Omega = f + X_w = f - \frac{I^2}{2f} - \frac{I^2\,4}{8f^3} - \ldots \ . \quad (31)$$

For $X_w = 0$, one finds the solution for a homogeneous wave field. The deviation from this solution is governed by the phase-mixing operator $X_w.X_w \ll \Omega \simeq f$ for small inhomogeneities.

In the case $q^s = 0$, (i.e. we considered the evolution of the inertial oscillations after the generation wave field has passed by), equation (30) represents an inertial oscillation with slowly varying amplitude and phase; the rate of change of phase can be interpreted as a frequency shift. The convergence of the expansion of (30) can be analysed in the normal-mode viewpoint. Quantitative estimates can be found in (I), in the simple case $N^2 = \text{const}$.

Since $X_w \ll \Omega$, it is normally sufficient to retain the first term in the expansion (31). This could also have been derived using the standart formulae for eigenvalue perturbation. If the operator H in the eigenvalue equation (13) is of the form

$$H = H_o + H' \quad (32)$$

where $H' << H_o$, the (negative) eigenvalue Ω^s can be expanded in a serie

$$\Omega^s = \Omega_o^s + \Omega_1^s + \Omega_2^s + \ldots \qquad (33)$$

where Ω_o^s is an eigenvalue of H_o and

$$\Omega_1^s = - \underline{\tilde{\beta}}_o^s \, H' \, \underline{\beta}_o^s \; ; \quad \Omega_2^s = \ldots \qquad (34)$$

Here, $\underline{\beta}_o^s$, $\underline{\tilde{\beta}}_o^s$ refer to the eigenvectors and the orthogonal vectors of the unperturbed operator H_o. In our case

$$H_o = \begin{pmatrix} -f & 0 & 0 \\ 0 & f & 0 \\ 0 & 0 & 0 \end{pmatrix}$$

$$H' = \begin{pmatrix} 0 & 0 & i\partial_+ \\ 0 & 0 & i\partial_- \\ \frac{iI\partial_-}{2} & \frac{iI\partial_+}{2} & 0 \end{pmatrix} \qquad (35)$$

and $\Omega^s = sf$. The vectors $\underline{\tilde{\beta}}_o^s = \underline{\beta}_o^s$ are the three unit vectors parallel to the coordinate axes. The eigenvectors $\underline{\beta}^s$ can be similarly expanded but, in the lowest - order phase - mixing approximation, one can set $\underline{\beta}^s = \underline{\beta}_o^s$ and need only the perturbation of the eigenoperator. This approach is used to consider further perturbation which destroy the zero wave number and produce phase-mixing.

PHASE-MIXING DUE TO THE HORIZONTAL CORIOLIS COMPONENT.

The analysis (I) shows that the horizontal Coriolis parameter $\hat{f}$ cannot always be neglected, particularly for weak stratifications and large lateral scales typical of deep-ocean conditions. The inclusion of $\hat{f}$ presents no computational difficulty.

PHASE-MIXING DUE TO WAVE-GUIDE INHOMOGENEITIES.

Lateral variations of the wave-guide parameters f, N^2 and h can be treated as perturbations if the lateral length scales are large compared with the ocean depth. The classical methods of geometrical optics are not applicable, since we are concerned with an ensemble of modes, rather than a single mode. Thus slow wave-guide variations again result in a diffusion- type behaviour. Detailled investigation (I) leads to the conclusion that planetary effects (f variation) can be neglected compared with the lateral variations of the wave-guide or the field.

PHASE-MIXING DUE TO NON LINEAR INTERACTIONS WITH GEOSTROPHIC CURRENTS.

Since the geostrophic currents are time independent in the linear, f-plane approximation, the quadratic interaction with an inertial oscillation yields a perturbation which is linear in the inertial oscillation, with a time-independent coefficient.

The phase-mixing operator for the geostrophic interactions follows from (34)

$$X_g^s = i \left[-U_j \frac{\partial}{\partial x_j} - \frac{(\partial_{-s} U_s)}{2} + \frac{(\frac{\partial}{\partial x_3} U_s) I_a \partial_{-s}}{2} \right] \quad (s=\pm) \qquad (36)$$

where $\underline{U}$ is the heostrophic current and $I_a = \int_{-h}^{x_3} dx_3'$. There is no summation over s.

The contribution to phase-mixing from this process appears at present marginal (I).

5. A NUMERICAL EXAMPLE.

The decay of an inertial oscillation due to lateral inhomogeneities of the initial field distribution has been computed using the phase - mixing expansion (30), (31); the initial distribution was taken as axisymmetric Gaussian in the horizontal coordinates, with an exponential vertical profile corresponding to generation by surface waves. The numerical values were adjusted to agree with observations at the site near Bornholm (Tomczak Jr., 1969).

Detailled discussion and figures will not be reproduced here and can be found in (I). In fact, many of the gross features of inertial oscillations observed in the Baltic were reproduced. These follow largely from a surface - wave source and are independent of the form of the decay process.

The time scale of the computed decay was not inconsistent with measurements, but the details were not everywhere convincing. Inclusion of lateral wave - guide inhomogeneities would probably remedy the shortcomings of the model.

6. CONCLUSIONS.

Estimates of the non linear generation of inertial oscillations by high frequency gravity waves agree in order of magnitude with inertial currents observed both near the surface and in the interior of the ocean. Surface gravity waves can drive inertial oscillations either through horizontal stresses (radiation stresses) or the vertical shear stress induced by the rotation of the earth. For horizontal scales smaller than 100 km, the horizontal stress is more important, whereas the shear stress dominates for larger scales. In the case of internal gravity waves, the horizontal stress is always negligible; estimates of the shear stress based on observed internal wave spectra yield values

comparable with shear stresses for surface waves.

The decay of inertial oscillations due to phase-mixing has been investigated for five processes. Lateral inhomogeneities of the inertial oscillation and lateral wave-guide variations yield comparable decay rates in reasonable agreement with observations; the influence of the horizontal component of the Coriolis vector and interactions with geostrophic currents appear to be of marginal significance; planetary effects are negligible.

REFERENCES.

Hasselmann, K., (1970) Wave driven inertial oscillations. Submitted to J. Geophys. Fluid Dynamics.

Hasselmann, K., (1970) On the mass and momentum transfer between short gravity waves and larger-scale motions (submitted for publication).

Longuet-Higgins, M.S. and R.W. Stewart, (1964) Radiation stresses in water waves. Deep-Sea Res., 11, 529-562.

Tomczak, M., Jr., (1969) "Uber interne Trägheitsbewegungen in der westlichen Ostsee", Deutsche Hydr. Zeitschr. 22, 158-162.

Ursell, F., (1950) On the theoretical form of ocean swell on a rotating earth, Monthly Not. Roy. Astron. Soc. Geophys. Suppl. 6, 1-8.

Webster, F., (1968) Observations of inertial-period motions in the deep sea. Rev. Geophys. 6, 473-490.

THE EFFECTS OF HORIZONTAL DENSITY GRADIENTS AND SLOPING BOUNDARIES ON THE PROPAGATION OF INERTIAL-INTERNAL WAVES

By Christopher N.K. Mooers
Department of Oceanography
Oregon State University, U.S.A.

INTRODUCTION -

Strong horizontal density gradients, or, equivalently, baroclinic-geostrophic flows, occur in many regions of the ocean, especially in oceanic fronts and boundary currents. Inertial-internal waves, i.e., waves under the influence of both the earth's rotation and the ocean's density stratification, are also prominent in coastal regions. Thus, it is of interest to determine the influence of horizontal density gradients and sloping boundaries on inertial-internal waves.

THE GOVERNING EQUATION -

The following assumptions are made :

1) the fluid is inviscid, non-diffusive, and incompressible.

2) the wave motion is linear.

3) the effects of the horizontal component of the Coriolis force and of the earth's sphericity are negligible; hence, it is valid to neglect the latitudinal variations of the Coriolis force and to use Cartesian coordinates.

4) the Boussinesq approximation is valid.

5) the mean flow, $\underline{\bar{V}}$, consists of an axial component oriented along the y-axis and the cross-stream components are neglected, i.e., $\underline{\bar{V}} = (0, \bar{v}, 0)$.

6) the mean flow is in hydrostatic and geostrophic equilibrium, i.e., the so-called thermal wind relation applies :

(*) Presently a NATO Postdoctoral Fellow · in the Department of Oceanography - University of Liverpool - Liverpool 3, England.

$$f\bar{v}_z = \frac{-g\bar{\rho}_x}{\rho_o} = M^2 = -sN^2 \ ,$$

where f is the vertical component of the Coriolis force,

g is the gravitational acceleration oriented along the z-axis, which is positive upwards,

ρ_o is the space-time-averaged mass density,

$s = \left|\frac{dz}{dx}\right| \bar{\rho}$ is the vertical slope of an isopycnal in the vertical plane transverse to the mean flow and the x-axis is the horizontal coordinate axis normal to the mean flow,

$N^2 = \frac{-g\bar{\rho}_z}{\rho_o}$ is the square of the Väisälä-Brunt frequency, and

M^2 ⟵ is the horizontal analogue of N^2.

The above assumptions yield the following system of equations :

the momentum equations :

$$(1.1)\quad D(u) - f\,v = -\pi_x \ ,$$

$$(1.2)\quad D(v) + (f+\bar{v}_x)\,u + \bar{v}_z w = -\pi_y \ ,$$

$$(1.3)\quad D(w) - b = -\pi_z$$

the equation of continuity :

$$(1.4)\quad u_x + v_y + w_z = 0$$

the bouyancy equation :

$$(1.5)\quad D(b) + M^2 u + N^2 w = 0,$$

where $v = (u,v,w)$ is the fluctuating component of the velocity;

$D(\ ) = (\ )_t + \bar{v}(\ )_y$ is the total time derivative;

$\tilde{\rho}$ is the total mass density field, which is partitioned such that

$$\tilde{\rho} = \rho_o + \bar{\rho}(x,z) + \rho(x,z,t),$$

where $\bar{\rho}$ and $\rho << \rho_o$;

$\pi = \dfrac{\rho+\rho_o gz}{\rho_o}$ is the fluid pressure, ρ, per unit mass density, which incorporates the Boussinesq approximation;
and

$b = \dfrac{-g\rho}{\rho_o}$ is the bouyancy.

Postponing discussion of the full three-dimensional case, the quasi-two-dimensional case, i.e., where $(\ )_y = 0$ though v is not neglected, is first examined. In this case, a stream function, ψ, exists such that $u = -\psi_z$ and $w = \psi_x$. Assuming simple harmonic time dependence, i.e., all fluctuating variables proportional to $e^{i\sigma t}$, system (1) reduces to the governing equation, (2) :

$$(2a) : (N^2-\sigma^2)\psi_{xx} - 2M^2\psi_{xz} - (\sigma^2-\sigma_f^2)\ \psi_{zz} = 0$$

or

$$(2b) : \psi_{xx} + (\lambda_1+\lambda_2)\ \psi_{xz} + \lambda_1\lambda_2\psi_{zz} = 0$$

or

$$(2c) : \psi_{\eta\zeta} = C(\psi_\eta, \psi_\zeta) ,$$

where $\sigma_f^2 = f(f+v_x)$ is the square of the effective inertial frequency,

$$\lambda_1, \lambda_2 = \frac{-M^2 \pm [M^4+(N^2-\sigma^2)(\sigma^2-\sigma_f^2)]^{\frac{1}{2}}}{(N^2-\sigma^2)}$$

are the slopes of the characteristics,

η, ζ are the characteristic coordinates,

$C(\psi_\eta, \psi_\zeta)$ is a function of ψ_η, ψ_ζ, and the partial derivatives of λ_1 and λ_2 and vanishes if λ_1 and λ_2 are constant.

Equation (2) is exact under the constraint that $\bar{\rho}$ and $\bar{v}$ satisfy the thermal wind relation.

From (2), the y-component of the vorticity, $\omega^{(y)}$, is

$$\omega^{(y)} = u_z - w_x$$

$$= -\nabla^2 \psi$$

$$= -\left[\frac{N^2}{\sigma^2}\,\psi_{xx} + \frac{2M^2}{\sigma^2}\,\psi_{xz} + \frac{f^2}{\sigma^2}\,\psi_{zz}\right] .$$

Hence, f, M, and N all contribute to the rotationality of the motion. In a similar way, they also contribute to the effective potential energy of the wave.

QUALITATIVE PROPERTIES -

A thorough discussion of the qualitative properties is given in Mooers (1970b) and only a limited discussion is given below. First, equation (2) is spatially hyperbolic for $\sigma_l < \sigma < \sigma_u$, i.e., for σ in the passband for free waves, where

$$\sigma_l^2 \approx \sigma_f^2 - s^2 N^2$$

and

$$\sigma_u^2 \approx N^2(1+s^2)$$

under the assumption that $\sigma_f^2 << N^2$. Since, for western and eastern boundary currents, $s \sim 10^{-3}$ to 10^{-2}, $N^2 \sim 10^{-5}$ to 10^{-4} $\sec^{-2}$, and $\sigma_f^2 \sim 10^{-8}$ $\sec^{-2}$, then $\sigma_u^2 \approx N^2$ and σ_l^2 can be appreciably less than σ_f^2. Hence, horizontal density gradients are likely to be far more important for low frequency than for high frequency inertial-internal waves. In fact, when $\sigma_f^2 = s^2 N^2$, $\sigma_l^2 = 0$ without approximation. Thus, the passband extends to

the zero frequency for $|s| = s_c = \frac{\sigma_f}{N}$, the critical slope, and to imaginary frequencies for $|s| > s_c$. Insight into the significance of s_c is obtained from the examination of the frontal Richardson number, FRN :

$$FRN = \frac{N^2}{(v_z)^2}$$

$$= \frac{f^2}{s^2 N^2}$$

$$\xrightarrow[s \to s_c]{} \frac{1}{(1+R_o)} ,$$

where $R_o = \frac{\bar{v}_x}{f}$ is the Rossby number, with sign, for $\bar{v}$. Thus, as s becomes critical, FRN becomes critical unless $R_o \simeq -1$; in which case the flow is barotropically unstable anyway.

Second, the passband divides into the three sub-bands summarized below for $s > 0$:

anomalously low frequencies (a.l.f.)	normal frequencies (n.f.)	anomalously high frequencies (a.h.f.)
$\sigma_l < \sigma \leq \sigma_f$	$\sigma_f \leq \sigma \leq \sigma_N$	$\sigma_N \leq \sigma < \sigma_u$
$\lambda_1 > 0$	$\lambda_1 > 0$	$\lambda_1 < 0$
$\lambda_2 > 0$	$\lambda_2 < 0$	$\lambda_2 < 0$, where $\sigma_N = N$.

The a.l.f. and a.h.f. are anomalous in two senses :

1) the fact of their existence,

and

2) the signs of λ_1 and λ_2 are the same; thus, all "wave beams" are oriented upwards in the a.l.f. and downwards in the a.h.f.

It also follows that $|\lambda_1| \neq |\lambda_2|$ except for $\sigma = \sigma_l$ or σ_u. Alternatively, the dispersion curves, Figure 1, imply distortion of the phase and group velocities for up-going and down-going "wave fronts" when $s \neq 0$. (Note : "wave fronts" and "wave beams" are orthogonal for inertial-internal waves.) It is necessary to realize that σ_f, σ_N, and s, and thus σ_l and σ_u, vary spatially in a frontal zone or baroclinic flow. Hence, when $s \neq 0$, not only is the passband altered but refractive effects, as indicated by the asymmetrization and variation of the slopes of the characteristics, occur as well. The refractive effects lead to phenomena termed frontal-blocking, frontal-trapping, and beam-splitting, c.f. Mooers (1970b).

Third, the primary effect of sloping boundaries on inertial-internal waves is summarized by the criticality, T, of the bottom slope, m :

$$T = \frac{-\lambda_2 + m}{(\lambda_1 - m)} ,$$

where $m \geq 0$ has been assumed. The amplification of wave amplitude and that of wave number upon reflection from a sloping boundary are proportional to T. There are three cases for T (Sandstrom, 1966) :

1) $T > 1$, subcritical or transmissive bottom slope;

2) $T < 1$, supercritical or reflective bottom slope;

and

3) $T \to \infty$, critical bottom slope, a degenerate case.

It is straightforward to prove that $T(s) < T(0)$ for $s > 0$ and $\sigma < N$ or $s < 0$ and $\sigma > N$. Hence, the criticality is reduced for σ in either the a.l.f. or n.f. when the slope of the bottom and that of the isopycnals have the same sign; the converse is true for σ in the a.h.f.

THE SOLUTION FOR CONSTANT COEFFICIENTS -

In the case of constant coefficients, equation (2c) becomes :

$$\phi_{\eta\zeta} = 0 \ ,$$

where $\eta = z - \lambda_1 x$ is the upgoing characteristic and $\zeta = z - \lambda_2 x$ is the downgoing characteristic. The general solution is then

$$\phi = \frac{1}{(\lambda_1 - \lambda_2)} \left[\lambda_1 F(\zeta) - \lambda_2 F(\eta)\right] \cos(\sigma t)$$

$$+ \left[G(\zeta) - G(\eta)\right] \cos(\sigma t + \Phi) \ ,$$

where F and G are the Cauchy, or initial, data which have at least piecewise continuous derivatives of the first order. Alternatively,

$$\phi = I\,U(\eta;t) + I\,D(\zeta;t) \ ,$$

where

$$I\,U = \frac{-1}{(\lambda_1 - \lambda_2)} \left[\lambda_2 F(\eta)\cos(\sigma t) + G(\eta)\cos(\sigma t + \Phi)\right.$$

is the upgoing Riemann invariant and

$$I\,D = \frac{1}{(\lambda_1 - \lambda_2)} \left[\lambda_1 F(\zeta)\cos(\sigma t) + G(\zeta)\cos(\sigma t + \Phi)\right.$$

is the downgoing Riemann invariant. The boundary conditions need only be applied to complete the solution, but, first, the geometry of the problem is examined.

A fundamental horizontal wavelength, L, exists only for waves with σ in the n.f. For uniform depth, H_o,

$$L(s) = \frac{H_o}{\lambda_1} + \frac{H_o}{(-\lambda_2)}$$

$$= \left[\frac{\lambda_1 - \lambda_2}{-\lambda_1 \lambda_2} \right] H_o$$

$$= \frac{[s^2 \mu^2 + \lambda_o^2]^{\frac{1}{2}}}{\lambda_o^2} \; 2H_o$$

$$\geqq L(0) = \frac{2H_o}{\lambda_o} \; ,$$

where

$$\lambda_o = \left[\frac{\sigma^2 - \sigma_f^2}{N^2 - \sigma^2} \right]^{\frac{1}{2}}$$

and

$$\mu = \frac{N^2}{(N^2 - \sigma^2)} \; .$$

Thus, for $s \neq 0$, the fundamental horizontal wavelength is increased regardless of the sign of s. Figure 2 illustrates the geometry of the limiting characteristics over a fundamental wavelength and the field of lines of constant phase, which shows zones of relative acceleration and retardation of wave fronts. In a similar fashion, for a subcritical, uniformly sloping bottom boundary, a fundamental horizontal wavelength, L_n, exists for a denumerable infinity of geometrically similar, contiguous sectors, $\{R_n;\ n : \text{interger}\}$, where

$$L_1(s) = \frac{H}{\lambda_1} \frac{(\lambda_1 - \lambda_2)}{(m - \lambda_2)}$$

$$= \left[\frac{-\lambda_2}{-\lambda_2 + m} \right] L(s)$$

$$\leqq L(s) \; ,$$

$$L_n(s) = (\gamma^{-1}\, T(s))^{1-n}\, L_1(s)\ ,$$

and

$$\gamma = -\frac{\lambda_2}{\lambda_1}\ .$$

Note : $L_n(s) \xrightarrow[n \to \infty]{} 0$ for the subcritical case.

When

$$s = 0,\ L_1(0) = \left[\frac{\lambda_o}{\lambda_o + m}\right] L(0),\ \gamma = 1,$$

and

$$L_n(0) = (T(0))^{1-n}\, L_1(0).$$

Figure 3 is analogous to Figure 2 and is for the case $s = 0$ and $m \neq 0$. Again, there are zones of relative acceleration and retardation of wave fronts over an effective wavelength. The case of $s \neq 0$ and $m \neq 0$ is an obvious generalization of Figures 2 and 3.

Since a fundamental wavelength exists, it is natural to expect the existence of a set of normal modes. In fact,

$$\psi \sim S = \sum_n a_n(t)\, c_n(x,z) + \sum_n b_n(t)\, s_n(x,z),$$

where

$$c_n(x,z) = \cos\left[\frac{k_n}{\lambda_2}(\zeta + H_o) - \cos\left(\frac{k_n}{\lambda_1}(\eta + H_o)\right)\right],$$

$$s_n(x,z) = \sin\left[\frac{k_n}{\lambda_2}(\zeta + H_o)\right] - \sin\left[\frac{k_n}{\lambda_1}(\eta + H_o)\right],$$

and

$$k_n = \frac{2\pi n}{L(s)}\ ,\ n : \text{integer}\ .$$

(The rigid boundary condition, i.e., $\psi = 0$ at $z = 0$ and $z = H_o$, has been imposed for simplicity.) Each mode is a strict (strong)

solution of (2) and the boundary conditions and has continuous partial derivatives of all orders. Yet, because ϕ has discontinuous first order normal derivatives across $\eta = -H_o, \zeta = 0$, etc.., ϕ is the general (weak) solution and S does not converge to ϕ. Further, when $s \neq 0$, the normal modes are non-separable in x and z, and they are not orthogonal over the interval $-H_o \leq z \leq 0$. Hence, it is awkward to expand the Cauchy data in terms of the normal modes. Similar effects occur in the case $s = 0$ and $m \neq 0$, where the discontinuous derivatives are due to the discontinuity in the bottom slope at the junction of a region of uniform depth and one of uniform bottom slope. Thus, several reasons have been presented for continuing with the analysis of the general solution.

The general solution will be constructed for the case $s \neq 0$ and $m \neq 0$. Again, rigid boundary conditions are applied for simplicity. They are now applied at $z = 0$ and $z = -H_o + mx$, $x \geq 0$. The solution for R_1 is constructed, and then the generalization to R_n follows by geometrical similarity. Several equivalent ways of carrying out the calculation have been found. The simplest and most concise is given below. First it is useful to recognize that each R_n has seven sub-sectors, I, II, ..., VII, in each of which the solution has a distinctive form. Referring to Figure 3 for the definition of the sub-sectors, writing the solution for each sector in terms of its Riemann invariants, and applying the boundary conditions sequentially to determine the unknown Riemann invariants, the solution for R_1 is written as

$$\phi_I = IU_I(\eta) + ID_I(\zeta) = IU(\eta) + ID(\zeta),$$

where IU and ID are as defined earlier and the time dependence is implicit;

$$\phi_{II}\ IU_{II}(\eta) + ID_{II}(\zeta) = IU(\eta) - IU(-\nu^{-1}\zeta)$$

$$\phi_{III} = IU_{III}(\eta) + ID_{III}(\zeta) = - ID[-(1+T)H_o - T\eta] + ID(\zeta)$$

$$\psi_{IV} = IU_{IV}(\eta) + ID_{IV}(\zeta) = -ID[-(1+T)H_o - T\eta] - IU(-\gamma^{-1}\zeta)$$

$$\psi_{V} = IU_{V}(\eta) + IF_{V}(\zeta) = -ID[-(1+T)H_o - T\eta]$$

$$+ID[-(1+T)H_o + \gamma^{-1}T\zeta]$$

$$\psi_{VI} = IU_{VI}(\eta) + ID_{VI}(\zeta) = IU\{\gamma^{-1}[(1+T)H_o + T\eta]\} - IU(-\gamma^{-1}\zeta)$$

and

$$\psi_{VII} = IU_{VII}(\eta) + ID_{VII}(\zeta)$$

$$= IU\{\gamma^{-1}[(1+T)H_o + T\eta]\} + ID[-(1+T)H_o + \gamma^{-1}T\zeta] .$$

It is a simple matter to verify ψ_{VII}; since

$$\psi_{VII}\Big|_{x=L_1} = IU(\gamma^{-1}T\ z) + ID(\gamma^{-1}T\ z),$$

$$\text{where } -\nu T^{-1} H_o \leq z \leq 0 ,$$

then $\psi_{VII}|_{x=L_1} \sim \psi_I|_{x=0}$, differing only in the fact that the argument of ψ_{VII} has been fractionally stretched in an amount inversely proportional to the fractional reduction in depth between $x = 0$ and $x = L_1$. For R_2, the solution is constructed in an analogous fashion, using ψ_{VII} as the new ψ_I. The generalization to the solution in R_n is then obvious.

THE THREE-DIMENSIONAL CASE -

A ray theory has been applied to the three-dimensional case in Mooers (1970b). A wave number vector, $\underline{k} = (k,l,m)$, and the intrinsic, or Doppler-shifted frequency, $\sigma = \sigma_o - \bar{v}_1$, where σ_o is the wave frequency, are introduced. Only the principal results are summarized below :

1) $$\frac{dk}{dt} = \bar{v}_x l \ ,$$

$$\frac{dl}{dt} = 0 \ ,$$

$$\frac{dm}{dt} = \bar{v}_z l \ ,$$

$$\frac{d\sigma_o}{dt} = 0 \ ,$$

and

$$\frac{d\sigma}{dt} = - \left[c_g^{(x)} \bar{v}_x + c_g^{(z)} \bar{v}_z \right] l \ ,$$

where t is travel time of a wave packet along a ray path, the group velocity is

$$\underline{c}_g = \left(c_g^{(x)}, c_g^{(y)}, c_g^{(z)} \right) \ ,$$

and the mean flow is assumed time independent.

2) Hence, l and σ_o are invariant, while $k \to \bar{v}_x t$ and $m \to \bar{v}_z t$ for large t <u>if</u> the ray-path-averaged $\bar{v}_x$ and $\bar{v}_z$ are non-vanishing. It is a consequence of this result that

$$\underline{c}_g \xrightarrow[t \to \infty]{} (0, \bar{v}, 0)$$

and, thus, that $\frac{d\sigma}{dt} \xrightarrow[t \to \infty]{} 0$ i.e., σ has a limiting value.

Further, <u>k</u> is turned into the vertical plane transverse to the mean flow and is oriented such that

$$\left. \frac{dz}{dx} \right|_\theta = \frac{-\theta_x}{\theta_z}$$

$$= \frac{-k}{m}$$

$$= \frac{-\bar{v}_x}{\bar{v}_z}$$

$$= \frac{dz}{dx}\Big|_{\bar{v}} \quad , \quad \text{i.e., the lines of constant phase,}$$

0, essentially coincide with the isotachs of $\bar{v}$. This result implies that the lines of constant phase tend to "wrap" themselves around the core of a geostrophic flow and to converge to the center of the core. Thus the group and phase velocities are also orthogonal, a basic property of inertial-internal waves, in the limit of large t.

3) The limiting value, σ_∞, of σ can be readily evaluated. In fact,

$$\sigma_\infty^2 = \left[\frac{N^2(\bar{v}_x)^2 - 2M^2\bar{v}_x\bar{v}_z + \sigma_f^2(\bar{v}_z)^2}{(\bar{v}_x)^2 + (\bar{v}_z)^2}\right]^{\frac{1}{2}} .$$

If $\bar{v}_x = 0$, $\sigma_\infty = f$; if $\bar{v}_z = 0$, $\sigma_\infty = N$.

Alternatively, with $\lambda = \frac{dz}{dx}\Big|_{\bar{v}}$,

$$\sigma_\infty^2 = \frac{N^2}{(1+\lambda^2)}\,(\lambda^2 + 2\lambda s + S_c^2)$$

and $\sigma^2 < 0$ if $|S| > |S_c|$ and $|\lambda+S| < (S^2-S_c^2)^{\frac{1}{2}}$.

Again, a supercritical isopycnal slope is a necessary condition for wave instability.

SUMMARY -

The Three-dimensional case can be employed to evaluate the significance of the quasi-two-dimensional case (l=0). If $l \neq 0$, the wave is refracted into the transverse in any event, and the intrinsic frequency is shiffted to a limiting value.Thus, for a frontal zone or geostrophic flow, a wave, in the case of $l = 0$, encounters, in a sense, an "open window", even though refractive effects in the transverse plane may still significantly affect the propagation of the waves. Though the limit of $t \rightarrow \infty$ is farfetched, and though the other idealizations employed deviate significantly from nature, the theoretical evidence is mounting for the existence of significant interactions between inertial-internal waves and geostrophic flows. The most important question remains open : is there appreciable energy exchange between inertial-internal waves and "mean" flows ?

BIBLIOGRAPHY -

MOOERS, Christopher N.K.(1970a) :
The Interaction of an Internal Tide with the Frontal Zone in a Coastal Upwelling Region. Ph.D.Thesis, Oregon State University, Corvallis, Oregon, 480 numb. leaves.

MOOERS, Christopher N.K.(1970b) :
The Effects of Horizontal Density Gradients on the Propagation of Inertial-Internal Waves. Geophysical Fluid Dynamics (submitted).

SANDSTROM, Helmuth(1966) :
The Importance of Topography in Generation and Propagation of Internal Waves. Ph.D.Thesis, University of California, San Diego, California, 105 numb.leaves.

LIST OF FIGURE CAPTIONS -

Figure 1. Dispersion Diagram (k>0)

downgoing and upgoing waves — — — , s = 0 ;

downgoing wave — . — . — . — , s > 0 ;
and
upgoing wave ———————— , s > 0 .

Figure 2. Wave Structure (s>0,m=0)

a. Geometry of the Characteristics

— . — . — . — , s = 0, m = 0 ;

and — — — — — , s > 0, m = 0 .

b. Lines of Constant Phase

———————— , s > 0, m = 0.

Figure 3. Wave Structure (s=0,m>0)

a. Geometry of the Characteristics

— — — — , s = 0, m > 0.

b. Lines of Constant Phase

———————— , s = 0, m > 0.

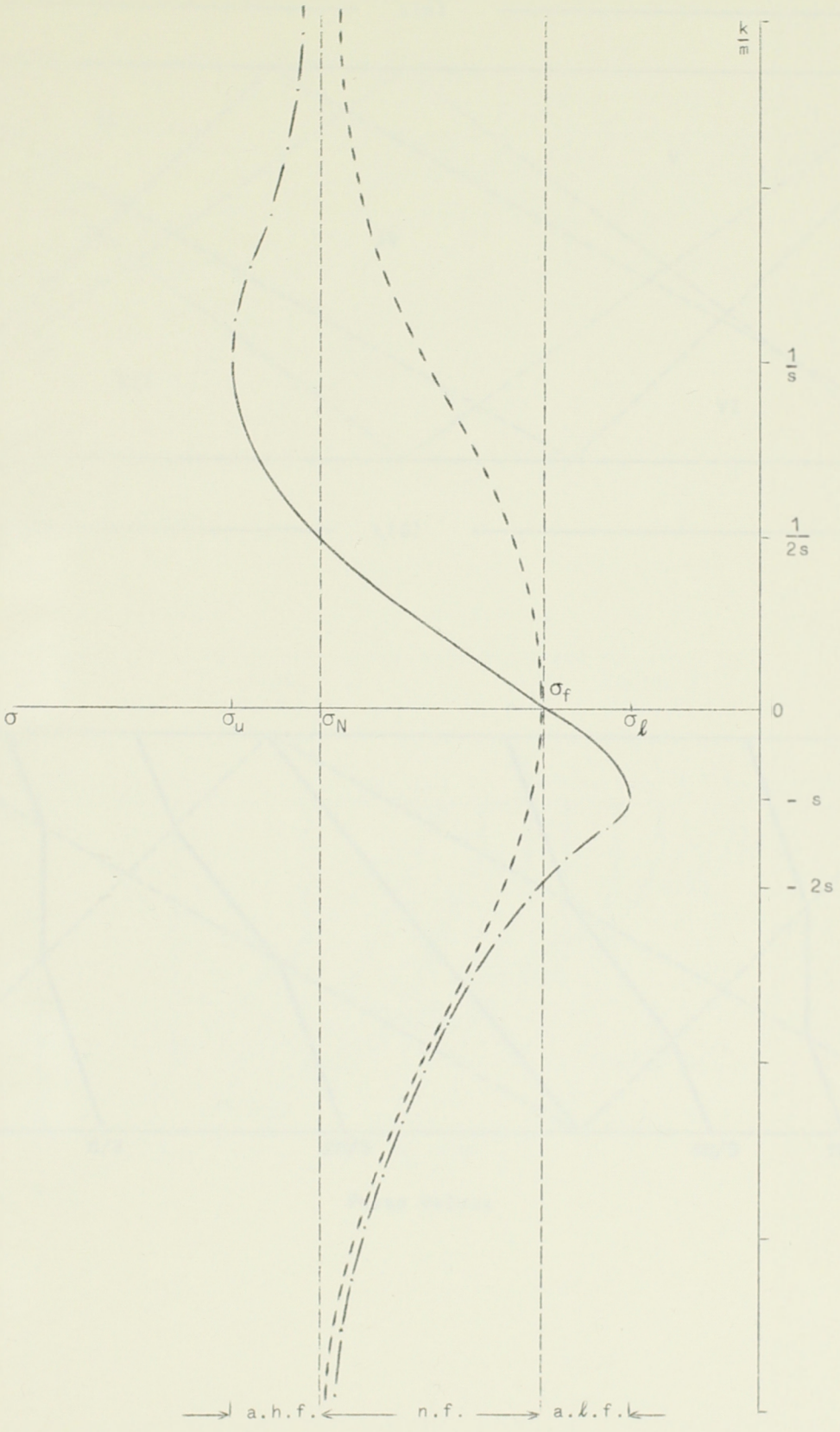

Fig. 1.

a.

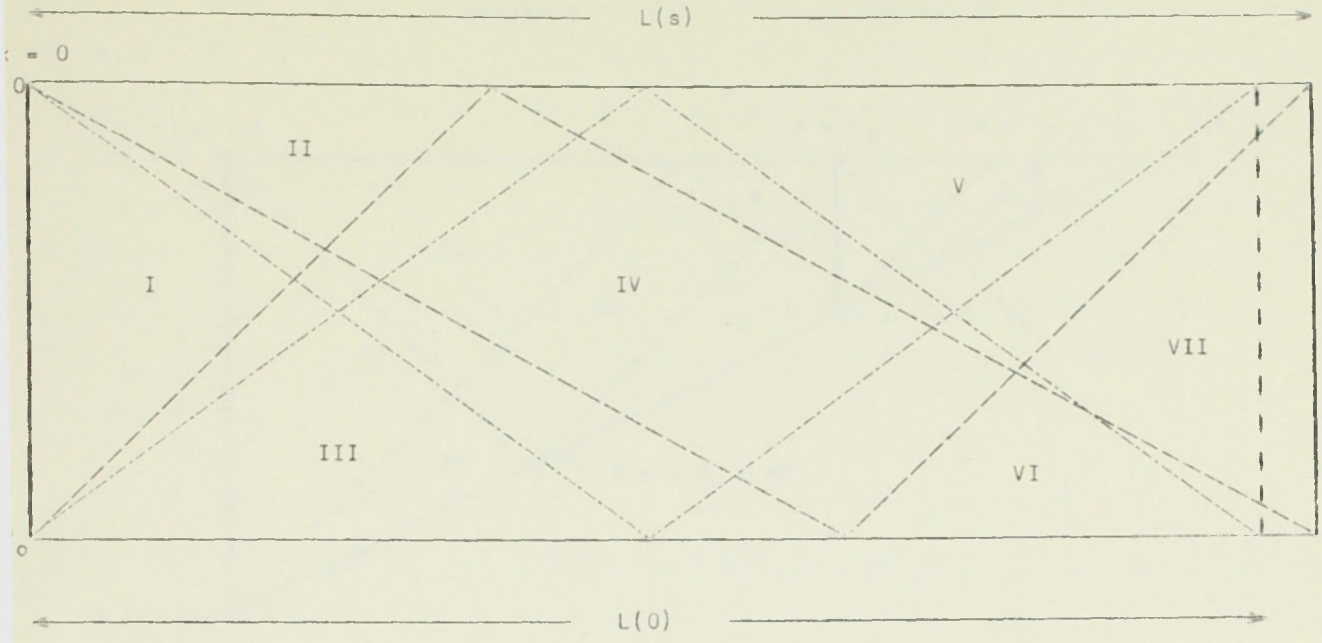

b.

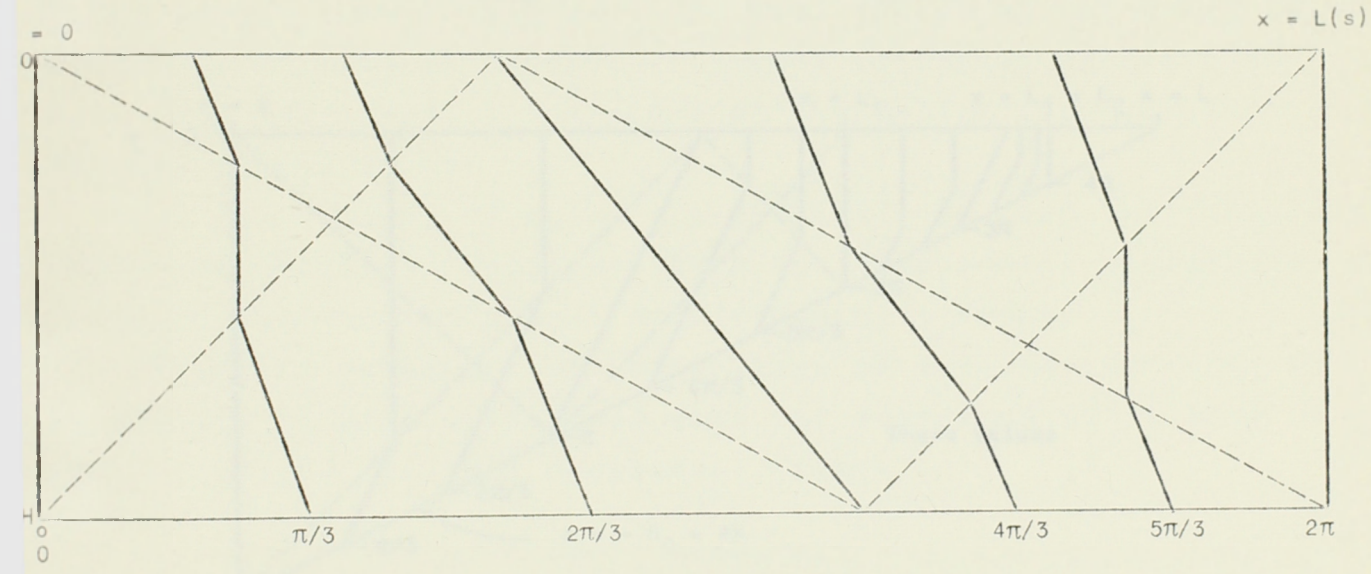

Phase Values

Fig. 2.

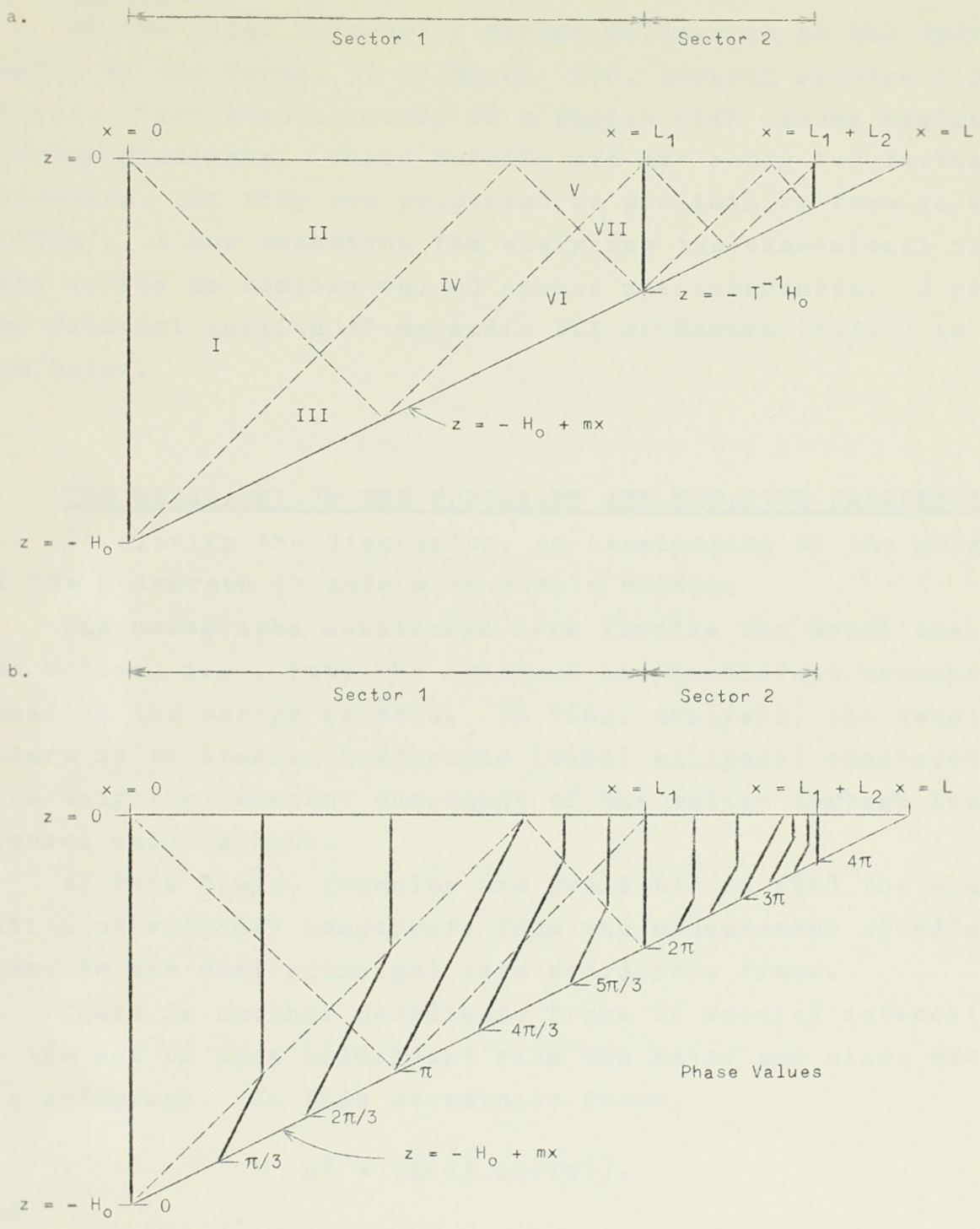
a.
Sector 1
Sector 2
x = 0
x = L1
x = L1 + L2
x = L
z = 0
I
II
III
IV
V
VI
VII
z = - T^-1 H0
z = - H0 + mx
z = - H0
b.
Sector 1
Sector 2
x = 0
x = L1
x = L1 + L2
x = L
z = 0
π/3
2π/3
π
4π/3
5π/3
2π
3π
4π
Phase Values
z = - H0 + mx
z = - H0
0

Fig. 3.

APPENDIX -

At the Liège University Second Colloquium on the Hydrodynamics of the Ocean, 17-20 March 1970, several spectra were displayed. They were observed in a region with strong horizontal density gradients. These results are not ready for further publication, but they are presented in preliminary form in Mooers (1970a). A new technique for analyzing two-dimensional velocity time series as complex-valued series was introduced. A copy of the relevant section of Appendix III of Mooers (1970a) is included below.

THE GEOGRAPHY OF THE HODOGRAPH AND NEGATIVE FREQUENCIES -

To clarify the discussion, an examination of the geography of the hodograph is made with simple models.

The hodographs considered here involve the total energy of the motion, i.e., both the coherent and incoherent components, based on the energy spectra. In tidal analysis, the usual procedure is to examine hodographs (tidal ellipses) constructed from only the coherent component of the motion through least squares calculations.

At this stage, formulae are available to find the transformation of velocity components from the measurement coordinate frame to the semi-principal axis coordinate frame.

There is another coordinate frame of special interest; it is the set of axes coincident with the major and minor axes of the hodograph. In this coordinate frame,

$$u'' = (A+C)\cos(\sigma t).$$

and

$$v'' = (A-C)\sin(\sigma t) ,$$

where A and C are amplitude factors. A and C can assume any non-negative, finite value. The eccentricity, ε , is $\varepsilon = A/C$ or C/A,

whichever is less than one. Since, in the semi-principal axis coordinate system,

$$P_{u'u'} = P_{v'v'} = \frac{P_{u''u''}+P_{v''v''}}{2}$$

$$= \frac{1}{2}\,(A^2+C^2)\ ,$$

the radius, R_o, of the hodograph along the semi-principal axes is $R_o = (A^2+C^2)^{1/2}$. By inspection,

$A = C$ gives rectilinear motion along the x"-axis,

$A = -C$ gives rectilinear motion along the y"-axis,

$C = 0$ gives anticlockwise circular motion,

$A = 0$ gives clockwise circular motion,

and

$A > C$ gives anticlockwise elliptical motion,

while

$C > A$ gives clockwise elliptical motion.

Thus, A is the amplitude of the anticlockwise component of the motion, while C is the amplitude of the clockwise component. The characterizing property of the ellipse-axes coordinate system is that $P_{u''v''} = 0$. The rotation from the (u,v) to the (u",v") velocity components through the angle θ_1 is then given by

$$\theta_1 = \frac{-1}{2}\,\tan^{-1}\left[\frac{2P_{uv}}{P_{vv}-P_{uu}}\right]\ ,$$

or

$$\theta_1 = \theta_o \pm \frac{\pi}{4}\ .$$

The component energy spectra in the ellipse-axes coordinate system are of special significance :

$$P_{u''u''} = \frac{P_{uu}+P_{vv}}{2} - \cos(2\theta_1)\frac{[P_{vv}-P_{uu}]}{2} + P_{uv}\sin(2\theta_1)$$

$$= \frac{P_{uu}+P_{vv}}{2} - \sin(2\theta_o)\frac{[P_{vv}-P_{uu}]}{2} - P_{uv}\cos(2\theta_o)$$

$$= \frac{P_{uu}+P_{vv}}{2} \pm \max P_{uv}$$

and, similarly,

$$P_{v''v''} = \frac{P_{uu}+P_{vv}}{2} \mp \max P_{uv} ,$$

which demonstrates that the Reynolds stress spectrum is related to the eccentricity of the hodograph. It is recognized that $P_{u''u''}$ and $P_{v''v''}$ are the eigenvalues of the real (or, even) part of the spectral matrix, thus they represent the squares of the lengths of the ellipse semi-axes, as they must.

There is an efficient means for solving for the amplitude and eccentricity of the hodograph from the spectral values : since

$$P_{u''u''} = \frac{(A+C)^2}{2}$$

and

$$P_{v''v''} = \frac{(A-C)^2}{2} ,$$

then

$$A \pm C = \sqrt{P_{uu}+P_{vv}+2 \max P_{uv}} = G$$

and

$$A \mp C = \sqrt{P_{uu}+P_{vv}-2 \max P_{uv}} = H ,$$

thus

$$\varepsilon = \frac{G-H}{G+H} .$$

Several properties of the hodograph can be deduced from the preceding formulae and model :

i) $J_1 = P_{uu} + P_{vv} = A^2 + C^2$,

ii) $J_2 = Q_{uv} = \frac{1}{2}(A^2-C^2)$,

($Q_{uv} = 0$ for $\varepsilon = 1$, i.e., for rectilinear motion)

iii) $J_3 = P_{uu}P_{vv} = (P_{uv})^2 = \frac{1}{4}(A+C)^2(A-C)^2 = (J_2)^2$, in the case of a single sinusoid), and

iv) $\max P_{uv} = [P_{uv}^2 + \frac{1}{4}(P_{vv}-P_{uu})^2]^{1/2}$

$= |AC|$, thus

$P_{uv} = 0$ for $\varepsilon = 0$, i.e., for circular motion.

An Example Hodograph. The geography of the hodograph is illustrated in Figure 4 for the following model. In the measurement coordinates, take

$$u = C \cos \sigma t + D \sin \sigma t$$

and

$$v = E \cos \sigma t + F \sin \sigma t ;$$

then

$$P_{uu} = \frac{1}{2}(C^2+D^2)$$

$$P_{vv} = \frac{1}{2}(E^2+F^2)$$

$$P_{uv} = \frac{1}{2}(CE+DF)$$

and

$$Q_{uv} = \frac{1}{2}(CF-DE).$$

For a quantitative example, take

$$C = \sqrt{3}, \quad D = 1/2 , \quad E = -1, \quad F = \sqrt{3/2} ;$$

a.

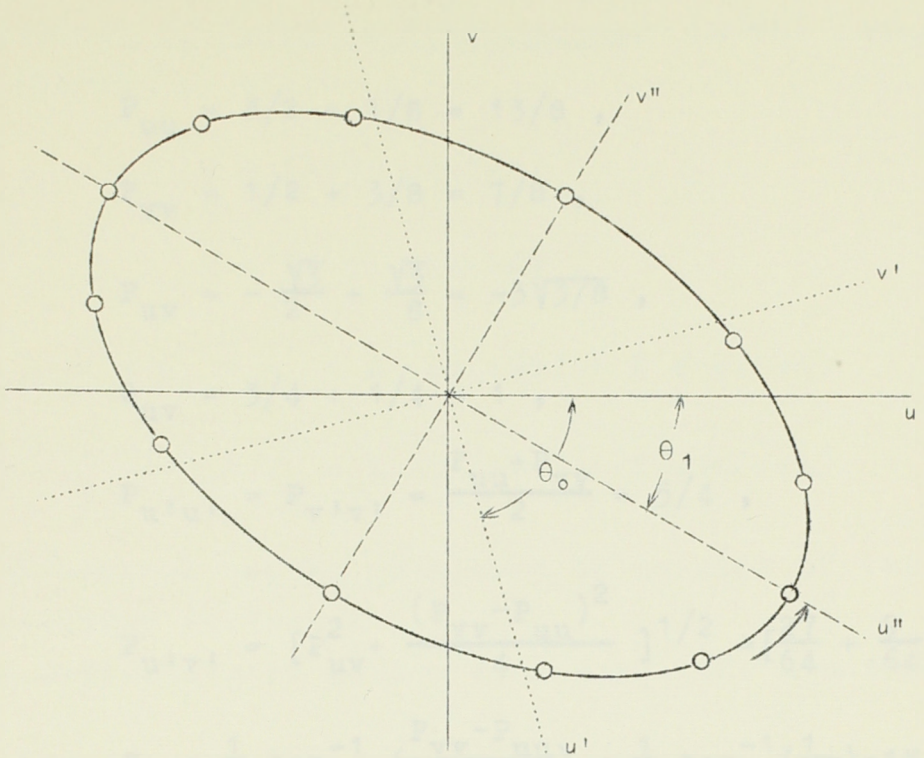

b.

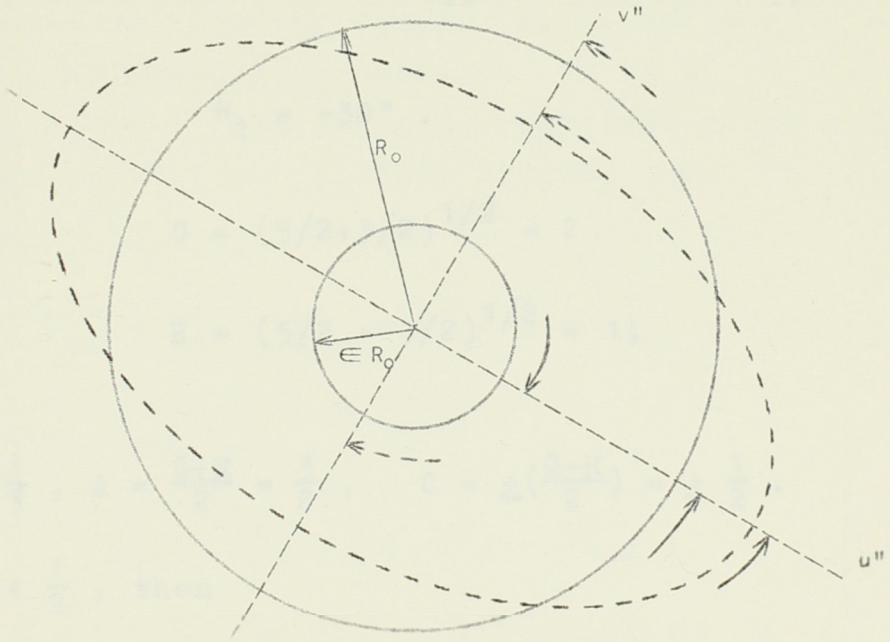

Fig. 4.- The geography of the hodograph.

a. The hodograph

(u,v) : geographic coordinates; (u',v') : semi-principal axes coordinates; (u",v") : ellipse-axes coordinates.

b. Decomposition of the hodograph into clockwise and anticlockwise components.

then

$$P_{uu} = 3/2 + 1/8 = 13/8 ,$$

$$P_{vv} = 1/2 + 3/8 = 7/8 ,$$

$$P_{uv} = -\frac{\sqrt{3}}{2} + \frac{\sqrt{3}}{8} = -3\sqrt{3/8} ,$$

$$Q_{uv} = 3/4 + 1/4 = 1 ,$$

$$P_{u'u'} = P_{v'v'} = \frac{P_{uu}+P_{vv}}{2} = 5/4 ,$$

$$P_{u'v'} = [P_{uv}^2 + \frac{(P_{vv}-P_{uu})^2}{4}]^{1/2} = [\frac{27}{64} + \frac{9}{64}]^{1/2} = 3/4 ,$$

$$\theta_0 = \frac{1}{2} \tan^{-1} (\frac{P_{vv}-P_{uu}}{2P_{uv}}) = \frac{1}{2} \tan^{-1}(\frac{1}{\sqrt{3}}) = 15^\circ ,$$

and

$$\theta_1 = -30^\circ .$$

Since

$$G = (5/2+3/2)^{1/2} = 2$$

and

$$H = (5/2 - 3/2)^{1/2} = 1,$$

then

$$\varepsilon = \frac{1}{3} , \quad A = \frac{G+H}{2} = \frac{3}{2} , \quad C = \pm(\frac{G-H}{2}) = \pm \frac{1}{2} .$$

Choose $C = + \frac{1}{2}$, then

$$u'' = (A+C) \cos(\sigma t) = 2 \cos (\sigma t)$$

and

$$v'' = (A-C) \sin(\sigma t)$$

$$= 1 \sin (\sigma t).$$

The Concept of Negative Frequencies. In the coordinates of the ellipse-axes, since

$$u = (A+C)\cos(\sigma t)$$

and

$$v = (A-C)\sin(\sigma t) ,$$

then

$$u = u^{+} + u^{-} = A\cos(+\sigma t) + C\cos(-\sigma t)$$

and

$$v = v^{+} + v^{-} = A\sin(+\sigma t) + C\sin(-\sigma t).$$

Thus, the hodograph can be conceived to consist of two counter-rotating velocity vectors :

i) An anticlockwise motion with amplitude A and frequency $+\sigma$, and

ii) A clockwise motion with amplitude C and frequency $-\sigma$.

The complex-valued velocity vector, w, is defined to be $w = u + iv$. It is clear that the autospectrum for w^{+} is $P^{+}_{ww} = A^2$ and that for w^{-} it is $P^{-}_{ww} = C^2$. Thus, there is physical meaning for spectra with negative as well as positive frequencies. The total auto-spectrum for w is

$$P_{ww} = P^{+}_{ww} + P^{-}_{ww} = A^2 + C^2 = P_{uu} + P_{vv} .$$

It also follows that

$$P^{+}_{ww} - P^{-}_{ww} = (A^2 - C^2) = 2Q_{uv} .$$

Thus, P^{+}_{ww} and P^{-}_{ww} are invariant under coordinate rotation.

The two counter-rotating vectors corresponding to the hodograph of Figure 42a are shown in Figure 42b.

C. Spectral Quantities for Pairs of Complex-Valued Time Series.

For the study of the coherency of a pair of two-dimensional

velocity vectors, in addition to the component-wise coherence and phase matrices, there is a quantity which measures the overall coherency of two velocity vectors. In essence, the coherency of a pair of horizontal hodographs is considered. Each horizontal velocity vector series is written as a complex-valued series with real argument, t, i.e., $w(t) = u(t) + iv(t)$. The material of this section was derived in a search for a technique which would provide quantitative results which were invariant under coordinate rotation.

Autovariance and Autospectrum Functions. The autovariance function for w is defined as,

$$R_{ww}(\tau) = \overline{w(t)w^{*}(t+\tau)}^{\,t},$$

where $(\ )^{*}$ is the conjugate operator; in coordinate form,

$$R_{ww}(\tau) = [R_{uu}(\tau)+R_{vv}(\tau)]+i[R_{vu}(\tau)-R_{uv}(\tau)],$$

$$= [R_{uu}(\tau)+R_{vv}(\tau)]-i2Q_{uv}(\tau),$$

which is invariant under coordinate rotation by Section A. Then the autospectrum is

$$P_{ww}(\sigma) = \text{F.T.}(R_{ww}(\tau))$$

$$= [P_{uu}(\sigma)+P_{vv}(\sigma)] + 2Q_{uv}(\sigma),$$

which is also invariant. $P_{ww}(\sigma)$ is not an energy spectrum in the usual physical sense because it is two-sided; i.e. it is neither odd nor even as a function of frequency. The variance of w does equal

$$\int_{-\infty}^{\infty} P_{ww}(\sigma)d\sigma \quad .$$

Covariance and Cross Spectrum Functions. The covariance function for w_1 and w_2 is defined as

$$R_{w_1 w_2}(\tau) = \overline{w_1(t) w_2^*(t+\tau)}$$

$$= [R_{u_1 u_2}(\tau) + R_{v_1 v_2}(\tau)] + i[R_{v_1 u_2}(\tau) - R_{u_1 v_2}(\tau)].$$

When w_1 and w_2 undergo a coordinate transformation to w_1' and w_2' by a rotation through an angle of θ_1 and θ_2, respectively, it follows that

$$R_{w_1' w_2'}(\tau) = R_{w_1 w_2}(\tau)\, e^{i(\theta_2 - \theta_1)}.$$

Thus, the absolute value of the covariance function is invariant. The cross spectrum is

$$\tilde{P}_{w_1 w_2}(\sigma) = F.T.(R_{w_1 w_2}(\tau)) = P_{w_1 w_2}(\sigma) + iQ_{w_1 w_2}(\sigma),$$

where the cospectrum is

$$P_{w_1 w_2}(\sigma) = [P_{u_1 u_2}(\sigma) + P_{v_1 v_2}(\sigma)] - [Q_{v_1 u_2}(\sigma) - Q_{u_1 v_2}(\sigma)]$$

and the quadrature spectrum is

$$Q_{w_1 w_2}(\sigma) = [Q_{u_1 u_2}(\sigma) + Q_{v_1 v_2}(\sigma)] + [P_{v_1 u_2}(\sigma) - P_{u_1 v_2}(\sigma)].$$

The absolute value of the cross spectrum is invariant under

coordinate rotation from the above. The forms of $P_{w_1 w_2}(\sigma)$ and $Q_{w_1 w_2}(\sigma)$ contain terms accounting for the component-wise coupling of the two velocity vectors; these terms are the elements of the component-wise cross spectral matrix.

Coherence Squared and Phase Functions. The coherence squared, γ^2, and phase, Φ, are defined in the usual way, dropping the frequency argument, σ, for convenience :

$$\gamma^2_{w_1 w_2} = \frac{|\tilde{P}_{w_1 w_2}|^2}{P_{w_1 w_1} P_{w_2 w_2}}$$

$$= \frac{[P_{u_1 u_2} + P_{v_1 v_2} + Q_{u_1 v_2} - Q_{v_1 u_2}]^2 + [Q_{u_1 u_2} + Q_{v_1 v_2} + P_{v_1 u_2} - P_{u_1 v_2}]^2}{[P_{u_1 u_1} + P_{v_1 v_1} + 2Q_{u_1 v_1}][P_{u_2 u_2} + P_{v_2 v_2} + 2Q_{u_2 v_2}]}$$

and

$$\Phi_{w_1 w_2} = \tan^{-1}\left[\frac{Q_{w_1 w_2}}{P_{w_1 w_2}}\right]$$

$$= \tan^{-1} \frac{[Q_{u_1 u_2} + Q_{v_1 v_2} + P_{v_1 u_2} - P_{u_1 v_2}]}{[P_{u_1 u_2} + P_{v_1 v_2} + Q_{u_1 v_2} - Q_{v_1 u_2}]} .$$

By the preceding remarks, γ^2 is invariant under coordinate rotation and $\Phi'_{w_1' w_2'} = \Phi_{w_1 w_2} + (\theta_2 - \theta_1)$.

It remains to prove that $\gamma^2_{w_1 w_2}$ is bounded above by 1.0. The most instructive way to do this is to use a model for w_1 and w_2 composed of a sum of sinusoids in each hypothetical measurement bandwidth. Form w_1 and w_2 from a set of sinusoids :

$$u_1 = A_1 \cos(\sigma t) + B_1 \sin(\sigma t),$$

$$v_1 = C_1 \cos(\sigma t) + D_1 \sin(\sigma t),$$

$$u_2 = A_2 \cos(\sigma t) + B_2 \sin(\sigma t),$$

and

$$v_2 = C_2 \cos(\sigma t) + D_2 \sin(\sigma t),$$

thus

$$w_1 = \sum_k [(A_1^{(k)} \cos(\sigma_k t) + B_1^{(k)} \sin(\sigma_k t)) + i(C_1^{(k)} \cos(\sigma_k t) + D_1^{(k)} \sin(\sigma_k t))],$$

and similarly for w_2, where k is summed over the number of frequencies in a measurement bandwidth. Dropping the superscript k for convenience, it is straightforward to show that

$$P_{w_i w_j} = \frac{1}{2} \sum_k [(A_i + D_i)(A_j + D_j) + (B_i - C_i)(B_j - C_j)]$$

and

$$Q_{w_i w_j} = \frac{1}{2} \sum_k [(A_i + D_i)(B_j - C_j) - (A_j + D_j)(B_i - C_i)].$$

Now take

$$\underline{I}(k) = [(A_i + D_i), (B_i - C_i)]$$

and

$$\underline{J}(k) = [(A_j + D_j), (B_j - C_j)],$$

thus

$$P_{w_i w_j} = \frac{1}{2}[\sum_k \underline{I} \cdot \underline{J}] = \frac{1}{2} \sum_k |\underline{I}| \, |\underline{J}| \cos \Phi$$

and

$$Q_{w_i w_j} = \frac{1}{2}[\sum_k \underline{I} \times \underline{J}] = \frac{1}{2} \sum_k |\underline{I}| \, |\underline{J}| \sin \Phi,$$

where Φ is the angle between $\underline{I}(k)$ and $\underline{J}(k)$.

With use of the C-B-S inequality in summation form, it follows that

$$|\tilde{P}_{w_i w_j}|^2 = \frac{1}{4}\{[\sum_k |\underline{I}||\underline{J}| \cos \Phi]^2 + [\sum_k |\underline{I}||\underline{J}| \sin \Phi]^2\}$$

$$\leq \frac{1}{4}\{[\sum_k |\underline{I}|^2 (\sum_k |\underline{J}|^2 \cos^2 \Phi + \sum_k |\underline{J}|^2 \sin^2 \Phi)\}$$

$$= \frac{1}{4} \sum_k |\underline{I}|^2 \sum_k |\underline{J}|^2$$

$$= P_{w_i w_i}(\sigma) P_{w_j w_j}(\sigma).$$

Therefore,

$$\gamma^2_{w_i w_j}(\sigma) \leq 1.0 ;$$

the equality holds only when $\underline{I} = \underline{J}$ all k or when there is only one sinusoid in a measurement band. γ^2 and Φ for complex-valued series obey the same statistics as they do for real series. The equations for the cospectrum and quadrature spectrum are in the proper form for use in band-averaging a set of Fourier coefficients.

Since $P_{ww} = \frac{1}{2} \sum_k [(A+D)^2 + (B-C)^2]$, then $P_{ww} = 0$ if and only if $A^{(k)} = -D^{(k)}$ and $B^{(k)} = C^{(k)}$ for all k. Thus, when the denominator of γ^2 vanishes, the numerator also vanishes.

Degenerate Cases. If one series is complex, e.g., velocity, and a second real, e.g., temperature, set $w_1 = w = u + iv$ and $w_2 = s$. Then

$$P_{w_1 w_2} = P_{ws} = P_{us} - Q_{vs}$$

and

$$Q_{w_1 w_2} = Q_{ws} = Q_{us} + P_{vs} ,$$

thus

$$\gamma^2_{ws} = \frac{[P_{us} - Q_{vs}]^2 + [Q_{us} + P_{vs}]^2}{P_{ss}[P_{uu} + P_{vv} + 2Q_{uv}]}$$

and

$$Q_{ws} = \tan^{-1} \left(\frac{Q_{us} + P_{vs}}{P_{us} - Q_{vs}} \right) .$$

If both series are real, i.e., v_1 and $v_2 = 0$, then the above formulae reduce to the ordinary forms in the cross spectrum analysis of real-valued series.

The Complex Spectrum of a Pair of Hodographs. As seen in Section B, the hodograph can be reduced to components with positive and negative frequencies. The spectrum of the hodograph, Section B, for positive and negative frequencies is recognized as the spectrum of a complex-valued series as discussed above. The detailed steps are illustrated for a pair of hodographs. Take $u_1 = (A_1 + C_1) \cos(\sigma t + \theta_1)$ and $v_1 = (A_1 - C_1) \sin(\sigma t + \theta_1)$, then

$$w_1 = u_1 + iv_1 = [A_1 e^{i(\sigma t + \theta_1)} + C_1 e^{-i(\sigma t + \theta_1)}]$$

and an analogous form is used for w_2. Thus,

$$R_{w_1 w_1}(\tau) = A_1^2 e^{-i\sigma\tau} + C_1^2 e^{+i\sigma\tau} ,$$

$$R_{w_2 w_2}(\tau) = A_2^2 e^{-i\sigma\tau} + C_2^2 e^{i\sigma\tau} ,$$

and

$$R_{w_1 w_2}(\tau) = A_1 A_2 e^{-i(\sigma\tau-(\theta_1-\theta_2))} + C_1 C_2 e^{i(\sigma\tau-(\theta_1-\theta_2))} .$$

Then

$$P_{w_1 w_1}(\sigma_o) = A_1^2 \delta(\sigma-\sigma_o) + C_1^2 \delta(\sigma+\sigma_o) ,$$

$$P_{w_2 w_2}(\sigma_o) = A_2^2 \delta(\sigma-\sigma_o) + C_2^2 \delta(\sigma+\sigma_o) ,$$

and

$$\tilde{P}_{w_1 w_2}(\sigma_o) = A_1 A_2 \delta(\sigma-\sigma_o) e^{i(\theta_1-\theta_2)} + C_1 C_2 \delta(\sigma+\sigma_o)\, e^{-i(\theta_1-\theta_2)} ,$$

thus

$$\left|\tilde{P}_{w_1 w_2}(\sigma_o)\right|^2 = A_1^2 A_2^2 \delta(\sigma-\sigma_o) + C_1^2 C_2^2 \delta(\sigma+\sigma_o) ,$$

where $\delta(\ )$ is a Dirac delta function.

For a sum of sinusoids in a measurement band, the coherence squared is then

$$\gamma^2_{w_1 w_2} = \begin{cases} \dfrac{(\Sigma A_1 A_2)^2}{\Sigma(A_1)^2 \Sigma(A_2)^2} , & \sigma \geq 0 \\ \dfrac{(\Sigma C_1 C_2)^2}{\Sigma(C_1)^2 \Sigma(C_2)^2} , & \sigma \leq 0 . \end{cases}$$

Thus, there is a value of $\gamma^2_{w_1 w_2}$ defined for the anticlockwise $(\sigma \geq 0)$ portion of w_1 and w_2 and a value for the clockwise, $(\sigma \leq 0)$ portion. Several special cases exist for the spectrum of the hodograph :

i) $A = C$, $P_{ww}(-\sigma) = P_{ww}(\sigma)$, rectilinear motion,

ii) $C = 0$, $P_{ww}(-\sigma) = 0$, pure anticlockwise motion,

iii) $A = 0$, $P_{ww}(\sigma) = 0$, pure clockwise motion.

In general, $P_{ww}(-\sigma) < P_{ww}(\sigma)$ for net anticlockwise motion and vice versa for net clockwise motion.

GENERATION OF TRANSIENT NEARLY INERTIAL INTERNAL WAVES BY THE INTERACTION BETWEEN INTERNAL WAVES AND A GEOSTROPHIC SHEAR CURRENT

By Claude J. Frankignoul
Institut de Mathématique, Université de Liège, 4000. Liège

1. INTRODUCTION.

There is evidence that the nonlinear coupling between modes is weak in the internal wave frequency range of the ocean-current spectrum (Fofonoff, 1969, Hasselmann, 1968). Hence, other mechanisms by which internal gravity waves exchange energy with their surroundings or with other types of motion might be mainly responsible, in some cases, of the observed spectrum.

Such energy exchange occurs when internal waves are in the presence of a mean shear flow (Bretherton, 1966, Phillips, 1966). An early attempt to evaluate the influence of this mechanism on the shape of the frequency spectra was made by Phillips (1966) for a simple non-rotating model. His result must nevertheless be interpreted with care, as they are restricted to a narrow band of frequencies and obscured by an algebraic error.

The influence of a steady shear on the internal wave spectra in a rotating medium has been recently investigated by Frankignoul (1970), on the basis of Phillips'work. The mean shear current was supposed to be in ageostrophic balance and the wave propagation directions isotropically distributed in the mean with respect to the horizontal. The comparison of the equilibrium spectral shapes with some relevant oceanic data indicated a good agreement.

In most deep sea situations, it is known that, if a steady

* Aspirant au Fonds National de la Recherche Scientifique.

shear flow is to be assumed, the hypothesis of geostrophic balance is more relevant. In the present paper, attention will be focused on the effect of a horizontal density gradient on the time-behavior and the equilibrium spectral shapes of the internal waves. An attempt will be made to evaluate the influence of the dissipations.

2. DERIVATION OF THE WAVE EQUATION.

It is assumed that the fluid is incompressible and non-dissipative. The horizontal component of the earth rotation is neglected and the mean shear flow is supposed to be steady, unidirectional and depending only upon the depth. To the Boussinesq approximation, the linearised equations of motion reads

$$\frac{du}{dt} - fv + wU' = -\frac{\partial \pi}{\partial x} \qquad (1)$$

$$\frac{dv}{dt} + fu = -\frac{\partial \pi}{\partial y} \qquad (2)$$

$$\frac{dw}{dt} - b = -\frac{\partial \pi}{\partial z} \qquad (3)$$

$$\frac{\partial u}{\partial x} + \frac{\partial v}{\partial y} + \frac{\partial w}{\partial z} = 0 \qquad (4)$$

$$\frac{db}{dt} - v\,M^2 + w\,N^2 = 0 \qquad (5)$$

where $(U(z),0,0)$ is the mean velocity, (u,v,w) the fluctuating velocity, b the fluctuating part of the buoyancy, π the non-hydrostatic pressure per unit mass, f the Coriolis parameter. $N^2 = -\frac{g}{\rho_o}\frac{\partial \bar{\rho}}{\partial z}$ and $M^2 = \frac{g}{\rho_o}\frac{\partial \bar{\rho}}{\partial y}$ are the Brunt-VÄisÄlÄ frequency and its horizontal analogue, g is the gravitational acceleration, $\bar{\rho}$ the mean non-hydrostatic density; $\frac{d}{dt} \equiv \frac{\partial}{\partial t} + U\frac{\partial}{\partial x}$.

Geostrophic and hydrostatic equilibria lead to

$$fU' = M^2 = -sN^2 \tag{6}$$

where s is the vertical slope of an isopycnal in the mean density field. For simplicity, it is assumed that

$$\begin{aligned} U'(z) &\equiv U' \equiv \text{constant} \\ N^2(z) &\equiv N^2 \equiv \text{constant} . \end{aligned} \tag{7}$$

For all these assumptions to be approximately valid, very small and very large scale motions must be disregarded. A typical region where the model applies roughly is the region below the main thermocline, far from boundaries.

By elimination, one gets an equation for w

$$\frac{d^3}{dt^3}\nabla^2 w + \frac{d}{dt}\left(f^2 \frac{\partial^2}{\partial z^2} + 2M^2 \frac{\partial^2}{\partial y \partial z} + N^2 \nabla_n^2\right) w - 2M^2 U' \frac{\partial^2 w}{\partial x \partial y} - 2M^2 f \frac{\partial^2 w}{\partial x \partial z} = 0. \tag{8}$$

Instead of using a normal mode expansion, we assume a wave decomposition of the form

$$w = W(t)\, e^{i(kx+ly - kU'zt)} \tag{9}$$

k and l being constant, on the basis of the stretching action of the shear, as found by examination of the ray equations (Jones, 1969, Mooers, 1970). The time-origin is chosen when the wave-number is horizontal so that negative time is allowed. In order to set-up a model which is amenable to analysis, W is assumed to be depth-independent. The medium is supposed to be infinitely deep and there is no boundary conditions.

As only wave-number components in the direction of the

mean shear undergo its influence, the form (9) is of no use if $k \equiv 0$: there is no energy exchange between the shear flow and the waves (at least to the Boussinesq approximation, see Healey and Leblond, 1969), and the present model does not apply. If the wave propagates obliquely, its wave number is rotated and increases as soon as it becomes horizontal. This was first noted by Phillips (1966).

Using the form (9), equation (8) reduces to

$$K^{-2} \frac{\partial^3}{\partial T^3}[(1+T^2)W] + \frac{\partial}{\partial T}[(1+2s \sin\Phi\, T+F^2T^2)W] + 2(F^2T+s \sin\Phi)W = 0 \qquad (10)$$

where Φ specifies the angle between the horizontal wave number vector and the steady current direction, and where

$$T = U' \cos\Phi\, t$$
$$K^2 = \frac{N^2}{U'^2 \cos^2\Phi} \,. \qquad (11)$$

3. ASYMPTOTIC SOLUTION FOR LARGE K^2.

As in the previous works based on the wave decomposition (9), an asymptotic solution can be found when K^2 is large. This corresponds usually to a very large dynamical stability of the mean flow. To the first order in K^{-1}, one has

$$W \sim G(1+T^2)^{-\frac{3}{4}} (1+2\, s \sin\Phi\, T+F^2T^2)^{\frac{1}{4}} e^{\pm i \frac{K}{N} \int n\, dT} \qquad (12)$$

where G is a constant and n the intrinsic frequency defined by

$$n = N\left(\frac{1+2\, s \sin\Phi\, T+F^2T^2}{1+T^2}\right)^{\frac{1}{2}} \,. \qquad (13)$$

The frequency n changes continuously with time and tends to the inertial frequency as t increases, so that energy is transferred towards low frequencies for $T > 0$. The frequency band in the geostrophic case is larger than in the cases where there is no mean flow or when the mean flow is in ageostrophic balance. Taking for simplicity F^2 and s^2 much smaller than unity, as is verified in most physical situations, the frequency limits are given by

$$f\left(1 - \frac{s^2 \sin^2\Phi}{F^2}\right)^{\frac{1}{2}} < n < N\,(1+s^2\sin^2\Phi)^{\frac{1}{2}} . \qquad (14)$$

As discussed by Mooers (1970) in the case where $\Phi = 90°$, only the low frequency limit can be effectively affected.

The vertical component of the group velocity Cg, given by

$$\frac{\partial n}{\partial t} = - k\, U'\, Cg ,$$

allows for an estimation of the vertical distance d over which the energy at any point runs from a time t_1 to a time t_2, by integrating (15) between t_1 and t_2. Typical value of d is d_Φ corresponding to $t_1 \equiv 0$, $t_2 \equiv \infty$. For conditions found at Site D (39°20'N,70°W) at a depth of 2000 meters, one has $d_o \sim O(2\lambda)$, λ being the horizontal wave-length. For not too large scale, the vertical displacement of the wave energy is small; this could partly justify the omission of boundary conditions. The dispersion relation is

$$(n^2-f^2)m^2 = (N^2-n^2)(k^2+l^2) + 2lm\, f\, U' \qquad (16)$$

where m is the vertical component of the wave number.

There is an energy exchange between the wave and the mean flow. The mean Reynolds stress produced by the wave is given by

$$-\rho_o \overline{uv} \sim -\frac{1}{2}\rho_o G^2 \cos\Phi\, T(1+T^2)^{-\frac{3}{2}}(1+2s\sin\Phi\, T+F^2T^2)^{\frac{1}{2}} \quad (17)$$

an overbar indicating the mean value. For $T > 0$, the Reynolds stress is negative and energy is extracted from the wave motion and transferred to the mean current. The rate of energy transfer is indicated by the behavior of the horizontal and vertical kinetic energy density of the wave

$$E_h \sim \frac{1}{4}\rho_o G^2T^2(1+T^2)^{-\frac{3}{2}}(1+2s\sin\Phi\, T+F^2T^2)^{1/2} \quad (18)$$

$$E_v \sim \frac{1}{4}\rho_o G^2(1+T^2)^{-\frac{3}{2}}(1+2s\sin\Phi\, T+F^2T^2)^{1/2}. \quad (19)$$

After a time long enough, E_h tends to a constant value whereas E_v vanishes, and the intrinsic frequency becomes the inertial frequency. Hence, the effect of the shear is to transform the internal wave motions into inertial oscillations, provided nothing interrups the process (see below).

If there is an energy transfer between waves and mean flow, one cannot rigourously assume the steadiness of the mean current. However, if the isotropy of the wave propagation directions is assumed, all wave energy contributions to the mean current balance. Then, the assumption of a steady shear, though being invalid locally, can be justified.

It must be noted that the transfer of the wave energy to the mean flow is identical to the phenomenon of critical layer absorption, as showed Booker and Bretherton (1967). No critical level occurs here as it corresponds to a fixed frequency (normal mode decomposition), while, in Phillips'model, the frequency is varying and the absorption of vertical momentum continuous.

4. SHEAR INSTABILITY AND DISSIPATIVE EFFECTS.

As an effect of the mean shear, the vertical scale of the wave motion is reduced, increasing the shear produced by the wave. This shear tends to become infinite as n tends to f, so that the Richardson number unavoidably becomes smaller than 1/4, the critical value for shear instability (necessary but not sufficient condition).

To calculate the frequency below which the motion might become unstable, we define a minimum Richardson number by adding the shear produced by the wave to the overall mean shear, which can be neglected as $K^2 >> 1$. Calling a the wave amplitude at $t = 0$ and λ the horizontal wave-length, a critical curve can be drawn in a $(n, \frac{a}{\lambda})$ diagram (fig.1). The larger is the wave amplitude, the smaller is the frequency below which instability may occur. Let us mention that the appearance of a dynamical instability does not imply that the wave itself is destroyed.

So far, dissipative effects have been neglected as is usually done in a wave theory. However, the evolution towards a vanishingly small scale in the vertical direction accelerate the viscous damping. This should prevent the wave from the occurrence of shear instability, in some cases.

Detailed investigation of the combined effects of viscosity, heat and salt diffusion leads to very tedious algebra, but bounds of their influence can be obtained more easily by using $\frac{d}{dt} \equiv \frac{\partial}{\partial t} + U \frac{\partial}{\partial x} - \nu \nabla^2$ in the basic equations instead of the former value. According to the choice of ν-kinematic viscosity or thermal diffusivity (the salinity being neglected)- one gets upper or lower bounds of the dissipative effects. The analysis is rigourous for unitary Prandlt number.

Calculation leads to an equivalent asymptotic solution; it can be shown that solution (12) is still valid, except that there is an additionnal factor

$$e^{-K\eta} \int_{T_o}^{T} (1+T^2)\, dT$$

with (20)

$$\eta = \frac{4\pi^2 \nu}{\lambda^2 N^2} \quad .$$

T_o corresponds either to the generation of the wave or to the time of entrance of a wave in such a region of shear, and must be introduced because the dissipations are irreversible.

It can be shown that, provided the ratio of the wave amplitude to the wave length is not large, there will be no dynamical instability. For illustration of the damping effect, one can calculate that the amplitude of a wave (λ=200 m) generated at Site D (2000 m) is reduced by a factor D such that $1.05 < D < 1.45$, after the lapse of time necessary for the frequency to decrease from N to 0.15 N.

The statement of section 3 must be modified to take into account the phenomenom described in this section. In most cases, the wave frequency will become rather close to f, but will never reach it. Two mechanisms - shift towards lower frequencies (when n becomes close to f), damping of the horizontal oscillations - will strongly contribute to give a transient character to a given low frequency Fourier component. Hence, the shear will act to transform the internal waves into nearly inertial transient oscillations, if the inertial angle of incidence of the wave is appropriate.

The action of the shear on internal waves could then be an important mechanism for the appearance of inertial oscillations in deep sea, and the observed transient character of those waves is easily explained in our model.

5. EQUILIBRIUM SPECTRAL SHAPES.

The main interest of the unusual wave decomposition (9) is that it allows to derive equilibrium spectral shapes from simple arguments.

In his paper, Phillips (1966) assumed there was a steady source of internal waves which has been acting long enough for a steady spectrum to develop. Then, the frequency spectra can be derived simply because, as each wave is rotated, its amplitude, velocity and frequency are modified. A fundamental problem is to find a suitable energy source in deep sea, far from boundaries; very little is known on this subject.

Phillips'results are based on the Doppler-shifted wave frequency and their use for time-dependent spectra at a fixed point must be interpreted with care. In fact, provided the source is fixed and steady, there will be no temporal variation in the frequency spectra at a given place, but only a direct dependance to the source frequency spectrum. Also, all wave energy transferred to the mean flow will accumulate and U cannot be supposed to depend only upon the depth, except to a rough approximation.

An assumption of more statistical character was made by Frankignoul (1970) and will be used here. We assume there is a large supply of many waves coming in the region of shear, in an undetermined manner but isotropically distributed with respect to the horizontal. This does not answer to the question of the source of the waves, but is not too restrictive. Because of the isotropy of the wave propagation directions, all Doppler-Shift effects balance in the mean and the frequency n can be used for measurements at a fixed point, provided they are long enough. Also, it is easy to see that the frequency spectra will be similar to the spectra obtained by assuming the existence of a steady source (by considering a pair of waves, symetric about the horizontal plane). Using Phillips'method (1966) to derive the spectral shapes, it is found that the horizontal and vertical kinetic energy density spectra E_h and E_v , and the potential energy

spectrum $P_{\varphi\varphi}$ are respectively of the form

$$E_h \propto T^2(1+2s\sin^2\Phi T+F^2T^2)(s\sin\Phi T^2+(1-F^2)T-s\sin\Phi)^{-1} \quad (21)$$

$$E_v \propto (1+2s\sin^2\Phi T+F^2T^2)(s\sin\Phi T^2+(1-F^2)T-s\sin\Phi)^{-1} \quad (22)$$

$$P_{\varphi\varphi} \propto (1+T^2)(s\sin\Phi T^2+(1-F^2)T-s\sin\Phi)^{-1} \quad . \quad (23)$$

To express the spectra in function of the frequency, formula (13) must be used. A simple analytical form is found when $\Phi \equiv 0$:

$$E_h \propto n^2(N^2-n^2)^{\frac{1}{2}}(n^2-f^2)^{-\frac{3}{2}} \quad (24)$$

$$E_v \propto n^2(N^2-n^2)^{-\frac{1}{2}}(n^2-f^2)^{-\frac{1}{2}} \quad (25)$$

$$P_{\varphi\varphi} \propto (N^2-n^2)^{-\frac{1}{2}}(n^2-f^2)^{-\frac{1}{2}} \quad . \quad (26)$$

The hypothesis of geostrophic balance only affects the low frequency part of E_v and $P_{\varphi\varphi}$ - they show a peak at the inertial frequency - , as compared with results obtained in the ageostrophic case, otherwise very similar.

To compare (24) - (26) with observations, it must be noted that both ends of the curves cannot be representative of the ocean-current spectra. Indeed, at very low frequency, the waves we have studied are subject to shear instability, whereas at very high frequencies, the model itself is invalid, since the microstructure has been neglected and only a mean N has been used. As, in the real oceans, other motions are also present at very low and very high frequency, a good agreement cannot be expected near the limits of the internal wave frequency range.

The model can be tested in a region, far from boundaries, where the mean Brunt-Väisälä frequency is roughly constant - this

is often observed below the main thermocline - and where there is a mean shear which is roughly steady and unidirectional, at least in periods long enough for the transfer process to occur. The value of the shear affects only the time scale of the frequency shift of the waves, and contributions from different periods of time where the model is valid will add in the same way, no matter what is the direction and magnitude of the mean shear.

Measurements made at Site D (39°20'N,70°W), below the main thermocline, seem to be suitable for a comparison with the computed spectral shapes (Frankignoul, 1970). Fig. 2 shows a comparison between the calculated horizontal kinetic energy spectrum and observations made at a depth of 2000 meter, in a region where the model applied best. The agreement is good, as in the ageostrophic case. There is no other really relevant observations which can be used to check the validity of the model. In (Frankignoul, 1970), comparison has been made with vertical kinetic energy and temperature fluctuations spectra recorded at the lower edge of the thermocline (where N is not constant) but the accuracy of the measurements is weak and the model rather inappropriate so that no conclusion can be drawn.

The effects of the dissipation on the equilibrium spectra cannot be investigated in detail but it can be seen intuitively that they will not seriously affect the value (24)-(26) in considering two waves coming in the region of shear, with propagation directions symetric about the horizontal plane. The frequency of one wave is shifted towards higher frequencies, while the frequency of the other one is shifted towards lower frequencies. As the dissipation depends only upon the time elapsed, the low and high frequency regions of the spectra will be affected in a similar way and the spectral shape will not be influenced by the dissipations.

6. CONCLUSIONS.

The effect of a constant steady and unidirectional shear on internal waves is to modify their frequency, wave-number and amplitude, and finally to transform them into inertial oscillations, after all vertical kinetic energy has been transferred to the mean current. Consideration of dissipative effects introduces a limited life-time of the wave and gives a transient character to the low-frequency waves, in agreement with the observations of inertial oscillations.

The good agreement between spectra of the horizontal kinetic energy computed from the model and some relevant observations bears out the interest of studying the effect of the shear on internal waves.

REFERENCES.

Bretherton, F.P. 1966. The propagation of groups of internal gravity waves in a shear flow. Q.J.Roy.Met.Soc.92,466-480.

Booker, J.R. and Bretherton, F.P. 1967. The critical layer for internal gravity waves in a shear flow. J.Fluid.Mech. 27, 513-539.

Fofonoff, N.P. 1969. Spectral characteristics of internal waves in the ocean. Deep-Sea Res., Suppl. to vol.16,59-71.

Frankignoul, C.J. 1970. The effect of weak shear and rotation on internal waves. Tellus, 22,2.

Hasselmann, K. 1968. Weak-interaction theory of ocean waves, pp.117-182 in Basic Developments in Fluid Dynamics (ed. M.Holt), 226pp. Academic Press.

Healey, D. and Le Blond, P.H. 1969. Internal wave propagation normal to a geostrophic current. J.Mar.Res.27,1,85-98.

Jones, W.L. 1969. Ray tracing for internal gravity waves. Journ. of Geophys.Res.74, 8, 2028-2033.

Mooers, C.N.K., 1970. The effect of horizontal density gradients on the propagation of inertial-internal waves. (Submitted to Geophysical Fluid Dynamics).

Phillips, O.M. 1966. The dynamics of the upper ocean, 261pp. Cambridge University Press.

LEGENDS FOR FIGURES.

Figure 1. Curves relating the non-dimensional frequency under which instability may occur to the ratio of the wave amplitude to the wave length, at t = 0. Numerical values correspond to site D, 2000 m. Dissipations are neglected.

Figure 2. A comparison of the horizontal kinetic energy density spectrum observed at Site D, 39°20'N,70°W; (2206, 2000m, June 1967) with the calculated spectrum. Arbitrary magnitude of the computed curve has been chosen to fit the observations.

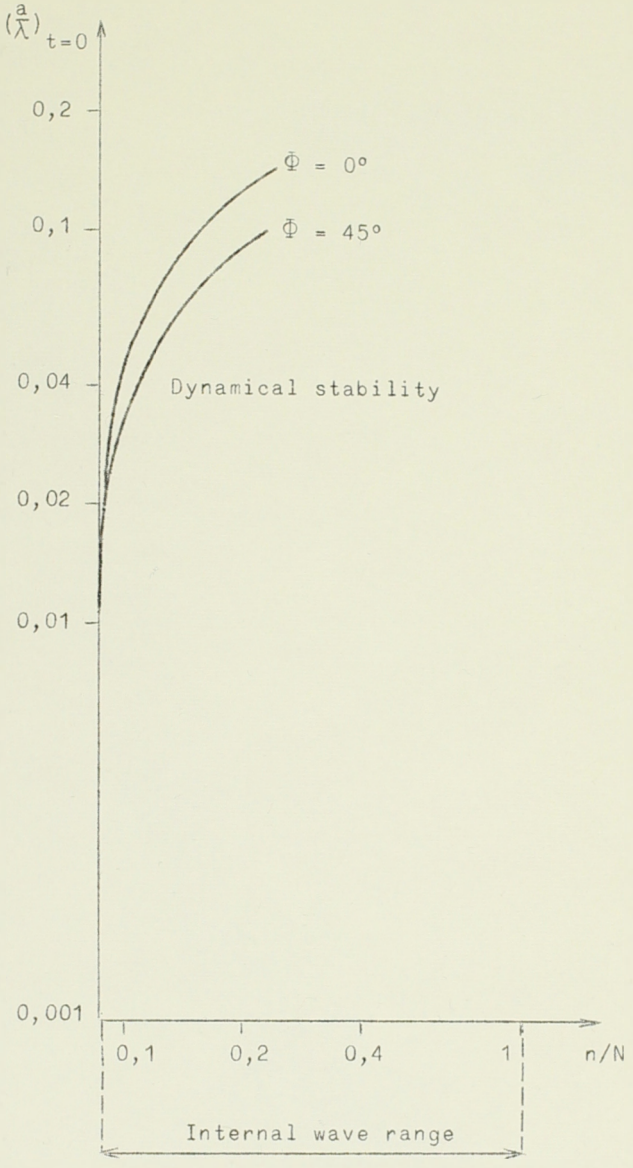
$(\frac{a}{\lambda})_{t=0}$
0,2
0,1
0,04
0,02
0,01
0,001
Φ = 0°
Φ = 45°
Dynamical stability
0,1
0,2
0,4
1
n/N
Internal wave range

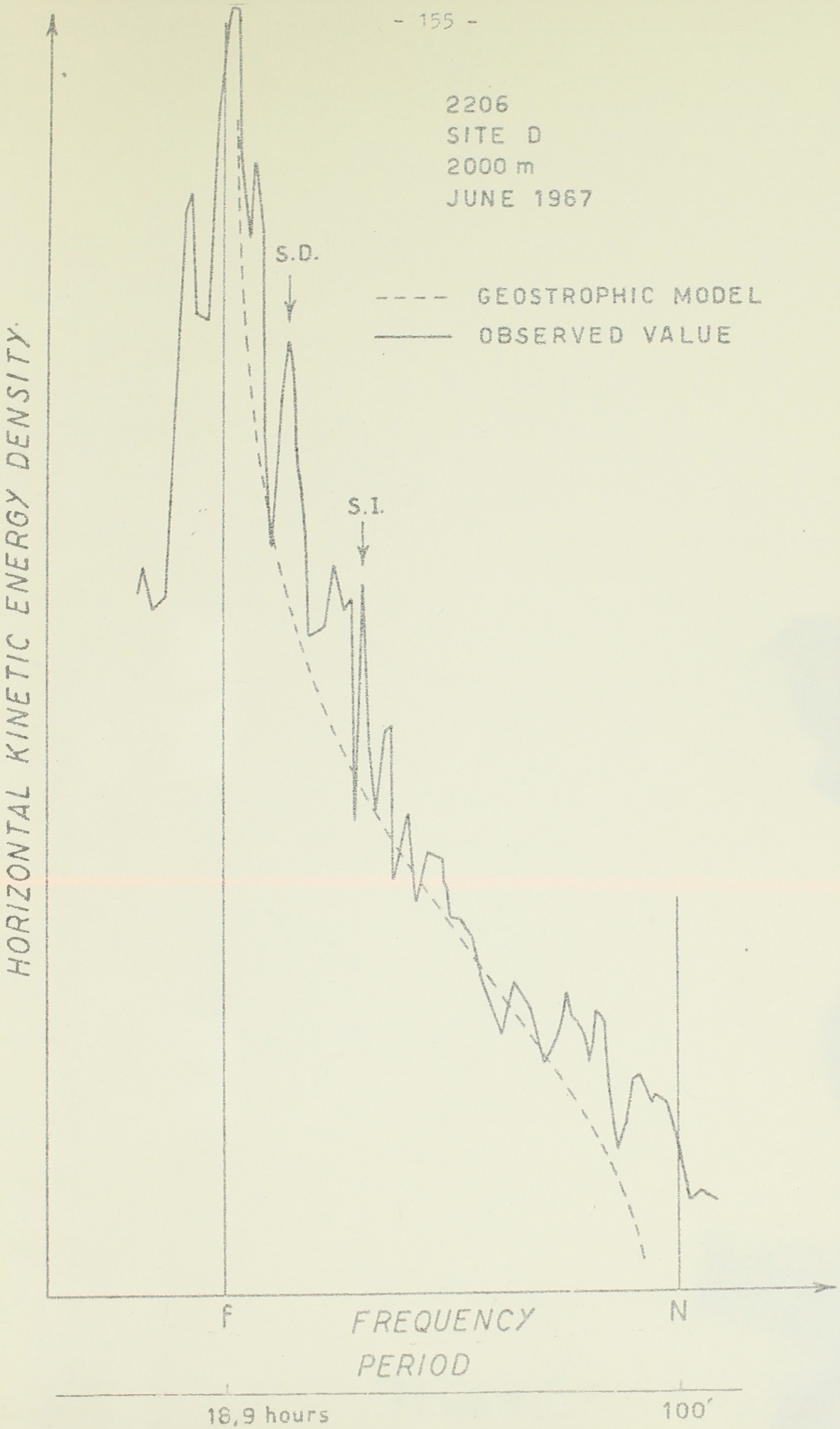
2206
SITE D
2000 m
JUNE 1967
S.D.
S.I.
GEOSTROPHIC MODEL
OBSERVED VALUE
HORIZONTAL KINETIC ENERGY DENSITY
f
N
FREQUENCY
PERIOD
18,9 hours
100'